AUSTRALIAN & NEW ZEALAND ORTHOPAEDIC RESEARCH SOCIETY

18TH Annual Scientific Meeting

The University Club of Western Australia
The University of Western Australia
Hackett Entrance 1, Hackett Drive, Crawley WA

30 August – 1 September
2012

CME Accreditation 14 hours at Category 1

ANZORS 18th Annual Scientific Meeting
Table of Contents

ANZORS 18th Annual Scientific Meeting
President's Welcome Address

A/Prof Hala Zreiqat

Dear ANZORS members,

Welcome to the 18th Annual Scientific Meeting, Perth, August 30 - 1 September 2012.

ANZORS is a multidisciplinary Society

For ANZORS to continue to flourish and succeed it needs a serious commitment to basic science in orthopaedics and that requires active interaction between basic scientists (bone /cartilage biology/biomechanics) and clinicians. I look forward to working with the new active ANZORS committee members to successfully plan towards achieving this goal.

We ensured maximal exposure Nationally and Internationally

In 2012, ANZORS continues to be widely recognised by a number of National and International Societies including AOA, COA, and EHS. I received invitations to speak at all of these societies in 2012. I ask board members to continue to promote the society nationally and internationally at the conferences they attend.

ANZORS expands its National and International profile

ANZORS must maintain contact with our overseas colleagues and maintain cordial interaction between the associations particularly with the Asia Pacific relationship. During 2012 I made sure that ANZORS was highlighted as frequently as possible. This year we are again holding a joint Session with ANZBMS sharing our invited international speaker and I would like to encourage maintaining this trend in the future and possibly engagement through concentrating on targeted Societies.

ANZORS engagement Nationally and Internationally (2012):

Nationally: This year we are holding a joint half-day symposium with the ANZBMS (second year in a row), following our highly successful joint session at the Gold Coast in 2011.

The Chinese Orthopaedic Association: For the second year we are holding a joint symposium with the 7thth International Congress of Chinese Orthopaedic Association. I organised a symposium to be attended by David Haynes, David Findlay and David Little.

Promoting PhD and Early Career Researchers (ECRs)

It is a pleasure to see the continuing support by ANZORS to PhD students where this year we awarded 19 Student Travel grants to attend the ANZORS annual conference.

We have implemented PhD and ECR awards to be presented at the Conference and are seeking sponsorship for these awards.

We have also supported oral presentations as 5+1 min short talks instead of poster sessions, giving everyone the opportunity to present their work and receive valuable feedback.

Showing gratitude:
To the invited speakers: ANZORS will continue to follow in its tradition to offer free registration and dinner to the invited speakers. This year we were able to offer airfares (within Australia) for several international/national speakers. We hope to continue with this gesture to ensure the growing status of ANZORS around the globe. Following up with letters of "thank you" will be equally critical. This gratitude should be shown in as many ways as possible both at the meeting and after returning home.
Ensuring continuation of interaction: Future requests that overseas speakers attend ANZORS scientific meetings is also a sign of appreciation for continuing interaction.
I trust that in my final year as President I have further cemented the high scientific reputation of ANZORS by many visits to key overseas Institutions.

Looking ahead: I would like to see more involvement with the AO (Davos), EORS and ESVOT. I have commenced planning to promote ANZORS at all these societies.

Abstract reviews: My sincere thanks to all member of the Scientific Committee who contributed to the abstract review process.

I am grateful to the enormous help given by the Secretary, Dr John Costi and the Treasurer, Professor Jiake Xu for working very closely with me throughout the year. A special thank you must go to Ms Diana Pham (PhD student, Biomechanics and Implants Research Group, The Medical Device Research Institute, School of Computer Science, Engineering & Mathematics, Flinders University, SA) for her substantial assistance with arranging and collating all abstract reviews with the Scientific Committee, collating all information for submitted abstract and travel grants, liaising with invited speakers and development of the program at a glance and final program booklet.

This meeting would not have been possible without the generous support of The Sydney University Tissue Engineering Network (SuTEN), The University of Sydney and the Harvard Club of Australia Foundation.

Thank you for giving me the honour and privilege of being the President of ANZORS and I look forward to working closely with the next President, Professor Jiake Xu in 2013.

Hala Zreiqat

President: Australian and New Zealand Orthopaedic Research Society

ANZORS 18th Annual Scientific Meeting
Committee Members

President

A/Prof Hala Zreiqat	NH&MRC Senior Research Fellow Head: Tissue Engineering & Biomaterials Research Unit School of AMME/Faculty of Engineering and IT and Bosch Institute The University Of Sydney, NSW

Secretary

Dr John Costi	Senior Lecturer Biomechanics & Implants Research Group The Medical Device Research Institute School of Computer Science, Engineering and Mathematics Flinders University, SA

Treasurer

Prof Jiake Xu	Winthrop Professor/Head of Molecular Laboratory School of Pathology and Laboratory Medicine The University of Western Australia, WA

2012 Host Organiser

Prof Jiake Xu	School of Pathology and Laboratory Medicine
A/Prof Nathan Pavlos	Centre for Orthopaedic Research, School of Surgery The University of Western Australia, WA

Immediate Past President

A/Prof David Haynes	Head of Anatomy and Pathology School of Medical Sciences The University of Adelaide, SA

Organising Committee

Hala Zreiqat

Jiake Xu

Diana Pham

John Costi

Nathan Pavlos

Dominic Thewlis

Scientific Committee (surname alphabetical order)

John Costi

Colin Dunstan

David Findlay

David Haynes

Julia Kuliwaba

Michelle McDonald

Ian Parkinson

Nathan Pavlos

Bogdan Solomon

Mark Taylor

Dominic Thewlis

Gethin Thomas

Yin Xiao

Jiake Xu

Hala Zreiqat

ANZORS 18th Annual Scientific Meeting
Travel Grant Recipients
(alphabetical surname order)

Melissa Cantley
University of Adelaide, SA

Adhiraj Chakrabarty
Royal Adelaide Hospital, SA

Nishant Chakravorty
Queensland University of Technology, QLD

Ashika Chhana
University of Auckland, NZ

Anjali Jaiprakash
Queensland University of Technology, QLD

Claire Jones
SA Pathology, SA

Jiao Jiao Li
University of Sydney, NSW

Pazit Levinger
Victoria University, VIC

Stephanie Low
University of Adelaide, SA

Saulo Martelli
University of Melbourne, VIC

David Musson
University of Auckland, NZ

Egon Perilli
Flinders University, SA

James Peters
Drexel University, Philadelphia, USA

Silpa Reddy
Drexel University, Philadelphia, USA

Seyed-Iman Roohani-Esfahani
University of Sydney, NSW

Yu-Wen Su
University of South Australia, SA

Marie-Luise Wille
Queensland University of Technology, QLD

Nicole Yu
Kids Research Institute, NSW

Yinghong Zhou
Queensland University of Technology, QLD

ANZORS 18th Annual Scientific Meeting
Venue and Transport Information

Venue: The University Club of Western Australia, The University of Western Australia
Hackett Entrance 1, Hackett Drive, Crawley

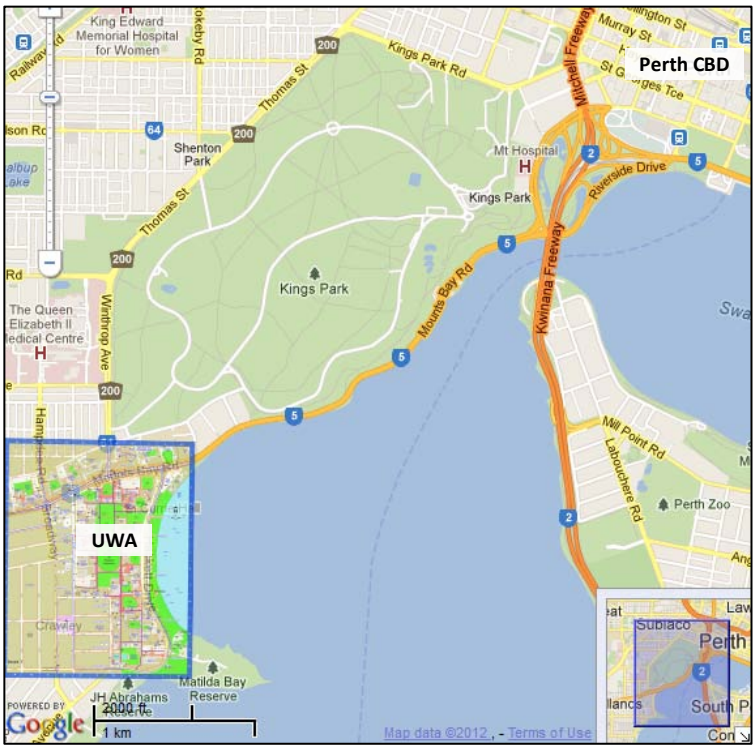

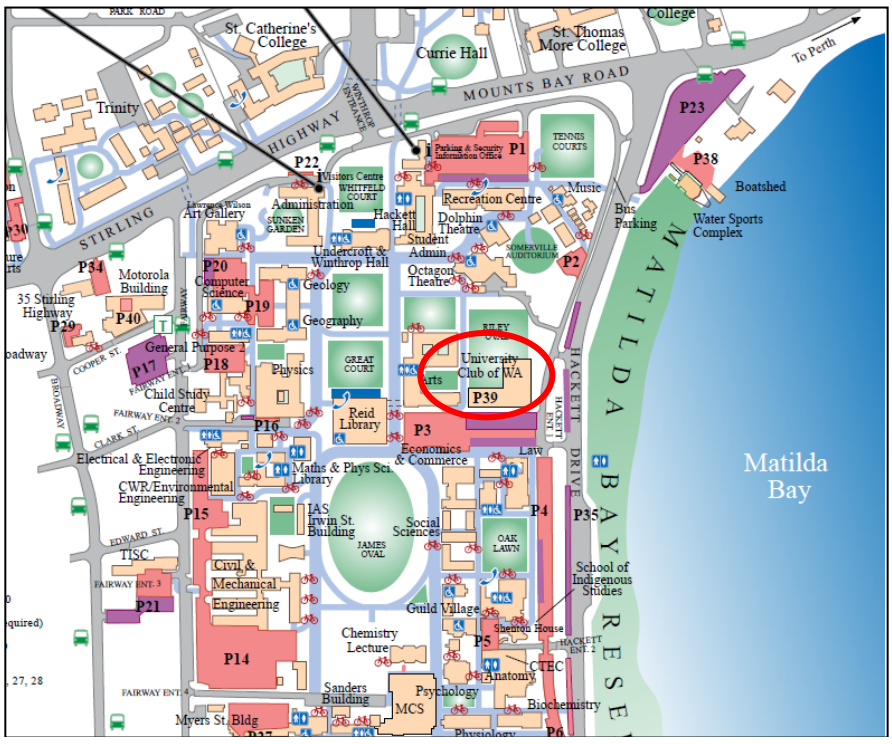

Bus Information

(http://www.uwa.edu.au/university/crawley/transport)

All of the below bus services use the bus stops on Stirling Highway at the north end of the Crawley Campus, except for the 97 (Subiaco Shuttle) that stops at the north end of Fairway.

Bus Routes to UWA

From	Route no.	Journey time to UWA	Frequency
Perth Wellington Street Bus Station	78, 79, 23, 102, 107	15 minutes	Every 5-10 minutes during peak times and every 15 minutes at other times
Perth Esplanade Busport	78, 79, 23, 102, 107	10 minutes	Every 5-10 minutes during peak times and every 15 minutes at other times
East Perth St Georges Terrace	24, 103	25 minutes	Every 20 minutes
Subiaco Train Station	97	20 Minutes	Every 15 minutes
Claremont Train Station	24, 23,107	10 Minutes	Every 10 minutes
Fremantle Train Station	98, 103	30 minutes	Every 15 minutes
Stirling Train Station	99	30 minutes	Every 15 minutes

ANZORS 18th Annual Scientific Meeting
Program at a Glance

Venue: The University Club of Western Australia, The University of Western Australia
Hackett Entrance 1, Hackett Drive, Crawley

DAY 1: Thursday, 30 August

6:00 PM	Welcome / registration
8:00 PM	Close

DAY 2: Friday, 31 August

8:15 AM	Registration / tea & coffee
8:55 AM	Presidential address: *A/Prof Hala Zreiqat*
9:00 AM	**SESSION 1: Biomedical Engineering & Imaging (1)** Invited speaker: *Prof Dennis Discher (University of Pennsylvania)*
10:40 AM	Morning tea
11:00 AM	**SESSION 2: Biomedical Engineering & Imaging (2)** Invited speaker: *Prof Pamela Yelick (Tufts University)*
12:35 PM	Lunch
1:20 PM	**SESSION 3: Clinical Orthopaedics & Kinematics** Invited speaker: *Prof William Lu (University of Hong Kong)*
2:40 PM	Afternoon tea
3:00 PM	**SESSION 4: PhD Award** Invited speaker: *Prof Alan Grodzinsky (MIT)*
4:25 PM	Annual general meeting
5:15 PM	Break
7:00 PM	ANZORS dinner / presentation of PhD award *Venue: The University Club Restaurant*
10:00 PM	Close

DAY 3: Saturday, 1 September

8:15 AM	Registration / tea & coffee
9:00 AM	**SESSION 5: Bone Biology & Joint Regeneration (1)** Invited speaker: *Assist. Prof Sarah Heilshorn (Stanford University)*
10:40 AM	Morning tea
11:00 AM	**SESSION 6: ECR Award** Invited speaker: *Prof Mark Taylor (Flinders University)*
12:25 PM	Lunch
1:20 PM	**SESSION 7: Biomaterials & Tissue Engineering** Invited speaker: *Prof Vicki Rosen (Harvard University)*
2:30 PM	Afternoon tea
2:50 PM	**SESSION 8: Bone Biology & Joint Regeneration (2)**
4:05 PM	Presentation of ECR award / closing speeches
4:15 PM	Meeting close

ANZORS 18th Annual Scientific Meeting
Full Program – DAY 2 and DAY 3

Venue: The University Club of Western Australia, The University of Western Australia
Hackett Entrance 1, Hackett Drive, Crawley

DAY 2: Friday, 31 August

8:15 AM	Registration / tea & coffee
8:55 AM	Presidential address: *A/Prof Hala Zreiqat*

SESSION 1: Biomedical Engineering & Imaging (1)
Chair: Dr John Costi

9:00 AM	***INVITED SPEAKER: Prof Dennis Discher*** *(University of Pennsylvania)* *From matrix to nucleus, ex vivo to in vitro*
9:25 AM	**John Davidson** A new poroelastic model of cartilage mechanics
9:37 AM	**Bo He** Elastic fibres display a versatile microfibril network in kangaroo articular cartilage
9:49 AM	**Claire Jones** A biomechanical comparison of rotator cuff repair techniques: suture bridge double row fixation with and without medial grasping suture
10:01 AM	**Silpa Reddy** Quantification of the normative adolescent pediatric rib cage to characterize age-dependent shape changes
10:13 AM	**Matthew Yalizis** Torque, compression and linear translation of novel hindfoot fusion screw
10:25 AM	**Song Chen** A mathematical model for prediction of intramedullary pressure trend during reaming in vivo sheep model
10:31 AM	**Pascal Buenzli** What is the role of bone surface availability in age-related endocortical bone loss? A combined experimental-computational approach
10:40 AM	Morning tea

DAY 2: Friday, 31 August (continued)

SESSION 2: Biomedical Engineering & Imaging (2)
Chair: Dr Dominic Thewlis

11:00 AM	***INVITED SPEAKER: Prof Pamela Yelick*** *(Tufts University)* *Progress and challenges in mineralized tissue engineering*
11:25 AM	**John Costi** Biomechanical assessment of segmental bone defect repair using impaction bone grafting
11:37 AM	**Stuart Callary** Effect of irradiation on allograft in a sheep model of femoral impaction grafting
11:49 AM	**Stephanie Low** 3D intraosseous micro-architecture of normal and avascular lunates (Kienböck's)
12:01 PM	**Tim Peltz** Changes in core suture geometry within repaired flexor tendons: an x-ray evaluation
12:13 PM	**Mark Kazzi** Software analysis of femoral cartilage volume after meniscal surgery
12:19 PM	**Corey Scholes** Quantitative analysis of computer navigation data before and after total knee arthroplasty
12:25 PM	**James Peters** Thoracic spine morphology comparison of a novel animal model
12:35 PM	Lunch

SESSION 3: Clinical Orthopaedics & Kinematics
Chair: Prof Pamela Yelick

1:20 PM	***INVITED SPEAKER: Prof William Lu*** *(University of Hong Kong)* *Bioactive Sr-HA bone cement for elderly osteoporotic bone fracture*
1:45 PM	**Adhiraj Chakrabarty** A new anterolateral approach to tibial plateau fractures – rationale and early results
1:57 PM	**Sébastien Lustig** Unsatisfactory accuracy with visionaire patient-specific cutting jigs for total knee arthroplasty
2:09 PM	**Dominic Thewlis** A ex vivo method to assess the influence of lunate morphology on carpal kinematics
2:21 PM	**John Abrahams** Radiostereometric analysis (RSA) of the migration of the trabecular metal acetabular revision system (TMARS) for severe bone loss at revision total hip replacement (THR)
2:27 PM	**Hossein Mokhtarzadeh** Feasibility evaluation of the Microsoft Kinect as a low cost alternative to motion capture systems
2:33 PM	**Hossein Mokhtarzadeh** Effect of high landing impact loads on tibial torques at different knee flexion angles
2:40 PM	Afternoon tea

DAY 2: Friday, 31 August (continued)

SESSION 4: PhD Award
Chairs: Prof David Findlay & Prof William Lu

3:00 PM	***INVITED SPEAKER: Prof Alan Grodzinsky*** *(MIT)* *Aggrecan molecular mechanics meets cartilage tissue nano-mechanics: relevance to cartilage repair via BMSCs in hydrogel scaffolds*
3:25 PM	**Yu-Wen Su** Expression and potential function of neurotrophic factors and their receptors in growth plate cartilage bony repair and skeletal cell formation
3:37 PM	**Marie-Luise Wille** Ultrasound transit time spectral analysis for derivation of density of cancellous bone
3:49 PM	**Anjali Jaiprakash** An in vitro model to study the regulation of osteocyte metabolism by chondrocytes
4:01 PM	**Melissa Cantley** Targeting HDAC 1 to suppress bone loss in peri-prosthetic osteolysis
4:13 PM	**Nicole Yu** In vivo synergy between rhBMP-2 and IKK-inhibitor PS-1145

4:25 PM	Annual general meeting
5:15 PM	Break
7:00 PM	ANZORS dinner / presentation of PhD award *Venue: The University Club Restaurant*
10:00 PM	Close

DAY 3: Saturday, 1 September

8:15 AM	Registration / tea & coffee

SESSION 5: Bone Biology & Joint Regeneration (1)
Chair: A/Prof Bogdan Solomon

9:00 AM	***INVITED SPEAKER: Assist. Prof Sarah Heilshorn*** *(Stanford University)* *Design of protein-based biomaterials for skeletal tissue engineering*
9:25 AM	**Pingping Han** Lithium (Li)-containing bioactive scaffolds improved cementogenic differentiation of periodontal ligament cells via the activation of Wnt/β-catenin signalling pathway by released Li+ ions
9:37 AM	**Xufang Zhang** Expression of angiogenic related cytokines in cartilage of osteoarthritis
9:49 AM	**Rachel Li** One's poison is another's food - heparanase for fracture healing
10:01 AM	**Jae-Won Shin** Hierarchical determination of nuclear deformability by lamins during marrow cell differentiation: implications in bone tissue engineering
10:13 AM	**Jiao Jiao Li** Design and fabrication of biphasic scaffold for osteochondral regeneration
10:25 AM	**Yinghong Zhou** Implantation of osteogenic differentiated donor mesenchymal stromal cells causes recruitment of host cells
10:31 AM	**Rosa Chung** Roles of Wnt/β-catenin signalling in bony repair of injured growth plate in young rats

10:40 AM	Morning tea

DAY 3: Saturday, 1 September (continued)

SESSION 6: ECR Award
Chair: Assist. Prof Sarah Heilshorn

11:00 AM	***INVITED SPEAKER: Prof Mark Taylor*** *(Flinders University)* *Moving towards population based computational modelling of total joint replacement*
11:25 AM	**Seyed-Iman Roohani-Esfahani** Strontium increases the bioactivity and degradability of magnesium silicate based scaffolds
11:37 AM	**Saulo Martelli** Comparison of two types of exercise for promoting bone growth in the femoral neck
11:49 AM	**Egon Perilli** High-resolution micro-CT examination of human bone: towards the entire organ
12:01 PM	**ZuFu Lu** TNF-α preconditioning promotes osteogenic differentiation of adipose-derived mesenchymal stem cells by modulating BMP-2 signalling pathway
12:13 PM	**Pazit Levinger** Lower limb biomechanical changes that impair gait performance following total knee replacement surgery
12:25 PM	Lunch

SESSION 7: Biomaterials & Tissue Engineering
Chair: Prof Mark Taylor

1:20 PM	***INVITED SPEAKER: Prof Vicki Rosen*** *(Harvard University)* *The role of BMP2 in bone graft healing*
1:45 PM	**David Musson** The osteogenic effects of a protein component extracted from a hydroxyapatite-based product
1:57 PM	**Murugan Ramalingam** Rapid screening of stem cells and engineering interface tissues using nanoscale gradient biomaterials
2:09 PM	**Nishant Chakravorty** Topographically and chemically modified titanium implant surfaces initiate differential regulation of micro-RNAs in osteoblasts
2:15 PM	**Jaydeep Ubeja** Human adult mesenchymal stem cell cultivation on a Bio-Oss hydroxyapatite matrix
2:21 PM	**Tao Wang** Development and optimization of ex vivo bioreactor system for tendon tissue engineering
2:30 PM	Afternoon tea

DAY 3: Saturday, 1 September (continued)

SESSION 8: Bone Biology & Joint Regeneration (2)
Chair: Prof Vicki Rosen

2:50 PM	**Ciara Murphy** Scaffold mechanical properties and composition regulates stem cell fate
3:02 PM	**William Cundawan** Seminal vesicle secretion (SVS) 7 is expressed by mature osteoclasts and acts to regulate osteoclast precursor proliferation, differentiation and bone homeostasis
3:14 PM	**Jasreen Kular** ENU-induced chemical mutagenesis reveals that choline kinase beta is an important regulator of osteoporosis
3:26 PM	**Anak Dharmapatni** TNF-like weak inducer of apoptosis (TWEAK) and its receptor, Fn14, are expressed by multinucleated cells in revision tissues and elevated during osteoclast development stimulated by polyethylene particles in vitro
3:38 PM	**Ee Cheng Khor** Central control of bone resorption: Neuropeptide Y, Y6 receptor signalling in the regulation of bone homeostasis
3:50 PM	**Ashika Chhana** Monosodium urate crystals inhibit tenocyte viability and function: implications for periarticular involvement in chronic gout
3:56 PM	**Shek Man Chim** EGFL7 is differentially expressed in osteoclasts and osteoblasts and mediates endothelial cell migration through the activation of extracellular signal-regulated kinase
4:05 PM	Presentation of ECR award / closing speeches
4:15 PM	Meeting close

SESSION 1 - ABSTRACTS

Biomedical Engineering & Imaging (1)

DAY 2: Friday, 31 August

9:00 AM – 10:40 AM

A MATHEMATICAL MODEL FOR PREDICTION OF INTRAMEDULLARY PRESSURE TREND DURING REAMING *IN VIVO* SHEEP MODEL

[1]Song Chen, [2]Paul Smith, [1]Qinghua Qin, and [2,3]Rachel Li

[1]Materials and Manufacturing Group, College of Engineering and Computer Science, Australian National University, ACT
[2]Trauma and Orthopaedic Research Unit, Department of Surgery, Canberra Hospital, ACT
[3]Department of Immunology and Genetics, John Curtin School of Medical Research, Australian National University, ACT
email: rachel.li@anu.edu.au

INTRODUCTION

Instrumentation of the intramedullary canal increases intramedullary pressure, which contributes to fat embolism syndrome (FES). We developed a computer-assisted reaming suction system (CARS) aimed to ameliorate the intramedullary pressure increase and thereby minimize the risk of FES. Using the experimental data obtained from a sheep femoral model with CARS, we have built a mathematical model to predict intramedullary pressure trend. The intramedullary pressure is dependent on the volume displacement, the revolution of reamer and the position of suction ports.

METHODS

Eighteen sheep were used to test CARS in monitoring and reversing the intramedullary pressure elevation. Six sheep of fractured femur with CARS were compared with 6 sheep of intact femur with CARS and 6 sheep of intact femur without CARS [1]. The mathematical model was built firstly on volume displacement dependency and then multiplied with a composite function of other factors including the rotation speed of a reamer. The composite function was derived from the experimental data fitting. The mathematical model had the y axis of pressure and the x axis of volume.

RESULTS AND DISCUSSION

The mathematical model is expressed as

$$\mathrm{Pr} = [A_1 * \exp(-\mathrm{Vr}/A_2) + A_3]\frac{\mathrm{Vr}}{1-\mathrm{Vr}} \qquad (1)$$

Where A_1, A_2 and A_3 are the parameters acquired from experimental data fitting. Pressure ratio (Pr) is equal to the pressure read from sensor divided by the normal intramedullary pressure. Volume ratio (Vr) is equal to the volume displacement divided by the total volume of intramedullary cavity. Examples of predicting the intramedullary pressure trends using the mathematical model are illustrated in Figure 1. Figure 1(a) demonstrated that high rotation speed caused a peak intramedullary pressure at the beginning of reaming. This peak could instantaneously reach to the threshold pressure of FES, especially without a suction system. It was also noticed that there was a dramatic reduction of the intramedullary pressure after the initial peak and this is consistent with previous literatures [2] that high revolution of reamer could reduce intramedullary pressure. However, the initial spark of the intramedullary pressure is much more significant than the subsequent decrease. Figure 1(b) represented that the peak pressure could occur at port 1 (proximal port) and the average high pressure could occur at port 4 (distal port). Hence, it is necessary to monitor the intramedullary pressure at both proximal and distal ports.

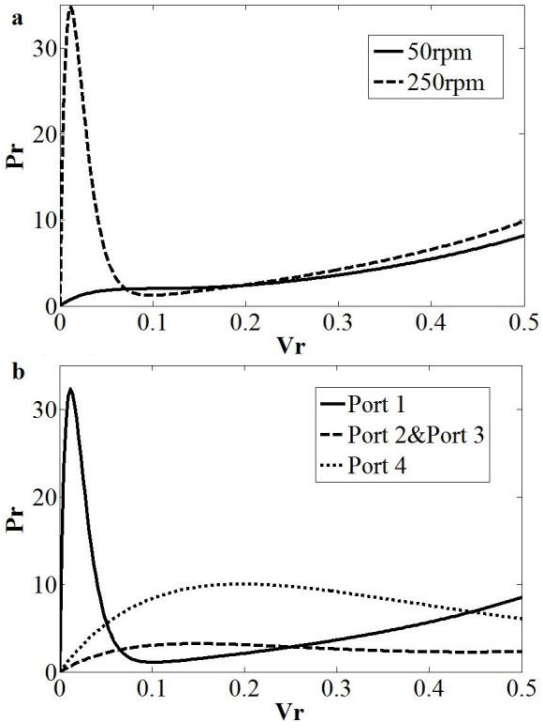

Figure 1: Prediction of the intramedullary pressure trend of intact femur from the mathematical model. (a) The influence of reaming revolution; (b) The influence of various ports at 250 rpm reaming.

CONCLUSIONS

The derived mathematical model is proven to be capable of predicating intramedullary pressure trend on various dependencies.

REFERENCES

1. Mousavi M, et al., *Clin Orthop and Relat Res*. **394**: 263-270, 2002.
2. Smith PN, et al., *J Orthop Res*. **26**(10):1327-1333, 2008.

TORQUE, COMPRESSION AND LINEAR TRANSLATION OF NOVEL HINDFOOT FUSION SCREW

Matthew A Yalizis and Elizabeth Clarke
The University of Sydney, Sydney Medical School, the Kolling Institute of Medical Research
email: myalizis@med.usyd.edu.au

INTRODUCTION

Hindfoot arthrodesis is reliably accomplished by removal of articular cartilage, attaining bony apposition and achieving sufficient interfragmentary compression by means of an internal fixation device, which in some cases is a compression screw. Various screw systems are available for use and have differing means of achieving interfragmentary compression. One method is to utilize a differential pitch thread (eg. Herbert, Acutrak). Another method is to include an unthreaded portion on the shaft of the screw as in a partially threaded cancellous screw. Estimating the amount of interfragmentary compression intraoperatively is possible by torque feedback on the screwdriver, however the two are not necessarily well correlated. The ability to accurately predict interfragmentary force intraoperatively would be an advantage. Additionally achieving complete bony apposition at the time of screw insertion can be difficult hence requiring the screw device to achieve greater translation between the bony surfaces. So we sought to compare torque, compression and linear translation of one novel dual component hindfoot fusion screw (Dynafuse) and 2 other available screws (Acutrak 6/7 and 6.5mm synthes cannulated screw).

METHODS

Simulated osteosynthesis was conducted on synthetic bone blocks made of polyurethane foam simulating the cancellous bone found in the hindfoot (Sawbones, Pacific Research Laboratories Washington USA). Compressive force between the two bone blocks was measured by means of a washer load cell (Omegadyne LC8125) and insertional torque was measured using a reaction torque cell (Omegadyne TQ202). There was a custom made testing platform designed to attach to the reaction torque cell and contain the bone blocks during the testing. Screws tested were N=12 Acutrak 6/7, N=12 6.5mm Synthes partially threaded cancellous cannulated screw and N=12 novel 7.0mm Dynafuse compression screw. Linear translation of bone blocks was recorded by means of camera tracking.

RESULTS AND DISCUSSION

The Acutrak and Dynafuse screws exhibited good correlation between screwdriver insertional torque and interfragmentary compression (correlation coefficient=0.92). The 6.5mm Synthes cannulated screw exhibited lower correlation between insertional screwdriver torque and compression (correlation coefficient=0.8). The highest peak interfragmentary compression force was achieved by the Dynafuse screw (331±41N). Linear translation of the bone blocks was greatest for the Synthes 6.5mm cannulated screw (1.51±0.2mm per half screwdriver revolution) and lowest for the Acutrak 6/7 (0.11±0.3mm per half screwdriver revolution). If bone fragments are not completely apposed at the time of screw insertion this may lead to a reduced final interfragmentary force. Hence the Synthes and Dynafuse screws could aid in apposition of bony surfaces as these require less screwdriver revolutions to achieve bone block apposition.

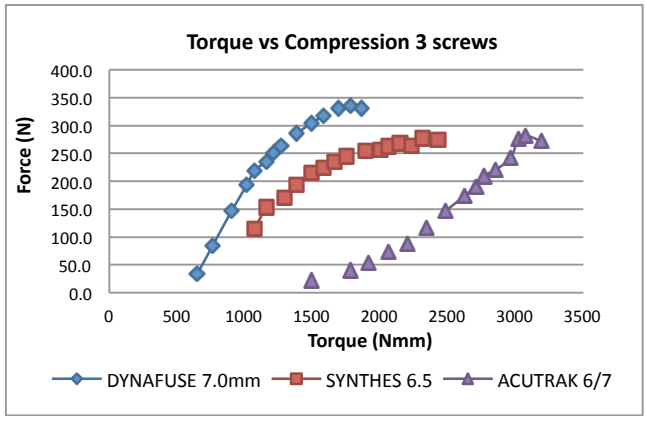

Figure 1: Average Torque vs Compression for 3 screw types

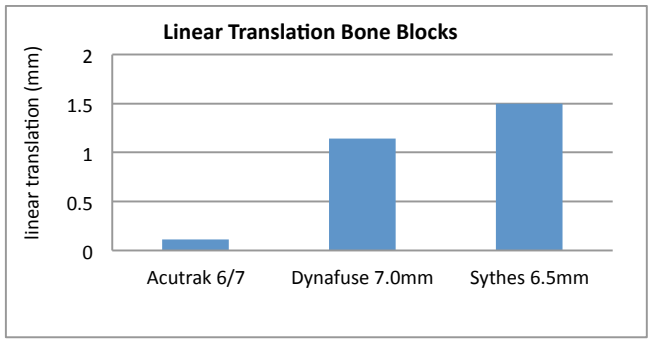

Figure 2: Average linear translation for 3 screw types (mm per half screwdriver revolution)

CONCLUSIONS

The Dynafuse compression screw exhibited the highest interfragmentary compression and both the Dynafuse and Acutrak exhibited good correlation between screwdriver torque and compression, which would aid in estimating compression during clinical use. The Synthes 6.5mm cannulated screw and the Dynafuse 7.0mm screw were best at drawing bone blocks together. The Acutrak 6/7 was not as effective in translating bone blocks and this implies that more care is needed intraoperatively to ensure that there is no interfragmentary gap at the time of screw insertion.

CONFLICT OF INTEREST DECLARATION

In the interests of transparency and to help reviewers assess any potential bias, ANZORS requires authors of original research papers to declare any competing commercial interests in relation to the submitted work. Referees are also asked to indicate any potential conflict they might have reviewing a particular paper.

If you have accepted any support such as funds or materials, tangible or intangible, concerned with the research by the commercial party such as companies or investors, choose YES below, and state the relation between you and the commercial party.

If you have not accepted any support such as funds or materials, choose NO.

Do you have a conflict of interest to declare? (DELETE TEXT as appropriate)

YES

If YES, please complete as appropriate:

1. Dr Yalizis declares as interest in the results of this study as he has designed the novel screw presented here.

QUANTIFICATION OF THE NORMATIVE ADOLESCENT PEDIATRIC RIB CAGE TO CHARACTERIZE AGE-DEPENDENT SHAPE CHANGES

[1]Silpa Reddy, BS., [2]Lucy Robinson, PhD., [3]Robert M. Campbell, Jr., MD., and [1]Sriram Balasubramanian, PhD.

[1]Orthopedic Biomechanics Laboratory, School of Biomedical Engineering, Science, and Health Systems, Drexel University, PA, USA
[2]Department of Epidemiology and Biostatistics, School of Public Health, Drexel University, PA, USA
[3]Division of Orthopaedic Surgery, The Children's Hospital of Philadelphia, PA, USA
email: silpa.reddy@drexel.edu

INTRODUCTION

Lack of information regarding adolescent rib cage geometry in the literature may lead to a poor understanding of normative and diseased adolescent thoracic cage structures and disease etiology. Age-related changes in rib cage structure and dimensions have been previously studied in adults [1, 2]. Yet previous attempts at quantifying diseased pediatric thoracic shapes have failed to include a large normative three-dimensional pediatric dataset for the basis of comparison [3]. Thus, there is a need to quantify the normative adolescent rib cage geometry to better understand what constitutes "normal" adolescent thoracoanatomy. The objectives of this study are to establish baseline parameter values of rib cage geometry for the normative adolescent population and determine age-related bilateral rib asymmetry and parameter trends.

METHODS

Chest CT scans were obtained from 21 skeletally-normative adolescent males who were within 5th to 95th percentile of BMI, height, and weight. Three-dimensional scan reconstructions were performed using Mimics image analysis software (Materialise Inc., Belgium). In order to describe rib cage shape, centerline geometry data for all rib pairs were input to a custom MATLAB (The MathWorks Inc., Natick, MA) code to compute geometric parameters of interest at each thoracic vertebrae level, namely measurements of rib length, normalized rib length by subject standing height, rib apparent unrolled curvature along each 10% of rib length, frontal angle, lateral angle, thoracic index and enclosed area of the rib.

Subjects were divided into four age groups, namely: 10 years (n=5) 12 and 13 years (n=4), 15 and 16 years (n=7), and 18 years (n=5). SPSS software (SPSS Inc., Chicago, IL) was used to perform non-parametric matched pair t-tests and one sample t-tests (with Bonferroni's correction) for interpretation of bilateral rib symmetry and parameter trends.

RESULTS AND DISCUSSION

Across all age groups, there is an underlying amount of bilateral asymmetry in the pediatric thorax that is statistically significant (α=0.05), but interpretation of 95% confidence intervals suggests that the asymmetry is not scientifically meaningful (Table 1). Larger standard deviations tended to prevail, for all parameters, at the false ribs. Normalization of the rib pair data yielded percentage differences between left and right ribs, characterizing the innate subject-specific and age-specific variability underlying rib shape. Thus, this validates the clinical assumption that the normative adolescent thorax is generally bilaterally symmetrical, and differences seen at rib pairs could be a general characteristic of the ribs or due to patient variability. Among the age groups, thoracic index appeared to decrease slightly (R^2 = 0.00 to 0.14) as age increased from 10 to 18, while enclosed area (R^2 = 0.25 to 0.83), normalized length (R^2 = 0.03 to 0.47), and length (R^2 = 0.19 to 0.86) all linearly increased with age. Differences in relationship strength between age and enclosed area, normalized length, and rib length could be attributed to varying growth rates per rib pair. This suggests that in adolescence, change is primarily in size rather than shape.

CONCLUSIONS

The normative pediatric adolescent male rib cage can be described quantitatively by age-dependent geometric characteristics.

REFERENCES

1. Mohr M, et al., *J Biomech*. **40** (6):1310-7, 2007.
2. Gayzik FS, et al., *J Biomech*. **41**(7):1545-54, 2008.
3. Stokes I, et al., *J Orthop Res*. **7**:599-606, (1989).

Table 1: Calculated rib length and absolute percent difference in rib length per rib across age groups.

PARAMETER	TYPE		T1	T2	T3	T4	T5	T6	T7	T8	T9	T10	T11	T12
RIB LENGTH (AVERAGE (SD)), mm	10 yo (n=5)	L	88.45 *(2.51)*	159.88 *(2.77)*	199.82 *(1.59)*	218.19 *(0.53)*	231.38 *(1.37)*	234.82 *(0.82)*	230.18 *(1.17)*	223.06 *(0.59)*	205.27 *(1.08)*	177.10 *(1.35)*	137.61 *(0.34)*	80.71 *(2.67)*
		R	84.90 *(9.67)*	155.96 *(10.18)*	197.57 *(10.18)*	217.44 *(11.83)*	229.43 *(10.94)*	233.66 *(9.05)*	231.84 *(8.16)*	223.90 *(8.77)*	206.79 (*7.83)*	179.01 *(4.89)*	138.09 *(5.70)*	84.48 *(8.04)*
	12 yo, 13 yo (n=4)	L	95.53 *(4.54)*	179.93 *(7.35)*	226.29 *(6.24)*	249.23 *(7.77)*	260.80 *(6.86)*	265.92 *(8.34)*	260.64 *(9.32)*	247.97 *(5.77)*	229.63 *(4.22)*	202.04 *(6.61)*	161.82 *(12.42)*	95.68 *(24.40)*
		R	94.31 *(6.10)*	178.22 *(5.39)*	223.27 *(8.19)*	248.46 *(9.59)*	261.68 *(9.98)*	265.01 *(11.46)*	262.45 *(13.10)*	249.75 *(13.2)*	232.56 *(11.43)*	206.89 *(11.21)*	164.99 *(16.04)*	108.12 *(20.31)*
	15 yo, 16 yo (n=7)	L	101.61 *(11.05)*	194.39 *(19.34)*	243.84 *(21.07)*	271.65 *(20.32)*	287.58 *(23.24)*	292.85 *(22.98)*	288.43 *(21.28)*	278.63 *(21.51)*	263.25 *(22.41)*	228.65 *(22.60)*	178.95 *(22.12)*	107.27 *(19.79)*
		R	101.27 *(11.27)*	191.21 *(16.84)*	243.53 *(19.40)*	273.45 *(21.12)*	288.13 *(20.34)*	293.36 *(21.90)*	289.99 *(20.72)*	282.29 *(22.32)*	263.86 *(23.15)*	231.49 *(23.60)*	180.48 *(23.86)*	107.55 *(21.79)*
	18 yo (n=5)	L	114.26 *(6.08)*	211.06 *(13.74)*	259.38 *(7.63)*	286.11 *(8.62)*	300.26 *(7.43)*	306.61 *(3.99)*	305.36 *(3.19)*	299.22 *(5.51)*	280.85 *(13.47)*	245.54 *(18.27)*	190.11 *(33.49)*	108.89 *(46.08)*
		R	115.09 *(9.38)*	208.81 *(12.40)*	258.65 *(5.75)*	285.53 *(3.88)*	301.53 *(2.89)*	307.91 *(2.71)*	305.94 *(1.98)*	298.94 *(9.88)*	281.22 *(17.56)*	246.51 *(21.28)*	195.28 *(34.59)*	117.44 *(39.63)*
ABSOLUTE PERCENT DIFFERENCE IN RIB LENGTH, ABS((L-R)/L) (AVERAGE (SD))	10 yo (n=5)	%	6.05 *(8.30)*	2.46 *(1.14)*	2.14 *(1.44)*	1.47 *(0.46)*	1.71 *(2.57)*	0.85 *(0.79)*	1.29 *(0.21)*	0.81 *(0.64)*	0.95 *(0.38)*	1.08 *(0.65)*	1.70 *(1.10)*	4.93 *(3.18)*
	12 yo, 13 yo (n=4)	%	2.42 *(0.77)*	2.29 *(0.74)*	1.77 *(1.26)*	1.04 *(0.53)*	1.14 *(0.55)*	1.15 *(0.78)*	1.05 *(1.28)*	2.26 *(2.15)*	2.31 *(2.85)*	2.51 *(3.22)*	3.45 *(3.92)*	16.11 *(17.82)*
	15 yo, 16 yo (n=7)	%	2.56 *(2.34)*	2.15 *(1.10)*	0.87 *(0.44)*	1.31 *(1.14)*	1.49 *(1.15)*	0.94 *(0.52)*	1.34 *(0.81)*	1.49 *(1.21)*	1.11 *(1.01)*	1.50 *(1.58)*	1.92 *(0.69)*	8.80 *(5.75)*
	18 yo (n=5)	%	3.45 *(2.93)*	1.59 *(1.81)*	0.99 *(0.87)*	1.32 *(0.87)*	1.34 *(1.08)*	0.67 *(0.88)*	0.51 *(0.24)*	1.46 *(1.60)*	1.93 *(1.53)*	1.97 *(1.62)*	4.63 *(3.32)*	15.90 *(16.44)*

A BIOMECHANICAL COMPARISON OF ROTATOR CUFF REPAIR TECHNIQUES: SUTURE BRIDGE DOUBLE ROW FIXATION WITH AND WITHOUT MEDIAL GRASPING SUTURE

[1,2]Claire F. Jones, [3]George EH. Awwad, [4,5]Kevin Eng, [3,4,5]Gregory I. Bain

[1]Adelaide Centre for Spinal Research, SA Pathology, SA. [2]School of Mechanical Engineering, University of Adelaide, SA. [3]Department of Orthopaedics and Trauma, Royal Adelaide Hospital (RAH), Adelaide, SA. [4]Department of Orthopaedics and Traumatology, University of Adelaide, SA. [5]Department of Orthopaedics and Trauma, Modbury Hospital, Modbury, SA.
email: claire.jones2@health.sa.gov.au

INTRODUCTION

Arthroscopic repair of rotator cuff tears has been widely accepted and complex reconstructions using transosseous tunnels, bone anchors and sutures have been introduced to more accurately recreate the cuff footprint [1]. The suture bridge double row (SBDR) repair has reduced re-tear rates compared to single or other double row techniques [2]. However, re-tears may occur and tend to be at the tendon-suture interface at the musculotendinous junction [3]. We hypothesised that a medial grasping suture may improve the stability of the construct. The aim of this study is to compare the biomechanical performance of the traditional SBDR and this new suture bridge medial mattress (SBMM) repair.

METHODS

Infraspinatus tendon-humerus specimens were isolated from 8-month-old sheep. Matched pairs were randomly assigned to either SBDR repair or SBMM repair (n=3, n=2, respectively to date). The tendon was detached from its insertion and repaired using a double row of anchors (3.5 mm Piton, Tornier, Edina, MN) with or without medial grasping sutures, by a single surgeon (KE). Dye markers were placed on the humeral head and on the tendon, and the test was recorded with a digital video camera (30 fps) (Figure 1). The proximal humerus was embedded in dental stone and fixed to the base of a materials testing machine (8874, Instron, Norwood, MA). The tendon was attached to the actuator with a clamp such that the tensile load was applied in the same plane as the insertion footprint. A tensile preload of 5 N was held for 5 seconds then cyclic loading of 10-30 N (0.5 Hz, 50 cycles) was applied before loading to failure at 1 mm/sec. Each repair was assessed for tendon displacement (i.e. gap formation) during the 1st and 50th cycle, and at 1mm and 2 mm of the ramp to failure, and the mode of failure was recorded.

RESULTS AND DISCUSSION

All specimens maintained tendon-bone contact throughout cyclic testing. The mean displacements of the tendon relative to the bone are shown in Table 1. The SBDR repair technique appeared to allow greater displacement of the tendon relative to the humeral head (relative to the displacement at 5 N preload), than the SBMM repair technique. There are insufficient data to complete statistical analyses at this time. During tensile loading to failure, both repair techniques failed by suture cutting through the tendon; no instances of anchor pull-out or suture failure were observed.

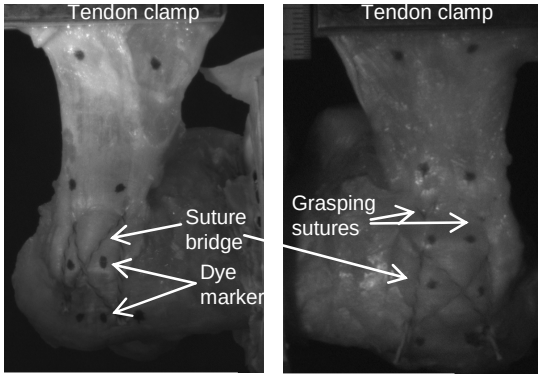

Figure 1: (left) SBDR and (right) SBMM repairs.

CONCLUSIONS

These preliminary results suggest that the SBMM repair may be more biomechanically stable than the SBDR repair technique. Approximately seven additional specimens per group will be tested and full data analysis will be completed in the coming month.

ACKNOWLEDGEMENTS

Bone anchors were donated by Tornier (Edina, MN).

REFERENCES

1. Baleani et al., *Clin Biomech* **21(8)**:799-803, 2006.
2. Mihata et al., *Am J Sports Med*, **39(10)**:2091-8, 2011.
3. Cho et al., *Am J Sports Med*, **38(4)**:664-71, 2010.

Table 1: Displacement between the tendon and bone markers (relative to that at 5 N preload) for Cycle 1 and 50, and 1 and 2 mm of actuator displacement during the ramp to failure.

	Displacement between tendon and bone (relative to 5 N preload) (mm)			
Repair Type	**Cycle 1**	**Cycle 50**	**1 mm**	**2 mm**
SBDR	2.21± 0.60	3.49 ± 1.18	3.99 ± 1.23	3.15 ± 0.60
SBMM	1.99± 0.61	3.07 ± 0.74	4.81 ± 1.37	3.45 ± 0.76

CONFLICT OF INTEREST DECLARATION

In the interests of transparency and to help reviewers assess any potential bias, ANZORS requires authors of original research papers to declare any competing commercial interests in relation to the submitted work. Referees are also asked to indicate any potential conflict they might have reviewing a particular paper.

If you have accepted any support such as funds or materials, tangible or intangible, concerned with the research by the commercial party such as companies or investors, choose YES below, and state the relation between you and the commercial party.

If you have not accepted any support such as funds or materials, choose NO.

Do you have a conflict of interest to declare? (DELETE TEXT as appropriate)

YES

If YES, please complete as appropriate:

1. The author(s) did receive payments or other benefits or a commitment or agreement to provide such benefits from a commercial entity.
   State the relation between you and the commercial entity:

The bone anchors were donated by Tornier. None of the authors has a relationship with the company.

ELASTIC FIBRES DISPLAY A VERSITLE MICROFIBRIL NETWORK IN KANGAROO ARTICULAR CARTILAGE

[1]Bo He, [2]Jianping Wu, [1]Jiake Xu, and [2]Thomas Brett Kirk

[1]School of Pathology and Laboratory Medicine, The University of Western Australia, WA
[2]Department of Mechanical Engineering, Curtin University of Technology, WA
email: brett.kirk@curtin.edu.au

INTRODUCTION

Elastic fibres are an essential extracellular matrix (ECM) component comprising an amorphous core of extensively cross-linked elastin, surrounded by fibrillin-rich microfibrils [1,2]. It is a significant component in the skin, lungs, arteries and elastic cartilage and has been the subject of a large number of publications. However, the study of elastic fibres in articular cartilage is relatively limited. Previous studies using histochemical methods reported that little elastin was present in articular cartilage but no architectural information was provided.

With the advancement of imaging techniques, multiphoton microscopy enables simultaneous imaging of the elastic fibres and collagen fibres with higher resolution. At long wavelength laser (near infrared light) excitation, two-photon excited fluorescence (TPF) from elastic fibres and the second harmonic generation (SHG) signal from collagen fibres can be collected, respectively. Long wavelength laser allows optical sectioning of the articular cartilage to a higher depth. Thus the three-dimensional structure of elastic fibres and collagen fibres can be reconstructed. The present utilized multiphoton microscopy to reveal the elastic fibre network in the articular cartilage and its relationship with collagen fibres.

METHODS

Fresh kangaroo forelimb and hindlimb joints were collected. Cartilage specimens were harvested from the weight bearing areas of the tibial plateau, femoral condyle and distal humerus. Cartilage corresponding to superficial zone and deep zone were sliced and recorded.

Multiphoton confocal laser scanning microscope (Leica TCS SP2 acousto-optical beam splitter (AOBS)) was used to image the elastin and coallagen fibres. The multiphoton laser is a Spectra Physics Mai Tai sapphire system, tunable between 710 and 990 nm. TPF and SHG were excited using 890 nm laser. The SHG signal was directed via collimating lenses onto a dichroic mirror and detected in the forwards direction. The SHG signal was expected at 445nm and collected by a Leica oil S2 condenser. TPF was collected in epi-direction at wavelength of 500 to 650 nm. All images were collected as a series of z stacks with a step size of 0.5 μm.

RESULTS AND DISCUSSION

Elastic fibres were extensively presented in the cartilage surface. Four types of elastin were found, including: straight lines, straight lines with branches, wiggling lines and fine elastin. Among them, straight line and straight line with branches were the majority patterns found in the ECM. Fine elastin was also found on the chondrocyte surface and in pericellular matrix. In the most superficial layer, cobweb-like elastic network, which did not show a dominant direction, was found parallel to the cartilage surface. Underneath the most superficial layer, elastic fibre is highly oriented and parallel to the collagen fibres in the superficial zone. In the deep zone, only fine elastin but no resolvable individual fibres was found on the chondrocyte surface and in pericellular matrix. Variations were also found between joints in terms of the density and pattern of elastic fibers: tibial plateau showed highest density followed by femoral condyle;

CONCLUSIONS

Our data reveals for the first time that elastic fibre is a complex and highly organized three-dimensional structure in the ECM of articular cartilage. The organization of elastic fibres varies with depth and joint surfaces. These results indicate the crucial role of elastin in maintaining the integrity and the elastic property of articular cartilage.

ACKNOWLEDGEMENTS

REFERENCES

1. Debelle L, et al., *Cell biology.* **31**:261-272, 1999.
2. Montes GS, *Cell biology international.* **20**:15-27, 1996.

A New Poroelastic Model of Cartilage Mechanics

[1]John B Davidson, [1]Bruce Gardiner, [2]Alan Grodzinsky, and [1]David Smith

[1]Computational Biology Group, School of Computer Science and Software Engineering, University of Western Australia
[2]Tissue Center for Biomedical Engineering, Massachusetts Institute of Technology, USA

INTRODUCTION

Poroelasticity, originally developed to model soil mechanics, has a long history of being used to model articular cartilage. The equations are equivalent to the bi-phasic and tri-phasic type cartilage models described in the literature. The framework presented here divides the standard 'solid' phase into collagen and aggrecan phases, allowing the effects of the properties and interactions of both to be teased apart.

METHODS

Cartilage is modelled as being composed of three separate phases, a homogeneous collagen network, mobile aggrecan molecules, and an extracellular fluid. Collagen is represented as a linear elastic solid with a modulus of 5MPa in tension and 0.5MPa in compression. Aggrecan concentration is modelled using an advection-diffusion equation, and extracellular fluid pressure is represented by Darcy's Law. The collagen matrix is subjected to body loads from the osmotic stress of the aggrecan, and the excess pore water pressure of the extracellular fluid. Osmotic pressure resulting from the aggrecan is calculated in the manner described in [1].

COMSOL Multiphysics was used to simulate deformation and aggrecan turnover in a cartilage explant subject to confined compression. Specifically, a 2D geometry 3mm x 0.1mm was used to represent a section of cartilage. A uniform source term in the aggrecan advection-diffusion equation simulated the effect of spatially homogenously distributed chondrocytes producing aggrecan at a constant rate. Only one surface of the cartilage was permeable to aggrecan and extracellular fluid, and mechanically unconstrained.

RESULTS AND DISCUSSION

Figure 1 shows the concentration of aggrecan along a central section through the length of the cartilage. Aggrecan concentrations are shown at 6 day intervals, along with the final equilibrium concentration, reached after approximately 46 days of aggrecan production at 4.3×10^{-5}mg/ml/s [2].

As aggrecan concentration increases in the geometry, the osmotic stress increases, drawing water into the construct and forcing the collagen to expand under tension. The cartilage geometry, initially at rest, begins to deform as a result of the increase in aggrecan concentration. The strain of the collagen matrix due to the osmotic pressure can be seen in Figure 2.

Upon initial application of an applied load, the extracellular fluid pressure increases to 'carry' this load. As the fluid leaves the tissue, local aggrecan concentration is seen to increase, raising the osmotic pressure, helping to balance the applied compressive load.

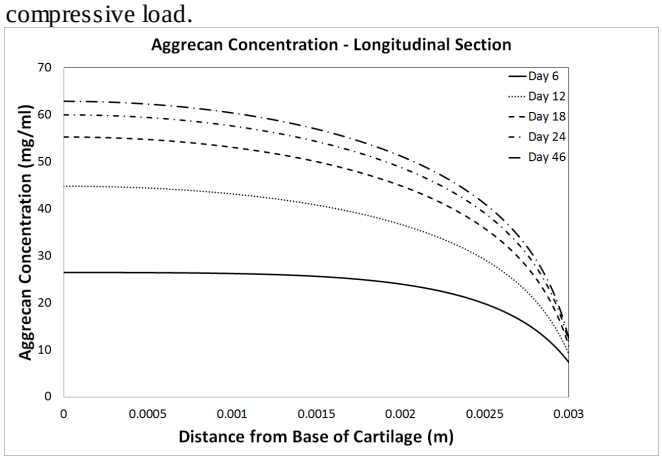

Figure 1: Aggrecan concentration.

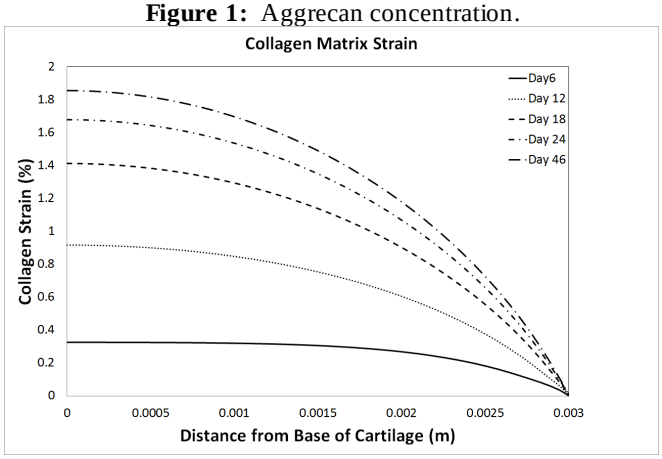

Figure 2: The strain of the collagen matrix.

CONCLUSIONS

This modelling framework allows the individual components of the cartilage matrix to be evaluated. This allows great flexibility, e.g. local stresses and strains of individual phases can be analysed, leading to more physiologically informed, time dependent, material properties. This will result in a tool to better replicate, interpret, and predict the complex, time and stress dependent properties of articular cartilage.

ACKNOWLEDGEMENTS

The authors would like to acknowledge the Australian Research Council DP0988001.

REFERENCES

1. Comper, *Cartilage: Molecular Aspects*. 1991.
2. Zhang, et.al., *J. Eng. Mech*. **135**:439-449, 2009.

FROM MATRIX TO NUCLEUS, EX VIVO TO IN VITRO

[1]Dennis E. Discher

[1]University of Pennsylvania, Philadelphia, PA, USA
email: discher@seas.upenn.edu

Collagen-I is not only a principal component of bone but is also the most abundant protein in animals. We profiled collagen-I amounts in many adult tissues by 'omic methods for mRNA and protein, and asked two questions: (1) is there any physical systematics to expression level, and (2) what cellular components correlate with collagen-I? The answer to what correlates with tissue collagen-I for more than a dozen soft tissue from brain to bone is the micro-elasticity of the tissue at the level of the cellular microenvironment. For bone, that means osteoid, and for cartilage, it is the pericellular matrix that is key. Many other matrix components, including crosslinking enzymes, also correlate, and the scaling of elasticity is remarkably consistent with simple polymer physics theory and rheology experiments.

With regard to the second question above, among the cellular components that correlate with collagen-I across tissues are the nuclear structure proteins, namely the lamins. We describe the consequence of lamin knockdown and overexpression on osteogenesis as couples to matrix elasticity effects on mesenchymal stem cells in vitro. Two simple matrix model systems will be described. A first is a 2 nm film of collagen-I fibers that is enzymatically crosslinked or not. We show that the effective rigidity of crosslinking strongly promotes osteogenesis in ways that couple to nuclear lamin levels. A second test system is based on synthetic polymer gels of controlled crosslinking that is also imbued with non-fibrous collagen-I, and a similar story emerges that is expanded to other lineages. In sum, we describe a mechanotransduction path from matrix to nucleus, with implications for disease, aging and development.

WHAT IS THE ROLE OF BONE SURFACE AVAILABILITY IN AGE-RELATED ENDOCORTICAL BONE LOSS? A COMBINED EXPERIMENTAL-COMPUTATIONAL APPROACH

[1]Pascal Buenzli, [1]Peter Pivonka, [2]C. David L. Thomas, and [2]John G. Clement

[1]Engineering Computational Biology Group, The University of Western Australia, Perth, WA, Australia
[2]The Melbourne Dental School, The University of Melbourne, VIC, Australia

INTRODUCTION

Age-related bone loss and postmenopausal osteoporosis are disorders of bone remodelling, in which less bone is reformed than resorbed. Yet, this dysregulation of bone remodelling does not occur equally in all bone regions. In long bones pronounced bone loss occurs near the endocortical surface, leading to cortical wall thinning and consequently to an expansion of the medullary cavity, a process sometimes referred to as "trabecularisation". Cortical wall thinning is of major concern in osteoporosis due to the strong reduction in bone mechanical properties that it is associated with.

In this contribution, we examine the hypothesis that the nonuniformity of bone surface availability within the tissue could explain the predominant loss of bone near the endocortical wall observed in osteoporosis. The idea that bone surface availability may influence bone loss in osteoporosis was proposed by RB Martin [1]. This question is challenging to address experimentally. Here, we investigate this hypothesis in a spatially nonuniform context using a simple computational model of bone remodelling, and a phenomenological relationship between bone specific surface and bone porosity. This enables us to follow the evolution of the medullary cavity area, or equivalently of the cortical wall width in a simulated osteoporotic condition. The results of the computational model are compared to experimental data from human femur midshafts of the Melbourne Femur Collection [2].

METHODS

We employ a simple computational model of bone remodelling to study local bone volume changes in small portions of bone tissue (1-3 mm^3). The computational model accounts for active osteoclasts and active osteoblasts, and for the fact that their numbers at the tissue scale depends on the microscopic availability of bone surface, i.e., depends on the bone specific surface. An age-related osteoporotic condition is assumed by specifying an imbalance between resorption and formation. The evolution of an initially nonuniform bone matrix volume fraction (volume of bone matrix per volume of tissue) is followed across the whole cross-section of a midshaft human femur. The evolution of the bone matrix volume fraction is governed by the number of active osteoclasts and active osteoblasts, which depend in turn on the specific surface. A phenomenological relationship provided by Martin [1] between the specific surface and the bone matrix volume fraction is used to update the cell numbers according to the changes in the bone microstructure. We also calculate the redistribution of the internal stresses within the cortical cross-section due to the evolving bone matrix volume fraction using the theory of elasticity applied to nonuniform beams.

RESULTS AND DISCUSSION

Our numerical results indicate that bone loss is increased near the endocortical surface where bone specific surface is highest, and that this leads over time to a substantial overall reduction in the cortical wall width progressing from the endosteum towards the periosteum (Figure 1). The associated expansion of the medullary cavity can be made to match experimentally observed data from cross-sectional studies of the Melbourne Femur Collection [2]. Furthermore, the redistribution of the stresses in the cortical cross section is such that mechanical load is increasingly and disproportionnally carried by periosteal cortical bone.

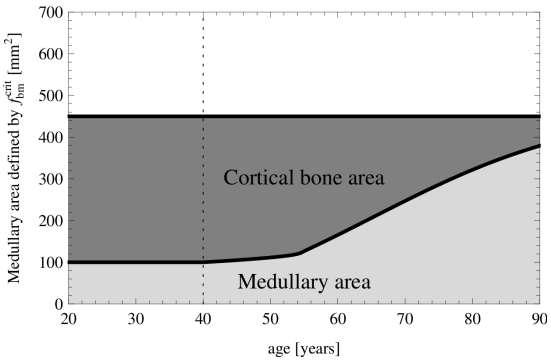

Figure 1: Evolution of the medullary area and cortical bone area over time after osteoporosis establishes at 40 years of age.

CONCLUSIONS

We conclude that the microscopic availability of bone surface within the tissue, needed for resorption and formation processes to occur, is potentially a significant factor in focal bone loss predominantly occuring near the endocotical wall in osteoporosis. Furthermore, the gradual redistribution of the internal stresses towards the periosteum is suggstive of the possibility to induce modelling responses at the periosteum.

REFERENCES

1. Martin RB, *CRC Crit. Rev. Biomed. Eng.*, **10**:179, 1984.
2. Feik SA, Thomas CDL, Clement JG, *J. Anat*. **191**:407, 1997

SESSION 2 - ABSTRACTS

Biomedical Engineering & Imaging (2)

DAY 2: Friday, 31 August

11:00 AM – 12:35 PM

QUANTITATIVE ANALYSIS OF COMPUTER NAVIGATION DATA BEFORE AND AFTER TOTAL KNEE ARTHROPLASTY

Corey Scholes[1], Sebastien Lustig[1], Joe Lynch[1], Bianca Albanese[1,2], David Parker[1]

[1]Sydney Orthopaedic Research Institute, Chatswood, NSW
[2]School of Aerospace, Mechanical and Mechatronic Engineering, The University of Sydney, NSW
email: cscholes@sori.com.au

INTRODUCTION

An advantage of navigation for TKA is real-time data provided by dynamic testing to assess range of motion and coronal laxity intraoperatively. To-date, there remains little guidance to the surgeon in applying these curves in an objective way. The purpose of this study was to investigate the effects of TKA on intraoperative knee laxity and balance assessed with computer navigation.

METHODS

A consecutive series of 200 patients were randomly selected from a prospective clinical database that underwent computer navigated TKA with the senior author using the Stryker PrecisioN system. TKA was performed in the standard fashion and the dynamic laxity of the knee assessed manually pre and post-procedure by moving the knee through the range of motion while applying varus and valgus stress to the joint. The surgical reports from the navigation system were stored electronically and the pre and post-procedure laxity curves extracted for further analysis. An image-processing toolbox in Matlab (Mathworks, USA) was used to apply an ellipse to the laxity curve and a range of measures were calculated. These comprised of the total area, the symmetry of the ellipse and the percentage of the curve in varus or valgus. Paired t-tests were used to detect differences between pre and post-TKA.

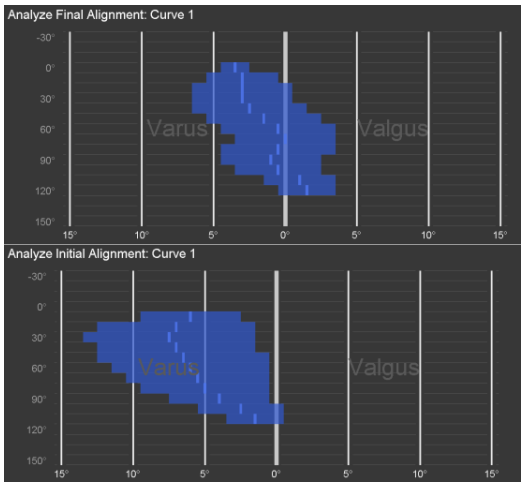

Figure 1. Initial alignment (top) and final alignment following arthroplasty (bottom) navigation curves generated by the Stryker PresisioN system.

RESULTS AND DISCUSSION

The method described provides objective information regarding dynamic knee laxity and balance previously inaccessible to the surgeon. Initial observations revealed that alignment at full extension did not fully represent the frontal alignment of the knee through the range of motion. In addition, the curves showed highly individual patterns with respect to their orientation, area and balancing between varus and valgus pre-operatively. Preliminary analysis revealed considerable between-patient variation in preoperative total curve area (CV 27%), curve symmetry (CV 76%) and the proportion of the curve in varus (CV 35%), which was not reduced by TKA. Importantly, the TKA significantly decreased ($p < 0.01$) the average total area of the laxity curve by 25% and the average proportion of the curve in varus (78.5% vs 65.1%, $p < 0.01$).

CONCLUSIONS

Navigation curve analysis provides objective data about dynamic knee laxity modifications related to total knee arthroplasty. This could enhance the knowledge about the implications of the procedure on knee balancing. A key limitation is that the association between navigation curves modifications and functional results remains unclear. Future work should explore links between these objective parameters and patient function.

CONFLICT OF INTEREST DECLARATION

In the interests of transparency and to help reviewers assess any potential bias, ANZORS requires authors of original research papers to declare any competing commercial interests in relation to the submitted work. Referees are also asked to indicate any potential conflict they might have reviewing a particular paper.

If you have accepted any support such as funds or materials, tangible or intangible, concerned with the research by the commercial party such as companies or investors, choose YES below, and state the relation between you and the commercial party.

If you have not accepted any support such as funds or materials, choose NO.

Do you have a conflict of interest to declare?

NO

SOFTWARE ANALYSIS OF FEMORAL CARTILAGE VOLUME AFTER MENISCAL SURGERY

Mark Kazzi[1,2], Corey Scholes[1], Joe Lynch[1], Ronnie Kapoor[3], Qing Li[2], Myles Coolican[1], David Parker[1]

[1]Sydney Orthopaedic Research Institute, Chatswood, NSW
[2]School of Aerospace, Mechanical and Mechatronic Engineering, The University of Sydney, NSW
[3]Macquarie Medical Imaging, North Ryde, NSW
email: cscholes@sori.com.au

INTRODUCTION

MRI offers a number of advantages over radiographs for the monitoring of knee cartilage changes. Software can be used to objectively quantify cartilage volume changes associated with osteoarthritis progression. Validity of such cartilage quantification software has been demonstrated [1, 2] however the reproducibility of cartilage volume analysis has not been well documented. This study aimed to assess the reproducibility of two different software packages across repeated measurements with respect to femoral cartilage volume.

METHODS

9 patients with previous meniscal surgery (age 25.5 +/- 10.3 years; BMI 25.57 +/- 5.1) undertook a 3T volumetric MRI of their affected knee with a T1 weighted fat suppressed sequence using 2mm slice thickness. Scans were semi-automatically segmented and three dimensional femoral cartilage volumes were calculated using ScanIP and 3D Slicer software packages (Figure 1). This analysis was then repeated to determine intra-observerreliability. Cartilage volumes calculated for the femoral condyles were compared between medial and lateral compartments, tests and software packages.

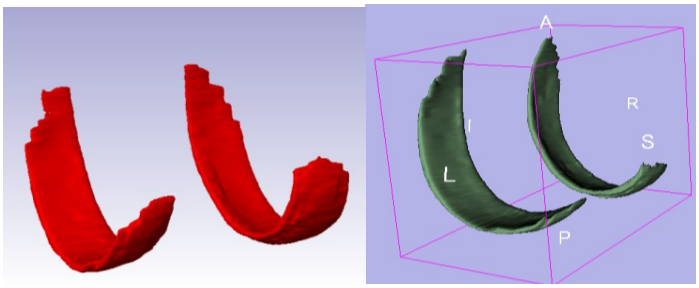

Figure 1. 3D Model generated using ScanIP (left) and 3D Slicer (right) of medial and lateral femoral cartilage.

RESULTS AND DISCUSSION

Results of the ANOVA showed no significant differences between test, compartment or software. Test-retest differences in cartilage volume for Scan-IP and 3D Slicer were 1.5% $\pm$0.6 and 1.8%$\pm$1.0 respectively. Inter-software reproducibility showed differences of 2.0% $\pm$1.6 for the medial femoral condyle, 3.2% $\pm$1.9 for the lateral condyle and 2.1 $\pm$1.2 overall.

CONCLUSIONS

Test-retest variation of femoral cartilage volume with the same software package was less than the differences between software packages. Nevertheless, the test-retest and inter-software variation were relatively high in this population when compared to the annual cartilage volume losses reported in the literature for healthy (3.1%/yr) and osteoarthritic (5-6%/yr) patients. Therefore, cartilage volume losses reported using these methods should be interpreted with caution. Further work is required to assess inter-observer reliability using the same software and explore ways of improving the reliability of quantifying cartilage volume. It is recommended that the test-retest variation be taken into account when planning the follow-up period between longitudinal measurements for monitoring cartilage volume changes.

REFERENCES

1. Peterfy C.G., et al., Radiology. **192**: 485-491. 1994
2. Cicuttini F., et al., Osteoarthritis and Cartilage, **7**: 265 271. 1999.

CONFLICT OF INTEREST DECLARATION

In the interests of transparency and to help reviewers assess any potential bias, ANZORS requires authors of original research papers to declare any competing commercial interests in relation to the submitted work. Referees are also asked to indicate any potential conflict they might have reviewing a particular paper.

If you have accepted any support such as funds or materials, tangible or intangible, concerned with the research by the commercial party such as companies or investors, choose YES below, and state the relation between you and the commercial party.

If you have not accepted any support such as funds or materials, choose NO.

Do you have a conflict of interest to declare?

NO

Changes in Core Suture Geometry within Repaired Flexor Tendons: an X-ray Evaluation

Peltz, TS; Haddad, R; Scougall, P; Nicklin, S; Hunt, J; Gianoutsos, M; Pelletier, M; Bertollo, N; Walsh, WR

University of New South Wales, Surgical & Orthopaedic Research Laboratories, Prince of Wales Hospital, Sydney, Australia
t.peltz@unsw.edu.au

INTRODUCTION:
Early mobilization of a repaired deep flexor tendon promotes better outcomes than immobilization. Tension on the reconstruction, however, produces gap formation at the repair site, which is detrimental. Much progress has been made in the optimization of repair techniques to minimize gapping. Notably, this has involved multi-strand techniques and the use of locking suture configurations. Nevertheless, the changes in the 3-dimensional suture geometry when the repair is strained, and the relationship this has to gap formation have not been fully characterized. Therefore, we present a X-ray technique to examine the three-dimensional changes in core suture configuration under tension.

METHODS:
40 adult sheep front limb deep flexor tendons were harvested and randomized into 4 repair groups of n=10 each. Tendons were cut at the long vinculum and a core suture performed in the proximal stump. The techniques used reflected a prevalent 2-strand and 4-strand method, using most commonly used grasping and locking variants of each. Namely, these repairs were the standard modified Kessler (figure 1); the conventional cruciate repair (figure 2); and the cross-locked cruciate repair (Adelaide repair) (figure 3). The final group was a novel technique we termed the "interlocked modification of the Adelaide repair" (figure 4). This involved an interlinking of the distal end of the locking-crosses in an Adelaide repair. 3-0 multifilament stainless steel wire (Ethicon. Sommerville, NJ) was used for all repairs. Anteroposterior (AP) and lateral X-rays were taken immediately after repair using a MX 20 Radiography system (Faxitron X-Ray. Lincolnshire, IL). The suture strands were then statically loaded to 35N and held at this tension for 60 seconds. X-rays of the tendon were repeated post-tensioning. A fixed length calibration device was included in the X-ray as a reference measure. Relative suture lengths within the tendon was measured before and after tensioning using ImageJ software (National Institute of Health).

RESULTS :
2-strand repairs (Figure 1)
Comparison of the AP images revealed considerable shortening of suture length within the tendon after loading. This is consistent with the formation of gap. One factor of the shortening was the significant narrowing ("bottle necking") of the tendon at the transverse suture component. However, this factor only contributed to part of the gapping tendency. We also witnessed a complete loss of the Kessler "pretzel" with transformation to a U-shaped configuration. The position of the transverse strand remained relatively constant.
Several changes were also apparent on the lateral films, including tendon buckling, and, more importantly a change in the angle of the exposed Kessler loop relative to the longitudinal axis of the tendon.

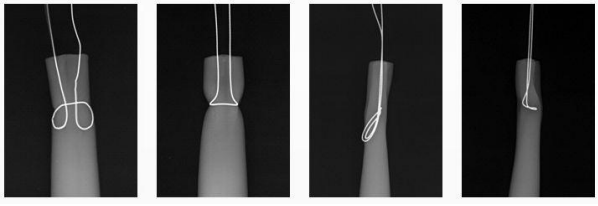

Figure 1

4-strand repairs (Figures 2/3/4)
In the cruciate repair significant cheese-wiring of the grasping loops was noted with a resultant propensity for repair site gap (Figure 2). In contrast, the cross-locking variants (Figure 3) tightened (locked) under tension and did cheese-wire much less. Changes were similar for both the standard and interlocking variants (Figure 4) of the Adelaide repair. In the lateral projections the flattening out of the cross-lock "pyramids" was more predominant in the standard Adelaide repair. A similar amount of buckling was noted for all 4-strand repair techniques. The relative length of suture elongation at the repair site was less for the Adelaide repairs compared to the loop-locking and 2-strand technique. The interlocked Adelaide repair showed least structural changes comparing pre tension X-rays to post tension X-rays.

DISCUSSION:
Several factors influence gap formation and these are intimately related to 3-dimensional changes in suture geometry. 2-strand grasping configurations like the Kessler technique not only allow great tendon constriction but also lose their three-dimensional configuration when tensioned. This results in elongation and therefore gapping. These effects are less observable in 4 strand configurations.
Cross locks, like used in an Adelaide repair stabilize the construct and prevent cheese wiring. The interlocked modification of the Adelaide technique showed least changes when put under tension.
This study looked at the core suture in isolation to exaggerate the geometric effects. No comment on in vivo performance can be made.

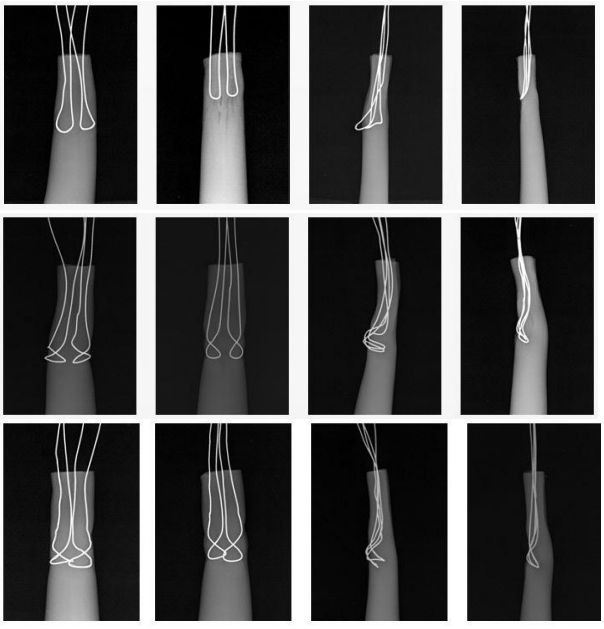

Figures 2,3,4

Conclusion:
X-ray is a useful method of investigating suture configuration changes in biomechanical experiments. This evaluation provides a valuable new insight into the behavior of prevalent flexor tendon repair constructs.

3D INTRAOSSEOUS MICRO-ARCHITECTURE OF NORMAL AND AVASCULAR LUNATES (KIENBÖCK'S)

[1]Stephanie CM Low, [1,2]Gregory I Bain, [1]David M Findlay, [1]Kevin Eng, and [3,2]Egon Perilli

[1]Department of Orthopaedic Surgery, Royal Adelaide Hospital, The University of Adelaide, South Australia, Australia
[2]Department of Anatomy and Pathology, School of Medical Sciences, The University of Adelaide, SA
[3]Medical Device Research Institute, School of Computer Science, Engineering and Mathematics, Flinders University, SA
email: stephanie.low@adelaide.edu.au

INTRODUCTION

Kienböck's disease is spontaneous lunate bone osteonecrosis, which presents with symptoms of pain and poor wrist function, ultimately leading to collapse and fracture of the lunate[1]. The etiology is poorly understood, and studies in the literature are limited[1,2,3]. The aim of this ongoing study was to characterize the internal micro-architecture of lunates with Kienböck's disease in 2D and 3D, using high-resolution micro-computed tomography (micro-CT) and histology, and to compare it with normal lunates[2,3].

METHODS

Three patients with Kienböck's disease were consented pre-operatively for donation of their lunates to be used in research. Lunates were surgically excised and examined by high-resolution micro-CT (17.4µm pixel size, Skyscan 1076). For the normal group, three non-avascular lunates from three cadavers were excised and examined.

The bone micro-architecture of the lunates was reviewed by means of 2D and 3D micro-CT images. For quantitative morphometric analysis, a cylindrical micro-CT volume of interest containing trabecular bone was chosen (length 3mm, diameter 3mm), and 3D morphometric parameters calculated: trabecular bone volume fraction (BV/TV), trabecular thickness (Tb.Th), trabecular number (Tb.N), trabecular separation (Tb.Sp). To test for changes in morphometric values between Kienböck's and normal lunates, a t-test was done. The significance level was set to $p = 0.05$. The pathological lunates were then decalcified and coronally sectioned, for H&E histological staining.

RESULTS AND DISCUSSION

Visual description of the internal micro-architecture: normal lunates exhibited a distal subchondral plate, characterized by a trabecular bone layer parallel to the articular surface, and connected to it by beam-like structures. Below the subchondral plate, the trabeculae were consistently arranged in a radial pattern, linking the proximal and distal articular surfaces. In the Kienböck's lunates, the bone was fragmented, most extensive toward the proximal pole. Subchondral collapse was evident, with destruction of the subchondral plate. There was absence of the radial pattern of the trabeculae as seen in normal lunates, with regions of trabecular bone interspersed by regions devoid of bone. Those regions containing trabecular bone appeared to have more dense bone, than in normal lunates (Fig.1).

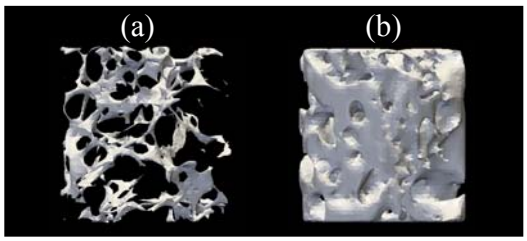

Figure 1: 3D micro-CT images, trabecular bone of (a) normal and (b) Kienböck's lunate. Cylindrical volume (L=D=3 mm).

Morphometric analysis of the trabecular bone showed that Kienböck's lunates had increased bone volume fraction, trabecular thickness and trabecular number, and decreased trabecular separation, compared to normal ($p<0.05$, Tab.1).

Table 1. Trabecular bone morphometry (mean±SD).

	Normal	Kienböck	t-test
BV/TV (%)	10.5±1.4	45.3±13.9	$p<0.05$
Tb.Th (µm)	185±35	359±80	$p<0.05$
Tb.N (1/mm)	0.59±0.17	1.24±0.13	$p<0.01$
Tb.Sp (µm)	765±90	475±41	$p<0.05$

In histological analysis, Kienböck's lunates showed a pattern similar to a healing fracture. Histology slides showed necrotic bone interspersed amongst areas of attempted healing, with immature osteoid and woven bone present. Large bone areas were replaced by fibrous tissue, likely representing scarring.

CONCLUSIONS

This ongoing study illustrates that lunate bone 3D micro-architecture exhibits design features typical of structures aimed at distributing loads of weight-bearing surfaces. Notwithstanding the small sample size, the micro-architecture of Kienböck's lunates is different from normal, with absence of the radial arrangement of the trabeculae compared to normals, showing locally significantly increased bone volume fraction, trabecular thickness and number. Histology showed similarities with a healing fracture. Characterisation of the changes will allow advances in treatment modalities and management techniques of avascular lunates.

REFERENCES

1. Dias JJ, et al., *JHS (E)* **35E (7)**:538 - 543, 2010.
2. Owers KL, et al., *JHS (E)* **35E (2)**:120 - 124, 2010.
3. Han K-J, et al., *JHS (E)* **0 (00)**:1 - 6, 2011.

EFFECT OF IRRADIATION ON ALLOGRAFT IN A SHEEP MODEL OF FEMORAL IMPACTION GRAFTING

[1]Stuart A Callary, [2]John R Field, [3]John J Costi, [3]Richard M Stanley, [1]Roumen Stamenkov, [1]Lucian B Solomon, [4]David Campbell
[1]Margaret A McGee, [1]Donald W Howie

[1]Department of Orthopaedics & Trauma, Royal Adelaide Hospital, Discipline of Orthopaedics & Trauma, University of Adelaide, SA ; [2]Comparative Orthopaedic Research (CORe) Facility, Flinders University, SA; [3]Biomechanics & Implants Research Group, The Medical Device Research Institute, Flinders University, SA; [4]Wakefield Orthopaedic Clinic, SA
email: stuart.callary@health.sa.gov.au

INTRODUCTION

Femoral impaction bone grafting (FIBG) at revision hip replacement is used to restore bone by impacting allograft bone in the femur prior to stem implantation. Initial clinical studies, including those using irradiated bone, had early failures characterised by gross progressive subsidence of the stem. Results using fresh frozen allograft bone are excellent, however the use of non-irradiated bone remains a risk for disease transmission. Australian bone banks have reduced irradiation dose from 25kGy to 15kGy as this dose has been shown to achieve an acceptable sterility assurance level. *In-vitro studies* have shown that bone irradiated at 15kGy does not compromise its mechanical and impaction properties, remodelling potential and pro-inflammatory activity. The aim of this study was to extend the *in-vitro* studies by investigating whether 15kGy radiation of bone affects its bioincorporation and thus the mechanical stability of the femoral stem in a clinically relevant *in-vivo* model of FIBG.

METHODS

Fourteen merino whether sheep underwent FIBG with a cemented double taper stem and morsellised allograft bone which was either non-irradiated (control) or irradiated at 15kGy. Radiostereometric analysis (RSA, precision±0.06mm) immediately post-operatively and at 2, 4, 6, 10 and 14 weeks was used to quantify subsidence of the stem, measured as cement displacement relative to femoral bone. Stem stability was defined as no progressive subsidence at the cement-bone (c-b) interface and stem micromotion of less than 50 microns. Tri-axial (medio-lateral, antero-posterior and supero-inferior (SI)) micro-motion (precision±0.01mm) of the proximal-lateral stem relative to the bone was measured in an Instron mechanical testing machine after applying cyclic loads to 40% of bodyweight. Undecalcified ground sections of the femur at the proximal, mid and distal levels of the stem were prepared. Bone graft incorporation and was assessed histologically.

RESULTS AND DISCUSSION

There were four exclusions, 2 for hip dislocation (1 control, 1 irradiated), one for periprosthetic fracture (irradiated) and one for an undersized femur (control). Five femurs in each group were retrieved for analysis at 14 weeks.

Stem Subsidence: There was no difference in subsidence at the c-b interface between the control group (mean±SD 1.32±1.55mm, median 0.62mm) and the irradiated group (2.27±2.26mm, median 1.41mm) (p=0.55) (Figure 1). The majority of subsidence occurred within the first 2 to 4 weeks post-operatively and then stabilised. In 2 (irradiated group) of the 3 hips with subsidence greater than 1mm by two weeks a healed cortical fracture, was observed histologically.

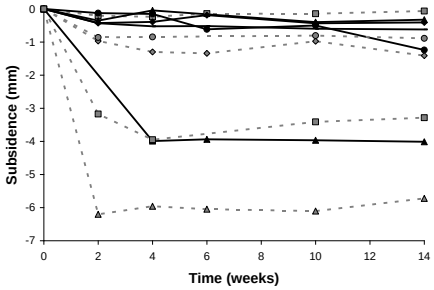

Figure 1: Subsidence at the cement-bone interface by animal (black line = non irradiated, grey dashed line = irradiated)

Stem micromotion: All stems tested were stable, with micromotion of less than 50 µm in each of axis (SI-axis: non-irradiated 5±24µm irradiated 13±43µm).

Bone graft incorporation: At 14 weeks, non-irradiated and irradiated allograft bone was incorporated with new bone tissue. For most femurs, incorporation was advanced at the proximal and mid levels of the stem, with trabeculation of the new bone and mature marrow interstitial tissue (Figure 2). Distally, there was active incorporation of the allograft bone. There was an absence of fibrous tissue at the cement-bone interface consistent with a stable stem-cement-bone complex.

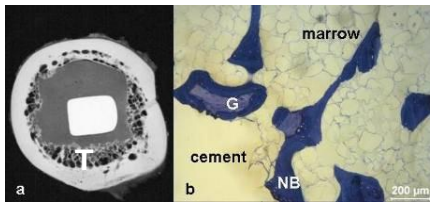

Figure 2: a) Contact radiograph and b) photomicrograph of mid-stem section (irradiated) showing incorporation by new bone (NB) and trabeculation (T) of bone graft (G)

CONCLUSIONS

The histological findings confirm the *in-vivo* RSA and *ex-vivo* mechanical testing results that stable fixation of the femoral stem after FIBG is achieved when using non-irradiated allograft bone or bone irradiated at 15kGy. Using a clinically relevant model, the conclusion from the prior *in-vitro* studies that 15kGy irradiation does not influence the biomechanical properties of morsellised bone graft for FIBG is supported. Further outlier analysis and histoquantitation is required.

ACKNOWLEDGEMENTS

This study was funded by the National Health and Medical Research Council Grant ID 453624.

BIOMECHANICAL ASSESSMENT OF SEGMENTAL BONE DEFECT REPAIR USING IMPACTION BONE GRAFTING

[1]John J Costi, [1]Richard M Stanley, [2]Boyin Ding and [3]Lucian B Solomon

[1]Biomechanics & Implants Research Group, The Medical Device Research Institute, School of Computer Science, Engineering and Mathematics, Flinders University, SA
[2]School of Mechanical Engineering, The University of Adelaide, SA
[3]Department of Orthopaedics and Trauma, Royal Adelaide Hospital, SA
email: john.costi@flinders.edu.au

INTRODUCTION

Bone allograft is used to facilitate the healing of fracture nonunion with segmental defects. However initial construct stability is poor until bone healing is achieved, which may take between 3-12 months [1] and even longer in complicated cases, accompanied with a significant cost burden to society [2]. The aim of this study was to compare initial stability of impaction bone grafting in a segmental defect to intramedullary nailing of a transverse mid-diaphyseal fracture.

METHODS

Seven sheep tibiae underwent biomechanical testing in compression (1000 N), bending and torsion (6 Nm) in a six degree-of-freedom hexapod robot. Each tibia underwent the same tests across three sequential groups: control (Group 1 - Intact), mid-diaphyseal transverse fracture stabilized by intramedullary nailing (Group 2 - Fracture), segmental defect stabilized with a nail and impacted bone graft in a compliant mesh (Group 3 - Defect). Stiffness was calculated for all tests in each group and normalised as a fraction of the intact tibia. Repeated measures ANOVA were conducted for each loading direction with significant differences accepted when $p<0.05$.

RESULTS AND DISCUSSION

Statistical analyses for normalised stiffness between each group revealed that the overall effect of Group was significant for all directions of loading (Figure 1, $p<0.028$). For compression, pairwise comparisons revealed that Group 1 was significantly different to Group 3 ($p = 0.044$), no significant differences were present between Groups 1 and 2 ($p = 0.225$, power = 0.62), and between Groups 2 and 3 ($p = 0.205$, power = 0.09). The difference between groups that could have been detected, to have a power of 0.8 (i.e. 80%) with the present sample size and assuming the standard deviations did not change was 24%. Pairwise comparisons between groups for bending and torsion (both left and right rotation) revealed significant differences between Groups 1 and 2, and Groups 1 and 3 ($p<0.010$), with no significant differences existing between Groups 2 and 3 ($p=1$, power ranged from 0.02-0.06 across the three test directions). The difference between groups that could have been detected, to have a power of 80% with the present sample size and assuming the standard deviations did not change ranged from 11-23% across the three test directions.

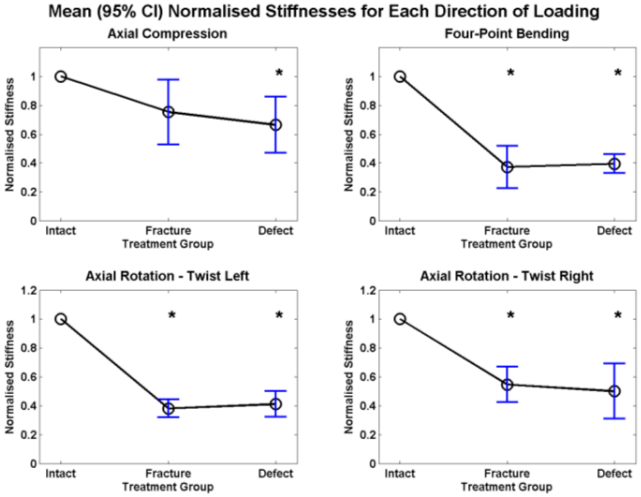

Figure 1: Mean (95% CI) stiffnesses expressed as a fraction of the intact tibia (normalised) for each direction of loading. Significant differences compared to the Intact group are denoted by *.

CONCLUSIONS

These results are encouraging in translating the technique of impaction bone grafting into the treatment of posttraumatic human long bone segmental defects that are known not only to be difficult to treat, but also require lengthy treatment time and significant patient compliance.

ACKNOWLEDGEMENTS

The authors would like to thank Associate Professor John R Field, Comparative Orthopaedic Research Surgical Facility, School of Medicine, Flinders University for providing the sheep tibiae, bone graft and intramedullary nails and surgical instrumentation. The authors would also like to thank Mr Isaac Lawless and Mr Nathan Hill from the School of Computer Science, Engineering and Mathematics, Flinders University for their assistance with the biomechanical testing.

REFERENCES

1. Coles CP and Gross M, *Can J Surg.* **43 (4)**:256-62, 2000.
2. Kanakaris NK and Giannoudis PV. *Injury* **38 (Suppl 2)**: S77-84, 2007

PROGRESS AND CHALLENGES IN MINERALIZED TISSUE ENGINEERING

[1]P.C. Yelick*, [1]W. Zhang, [1]Andreeva, V., [1]E. Smith, [2]S. Sant, G. [2]Camaci-Unal, [1]C. Stewart-Swift and [2]A. Khademhosseini

[1]Department of Oral and Maxillofacial Pathology, Division of Craniofacial and Molecular Genetics, Tufts University, Boston MA; [2]Harvard-MIT Division of Health Sciences and Technology, Brigham and Women's Hospital, Harvard Medical School, Boston MA
E-mail: pamela.yelick@tufts.edu

INTRODUCTION

Our research works to elucidate molecular pathways regulating mineralized tissue development, homeostasis, disease and regeneration. Our models include: 1) three dimensional tissue engineering bone and tooth models; and 2) the zebrafish as a model for the discovery and functional characterization of genes regulating mineralized tissue development, disease and regeneration.

METHODS

Our research has examined the utility of synthetic PGA/PLGA scaffolds as well as natural collagen, fibrin and GelMA scaffolds for dental and bone tissue engineering. We have also used a forward genetic chemical mutagenesis screening approach to identify adult mineralized tissue zebrafish mutants as models for viable human mineralized tissue disease.

RESULTS

Our results have identified a number of scaffold materials that show promise for dental tissue and bone regeneration. We have also identified a variety of zebrafish mineralized tissue mutants as potentially informative models for human mineralized tooth and bone diseases.

DISCUSSION

The novel combined use of zebrafish and tissue engineering models is a powerful approach to identify novel signals regulating mineralized tissue development and regeneration.

CONCLUSIONS

We anticipate that this approach will identify novel signals that can be used to facilitate tooth and bone regeneration in humans.

ACKNOWLEDGEMENTS

This research was supported by NIH/NIDCR/NIBIB grant R01DE016132 (PCY) and NIH/NIDCR grant R01DE018043 (PCY).

REFERENCES

1. Traphagen et al., 2012 Biomaterials 33:5287-96.
2. Duailibi et al., 2011 Artif Organs 35:1525-1594.
3. Zhang et al., 2011 J Biomed mater Res 97:414-22.
4. Andreeva et al., 2011 Genesis 49:360-6.
5. Lin et al., 2011 J Dent Res 90:251-6.
6. Zhang et al., 2010 Biomaterials 31:7995-8003.
7. Young et al., 2002 J Dent Res 81:695-700.

THORACIC SPINE MORPHOLOGY COMPARISON OF A NOVEL ANIMAL MODEL

James Peters BS [1], Lucy Robinson PhD [2], Richard Kent PhD [3], Sriram Balasubramanian PhD [1]

[1] School of Biomedical Engineering, Science and Health Systems, Drexel University, Philadelphia, PA
[2] School of Public Health, Drexel University, Philadelphia, PA
[3] Center for Applied Biomechanics, University of Virginia, Charlottesville, VA

INTRODUCTION

Large quadruped mammals are commonly used to simulate the human spine *in vitro*, and much literature is available on the morphological comparison between human and quadruped spine. However, these models ignore factors such as loading condition, range of motion, and associated ligamentous structures that contribute to the structure and stability of the spine. Also, no current quadruped model can be shown to accurately mimic the upright biomechanical function of the erect human spine.

Based on similarities in posture and loading, the kangaroo may be better suited as a model for the human thoracic spine. As a first step in validating this novel animal model, thoracic spine geometry of the kangaroo was quantified and compared with data available in the literature on the human, pig, sheep, and deer [1-6].

METHODS

Whole body computed tomography (CT) scans were obtained from 10 juvenile kangaroos (ages 11-14 months) post-mortem. The thoracic vertebrae were digitally reconstructed (Mimics, Materialise Inc., Belgium) and the height, width and depth of the vertebral bodies (VB), intervertebral discs (ID), endplates (EP), spinal canal (SC), and spinous (SP) and transverse processes (TP) were computed as well as inter-facet (IF) dimensions at each vertebral level and compared to data available in the literature on the sheep, pig, deer, and human. A Spearman Rho's correlation test (Table 1) was used to assess similarities in trend between the animal and human data.

RESULTS AND DISCUSSION

Trend comparisons were conducted by minimizing the sums of squared errors between the human and animal data sets for each parameter. By minimizing the error, correlation values could be evaluated based solely on the greatest amount of overlap between the human and each animal model. Linear offsets and scaling factors resulting from differences in age, height, weight, and gender which have not been considered in previous studies were taken into account through the use of this method. Human data were obtained from adults, 18 years of age or older, while data for all animals except the deer were taken from specimens of less than two years of age. Therefore, a trend analysis may provide more insight into the compatibility of each animal model with the human.

TABLE 1. Spearman's Rho Correlations: Animal Data Compared With Human.

	Pig	*Sheep*	*Deer*	*Kangaroo*
VB^H_a	.907**	.752**	-.409	.879**
VB^H_p	.993**	.594*	-.445	.972**
EP^W_s	.828**	.621*	0.067	.842**
EP^W_i	.967**	0.414	0.452	.967**
EP^D_s	.754**	-.250	-.888**	.993**
EP^D_i	.942**	-.870**	-0.469	.998**
PD^H_r	.928**	n/a	0.172	.900**
PD^H_l	.903**	n/a	0.267	.849**
PD^W_r	0.472	n/a	0.397	.872**
PD^W_l	0.524	n/a	0.361	.907**
SC^W	.928**	-.573	0.172	.900**
SC^D	0.304	0.364	0.241	-.246
SP^L	0.525	n/a	.697*	0.49
SP^A	.958**	n/a	.888**	.846**
TP^W	.664*	n/a	0.394	0.13
IF^H_r	n/a	n/a	n/a	.944**
IF^W_s	n/a	n/a	.662*	.933**
IF^W_i	n/a	n/a	n/a	.905**
ID^H	-.615*	n/a	.735*	.834**

Height (H), width (W), depth (D), length (L), angle (A), anterior (a), posterior (p), superior (s), inferior (i), right (r), left (l), not available (n/a). * ($\rho \leq 0.05$), ** ($\rho \leq 0.01$)

CONCLUSIONS

Thoracic spine morphology trends of the kangaroo are more similar to the human than those of other quadruped animal models. In the biological sense, form often defines function. This limits the amount of beneficial information that may be gained from the use of a quadruped as a model for the human. Based on these results presented here and the biomechanical compatibility of the pseudo-biped and biped spines the kangaroo may provide a better model for human thoracic column.

REFERENCES

1. Bozukus, H., *Surg Endosc* **19**: p 1652-1665. 2005
2. Busscher, I., *Eur Spine J* **19**: p 1104-1114. 2010
3. Hasler, C., *SPINE* **35**(23): p E1262-E1272. 2010
4. Kumar, N., *The Anatomical Record* **260**: p 189-203. 2000
5. Panjabi, M.M., *SPINE* **16**(8): p 888-901. 1991
6. Panjabi, M.M., *SPINE* **18**(10): p 1298-1310. 1993

SESSION 3 - ABSTRACTS

Clinical Orthopaedics & Kinematics

DAY 2: Friday, 31 August

1:20 PM – 2:40 PM

Feasibility Evaluation of the Microsoft Kinect as a Low Cost Alternative to Motion Capture Systems

[1]Hossein Mokhtarzadeh, [2]Amber Emmens, [1]Peter Vee Sin Lee and [1]Denny Oetomo

[1]Department of Mechanical Engineering, the University of Melbourne, Australia
[2]Mechanical Engineering, Faculty of Engineering Technology, University of Twente, the Netherlands
Email: mokhtarzadeh.hossein@gmail.com

INTRODUCTION

Motion capture systems are widely used in biomechanical studies to collect marker position data from anatomical landmarks with high accuracy. Their results are used to estimate joint moments and muscle forces where external loads are available. The system benefits from high accuracy and precision of about 0.2cm, however, they are costly and the set up and the post-processing procedure are time consuming [1]. On the other hand, the recently released Microsoft Kinect sensor for the Xbox is able to detect motions with lower depth accuracy (a few mm up to ~4cm at maximum sensor range) [2], but it requires minimum setup procedure while joint kinematics could be obtained in real-time. Kinect is also cost effective (~$200 for a Kinect vs. >$80K for 8-camera Vicon) and is capable of collecting data with up to 30Hz sampling frequency, which is sufficient for normal gait analysis. In this study, we present the comparison of Kinect and Vicon performance, with the aim of providing a low cost alternative with quick processing to the motion capture facility. The joint motion data was then imported to a musculoskeletal model in OpenSim [3] to calculate the joint moments and muscles forces.

METHODS

Two simple movements were performed by a male participant (age 73, height 174cm and 85.5kg): Arm movement and knee flexion/extension. An OpenNI framework was used to develop a platform with PrimeSense NITE middleware. These software packages helped us to do skeleton tracking. Fifteen joint positions were obtained using OpenNI. All the data captured by Kinect were imported into Matlab for post processing. In the meantime, the same arm and leg movements were collected using Vicon (Oxford, UK) with 38 marker sets placed on anatomical landmarks at 120 Hz. Joint angles data from the Kinect and the Vicon systems were fed as inputs to OpenSim (open-source software for analyzing musculoskeletal models, SimTK). After scaling the model based on marker positions, the inverse kinematics and inverse dynamics were executed in OpenSim to predict joint motions measured in the experiments and joint moments based on the kinematic data. The Residual Reduction Algorithm was also utilized to generate dynamically consistent model for further analysis, such as the static optimization to obtain muscle forces.

RESULTS AND DISCUSSION

Elbow joint flexion angles resulted from Kinect data were found to be in good agreement with the ones obtained from the Vicon measurement. However, large differences in joint angles were noticed at the beginning of movements (Fig 1). An absolute mean difference of 10° in the entire trajectory was obtained. One possible explanation is that there were mismatch between marker positions between OpenNI and Vicon. Vicon detects marker positions on bony landmarks and a large number of markers help produce accurate joint centers, whereas OpenNI obtained joint centers based on 15 virtual markers. More accurate joint motions could be obtained if the number of Kinect devices would increase. This would allow us to define joint centers close to the in vivo experiments. Net joint torques was found to be in good agreement in either methods (<1Nm at peak elbow torque). The discrepancies may come from the inaccuracy in evaluating joint centers in either methods as well as lack of unique scaling method. Scaling the arms could alter not only the joint motion but also the net torques at each joint. Although only one subject was used in the comparison study, the feasibility of using this technique in Kinect has been found to show tremendous potential. Future studies should focus on accuracy of the models, adding ground reaction forces, and finding individual muscle forces.

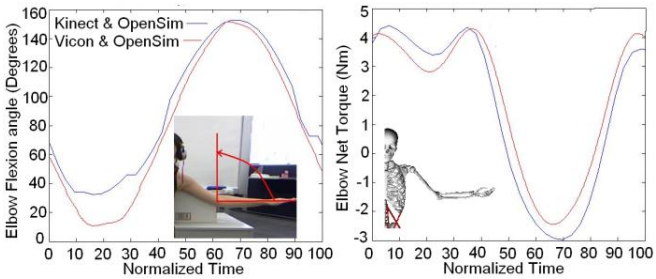

Figure 1: A representative of elbow flexion angle (left) and net elbow torque (right) comparison between Kinect and Vicon measurement in OpenSim

CONCLUSIONS

A good agreement was observed between Vicon and Kinect data using OpenSim musculoskeletal model. However, there are still challenges to overcome including multi-plane measurements, workplace coverage, sampling rate and depth accuracy of the Kinect results. Our findings suggest that combination of Kinect and musculoskeletal modeling is possible. Also, these low-cost and accessible tools will find tremendous potential among clinicians, and sport scientists.

REFERENCES

1. Richards, J.G., *Human Movement Sci* 18, 589-602, 1999
2. Khoshelham, K., et al., *Sensors.* 12, 1437-1454, 2012
3. Delp, S.L., *et al., IEEE T. Biomed Eng.* 54, 1940-50, 2007

RADIOSTEREOMETRIC ANALYSIS (RSA) OF THE MIGRATION OF THE TRABECULAR METAL ACETABULAR REVISION SYSTEM (TMARS) FOR SEVERE BONE LOSS AT REVISION TOTAL HIP REPLACEMENT (THR)

John M Abrahams, Lucian B Solomon, Stuart A Callary, Susan Neale, Roumen Stamenkov, Susan Pannach, Donald W Howie

Department of Orthopaedics and Trauma, Royal Adelaide Hospital and
Discipline of Orthopaedics and Trauma, University of Adelaide, Adelaide

INTRODUCTION

The Trabecular-Metal Acetabular Revision System (TMARS) is used for acetabular reconstruction in hips with extensive bone loss at revision surgery. The TMARS includes a trabecular-metal (TM) acetabular component with or without an augment and/or cage. Stability of the TM system in-vivo has only been determined using relative insensitive manual radiographic techniques. Radiostereometric analysis (RSA) is a more accurate computer-assisted method that can only be performed prospectively. In two previous studies where manual techniques were used it was reported that the TM system achieved good stability, defined as a migration of less than 6 mm on plain radiographs [1,2]. This study aimed to i) measure the migration of the TM system in a prospective cohort and ii) relate migration data to clinical outcomes.

METHOD

Between 2003 and 2011, the TM system was used selectively at revision hip replacement in 21 hips (21 patients) with severe acetabular bone deficiency (Fig 1). The Paprosky grade of acetabular bone deficiency at revision [3] was 2B in 1 hip, 3A in 3 hips and 3B in 17 hips (81%). The reconstructions included a TM acetabular component alone in 7 hips; an additional augment in 9 hips; an additional cage in 3 hips and an augment and cage in 2 hips. Tantalum markers were implanted intraoperatively to allow RSA analysis.

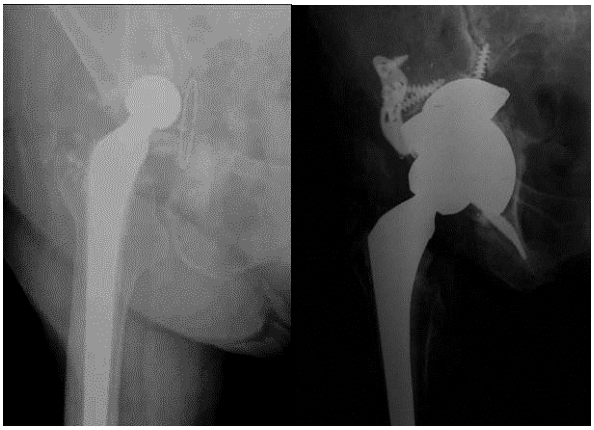

Figure 1 – Pre- (a) and post-revision (b) of a patient treated with a TM acetabular component with an augment and cage.

Two dimensional migration of the TM acetabular component was calculated as the vectorial sum of medial and superior migration and measured by RSA at three and/or six and 12 months, and at each follow-up thereafter. Reoperations were documented and patients were assessed clinically. The median follow-up to reoperation or latest follow-up was 3.5 years, range 1 – 7 years.

RESULTS & DISCUSSION

The migration of the TM system over time, as determined using the RSA analysis technique, is presented in Figure 2.

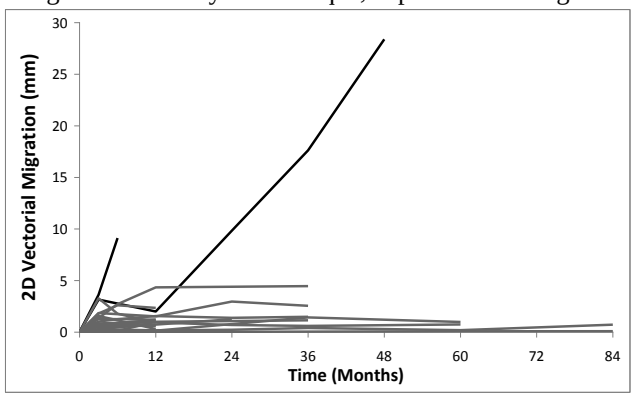

Figure 2 – The 2D Migration for each individual in all four groups. The two individuals highlighted had continuing migration and were revised.

Two acetabular components from the TM and augment group migrated 3.6mm and 3.2 mm respectively at three month and then progressed to 9.1 mm and 28.4 mm respectively at one and 3.5 years. These cases were symptomatic and subsequently revised.

One acetabular component, from the TM and cage group migrated 2.7mm at 6 months, progress to 4.3 at 1 year and remained asymptomatic with a migration of 4.5mm at three years. The remainder of the components from all groups had a median migration at the last follow-up of 0.8mm (range 0.2 – 2.5mm).

CONCLUSION

Using the sensitive technique of RSA, we have shown that the majority of TM components are stable at early follow-up. Early migration of TM reconstructions of severe acetabular defects, exceeding 3 mm in the first three months, are indicative of continuing migration and ongoing symptoms leading to revision surgery.

REFERENCES:

1. Sporer SM, et al., J Arthroplasty. **21**: 83-86, 2005.
2. Del Gazio DJ, et al., Clin Ortho Rel Research. **470**: 395-401, 2012.
3. Paprosky, et al., J Arthroplasty. **9**: 33 – 44, 1994.

A *EX VIVO* METHOD TO ASSESS THE INFLUENCE OF LUNATE MORPHOLOGY ON CARPAL KINEMATICS

[1]Dominic Thewlis, [1]Francois Fraysse, [2]Kevin Eng, [2,3]Greg Bain, [4]Richard Stanley, [5]Boyin Ding and [4]John J Costi
[1]School of Health Sciences, University of South Australia, Adelaide, SA
[2]Department of Orthopaedics and Trauma, Modbury Public Hospital, South Australia, Australia, SA
[3]Department of Orthopedics and Traumatology, University of Adelaide, South Australia, Australia, SA
[4]Biomechanics & Implants Research Group, The Medical Device Research Institute, School of Computer Science, Engineering and Mathematics, Flinders University, SA
[5]School of Mechanical Engineering, The University of Adelaide, South Australia, SA
email: dominic.thewlis@unisa.edu.au

INTRODUCTION

The lunate has been shown to have two distinct morphologies. The type II lunate, present in 70% of the population, is characterised by an extra articular surface with the hamate and an increased incidence of arthrosis [1]. Measuring the complex kinematic interactions of the carpal bones is impossible when using surface markers. The small carpal articulations have either been lumped into a single joint or studied using static imaging methods [2]. *Ex vivo* assessment allows measuring motion instead of static positions; however, many of the previous experiments have tested specimens through a non-physiological range of motion [3]. Therefore, the aim of this study was to develop an *ex vivo* method to quantify inter-carpal kinematics through a physiological range.

METHODS

In order to define the physiological range of the wrist during a functional activity, we recruited 21 participants who were free of wrist pathology or pain. The participants were required to perform a hammering task for 45 cycles at a frequency of 1 Hz, which was designed to simulate a common functional movement through the 'dart thrower's arc'. The kinematics of the hand and forearm were captured using a 12-camera Optitrack V100:R2 system (NaturalPoint, USA) at 100 Hz. The mean wrist joint angles were calculated for the population (Figure 1) assuming 3 rotational degrees of freedom (DoFs) with the joint centre located at the midpoint between the capitate and lunate.

Eight upper extremity specimens were obtained from fresh frozen cadavers. The eight specimens were identified as type I or II wrists based on lunate morphology. In preparation for the *ex vivo* testing, all specimens were prepared at the Ray Last Anatomy labs. Custom built clusters of markers affixed to 1.6 mm k-wires were inserted into the radius, ulna, scaphoid, lunate, triquetrum, capitate and third metacarpal. The location of the wire placement was checked under x-ray. The specimens were then CT scanned prior to refreezing. The CT scans were then reconstructed into a 3D model of the wrist using ScanIP (Simpleware, UK). From the 3D model the principal axes of inertia were calculated and used to define the local coordinate systems for the carpal bones. The specimens were then transported to Flinders University and fixed in a six DoF hexapod robot designed for biomechanical testing. The average motion from the collected in vivo data was reproduced on the specimens by the hexapod robot. Simultaneously, bone pins motions were recorded using the Optitrack system. The motion of the pins combined with the CT data allowed to reconstruct the motions of the carpal bones during the reproduced hammering task.

RESULTS AND DISCUSSION

We have developed a method that uses physiological motion from a functional task to move the wrist through a range of motion. Data collection and processing is still on going with the anticipation of completing this process by mid July 2012.

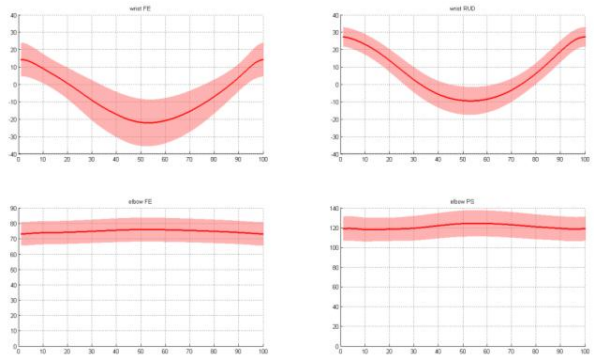

Figure 1: The wrist joint kinematics used in combination with the CT scans to develop the hexapod control file (mean±1SD).

ACKNOWLEDGEMENTS

Modbury Hospital Foundation and Arthritis Australia

REFERENCES

1. Viegas, S.F. *J Arthroscopic & Rel Surg*. 6:5-10, 1990
2. Haasse, S.C et al. *J Hand Surg Am.* 32:1009-1012, 2007
3. Werner, F.W et al. *J Hand Surg Am.* 29:418-422, 2004

Unsatisfactory accuracy with VISIONAIRE patient-specific cutting jigs for Total Knee Arthroplasty

Sébastien Lustig[1], Corey Scholes[1], Sam Oussedik[1], Vera Kinzel[1], Myles Coolican[1], David Parker[1]

[1]Sydney Orthopaedic Research Institute, Chatswood, NSW
email: cscholes@sori.com.au

INTRODUCTION

Patient-matched instrumentation is advocated as the latest development in arthroplasty surgery [1]. Custom-made cutting blocks created from preoperative MRI scans have been proposed to achieve perfect alignment of the lower limb in total knee arthroplasty (TKA) [2]. The aim of this study was to determine the efficacy of patient-specific cutting blocks by comparing them to navigation, the current gold standard.

METHODS

60 TKA patients were recruited to undergo their surgery guided by Zimmer PSI cutting blocks. Continuous computer navigation was used during the surgery to evaluate the accuracy of the cutting blocks. The blocks were assessed for the fit to the articular surface, as well as alignment in the coronal and sagittal planes, sizing and resection depth. Actual postoperative alignment was then assessed by detailed CT scans following the Perth protocol, comparing the results with intraoperative measurements.

.

RESULTS AND DISCUSSION

All patient-matched cutting blocks were a good fit intra-operatively. Analysis detected significant differences between the planned alignment and the alignment verified intraoperatively with navigation for femoral frontal alignment (0.9 ± 1.0, $p < 0.01$), femoral flexion (1.5 ± 1.2, $p < 0.01$) and femoral rotation (2.8 ± 3.5, $p < 0.01$). In contrast, tibial frontal alignment was not significantly different to the plan ($p = 0.87$), while the slope differed by 1.9° (±1.6, $p < 0.01$).

The cutting blocks would have placed 79.3% of the sample within ±3° of neutral in the coronal plane (Figure 1), while the rotational and sagittal alignment results within ±3° were 77.2% and 54.5% respectively.

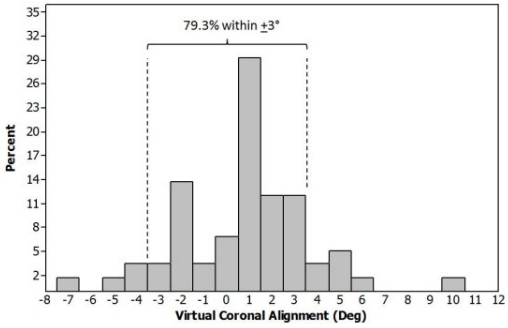

Figure 1. Total coronal alignment: when the femoral and tibial alignments were summed to produce a virtual limb alignment, the PSCB would have placed 79.3% of the sample within ±3°.

CONCLUSIONS

This study suggests the use of patient-matched cutting blocks is not accurate, particularly in the guidance of the femoral alignment in total knee arthroplasty. Despite this technique creating well-fitting cutting blocks, intraoperative monitoring with computer navigation revealed an unacceptable degree of potential limb mal-alignment, resulting in increased outliers particularly when compared with standard computer navigation.

REFERENCES

1. Lombardi A.V. Jr, et al. Orthopedics; **31**:927. 2008
2. Ng VY, et al. Clin Orthop Relat Res; **470**:99. 2012.

CONFLICT OF INTEREST DECLARATION

In the interests of transparency and to help reviewers assess any potential bias, ANZORS requires authors of original research papers to declare any competing commercial interests in relation to the submitted work. Referees are also asked to indicate any potential conflict they might have reviewing a particular paper.

If you have accepted any support such as funds or materials, tangible or intangible, concerned with the research by the commercial party such as companies or investors, choose YES below, and state the relation between you and the commercial party.

If you have not accepted any support such as funds or materials, choose NO.

Do you have a conflict of interest to declare?
YES

If YES, please complete as appropriate:

1. The author(s) did receive payments or other benefits or a commitment or agreement to provide such benefits from a commercial entity.
   State the relation between you and the commercial entity:

2. A commercial entity paid or directed, or agreed to pay or direct, any benefits to any research fund, foundation, educational institution, or other charitable or nonprofit organization with which the authors are affiliated or associated.

   - Smith and Nephew paid for the postoperative CT scans

A NEW ANTEROLATERAL APPROACH TO TIBIAL PLATEAU FRACTURES – RATIONALE AND EARLY RESULTS

[1]Adhiraj Chakrabarty, [1]Boopalan Ramasamy, [1]AW Stevenson, MV Price, [1,2]SA Callary, and [1,2]LB Solomon

[1] The Department of Orthopaedics and Trauma, The Royal Adelaide Hospital, Adelaide, SA
[2]University of Adelaide, Adelaide
email: adhirajc@gmail.com

INTRODUCTION

The angiosomes covering the knee are: the anterior tibial, the descending genicular and the popliteal [1]. Dissection between angiosomes is considered safest. The aim was to identify a surgical approach for reducing and stabilizing lateral tibial plateau fractures that would allow access for anatomical reduction and preserve the anterior tibial angiosome.

METHODS

Dissections of 20 cadaveric knees showed that the common lateral oblique skin incision compromises the skin blood supply and detachment of the tibialis anterior origin may potentially devascularise the split components of the lateral tibial plateau delaying bone healing. Based on the dissection findings, a new anterolateral approach to the knee was developed. 33 consecutive patients were operated through anterolateral or combined with posteromedial and/or anteromedial approaches. Complications, radiographic assessment of fracture healing and patient reported Lysholm scores were prospectively collected. In 15 patients fracture reduction was also assessed by radiostereometric analysis (RSA).

RESULTS AND DISCUSSION

There were 20 males and 13 females. The median age was 45 yrs (range 22–69). There were 19 Schatzker II, 3 Schatzker V and 11 Schatzker VI fractures. The mean injury severity score was 9.5 (range 9–25). 19 patients were operated through the anterolateral approach, 9 patients through anterolateral and posteromedial approaches and 5 patients through anterolateral, posteromedial and anteromedial approaches. All surgical wounds healed uneventfully within two weeks of surgery. All fractures were reduced to within 2mm of articular congruency and maintained reduction at two years. Limb alignment was within normal values in 30 of the 33 patients at two years. Three patients, with Schatzker VI fractures, had varus angulation. The Lysholm knee score improved for all available 21 patients at one year to a median of 76 (range 29–100). Longitudinal monitoring of fracture fragment displacement over time using RSA demonstrated that the loss of fracture reduction was below the 3mm threshold, thought to influence the outcome of these injuries [2].

CONCLUSIONS

The anterolateral approach allows for anatomical reduction of lateral tibial plateau fractures either in isolation or combined with other approaches (i.e. posteromedial, anteromedial). The preservation of the blood supply to the anterior tibial angiosome ensures that this approach can be performed safely.

ACKNOWLEDGEMENTS

I acknowledge my co-authors for their contribution in the project. No financial and/or conflicting interests.

REFERENCES

1. Taylor, G; Pan, Wei. Angiosomes of the Leg: Anatomic Study and Clinical Implications. Plastic and Reconstructive Surgery. **102**(3):599-616, September 1998.
2. Honkonen SE. Indications for surgical treatment of tibial condyle fractures. CORR. 1994:199-205.

BIOACTIVE SR-HA BONE CEMENT FOR ELDERLY OSTEOPOROTIC BONE FRACTURE

William Lu, PhD

Department of Orthopaedics & Traumatology
The University of Hong Kong, Hong Kong, PR China
E-mail: wwlu@hku.hk

Among many potential biomaterials, PMMA bone cements or similar derivatives are considered to be one of the most applicable to orthopaedics. Conventional PMMA bone cement have been used in orthopaedic surgery for about 40 years. However, it has elemental complications, such as its non-adhesiveness to bone surfaces, exothermically high reaction and monomer toxicity. It has been used in spinal surgery by means of vertebroplasty treatment, but the associated drawbacks and risks limit its use.

We propose that the ideal bone cement for osteoporotic bone fracture, such as vertebroplasty, should be one that is injectable, has a stiffness close to bone, is bioactive, can osseointegrate, has a low setting temperature, allows immediate load bearing, and is radiopaque. Based on these requirements, a novel nano bioactive bone cement was developed (U.S. Patent No.6,593,394). It mainly composes of strontium-containing hydroxyapatite (Sr-HA) filler and bisphenol A diglycidylether dimethacrylate (BIS-GMA) resin. Bis-GMA is a bio-glass commonly used in dental practice, and HA is osteoconductive. While strontium belongs to the same group as barium and calcium, is radiopaque, and has been shown to stimulate bone formation and inhibit bone resorption *in vitro* as well as *in vivo*. Recently, strontium salts have been shown in human clinical trials to be an effective treatment for osteoporosis, and one of a few drugs that acts by promoting bone formation. In the talk, the updated *in vitro*, *in vivo*, and clinical evidence for the effectiveness of this Sr-HA cement will be discussed in depth.

Effect of high landing impact loads on tibial torques at different knee flexion angles

[1]Hossein Mokhtarzadeh, [2]Chen Hua Yeow, [1]Fatemeh Malekipour, [1]Denny Oetomo and [1]Peter Vee Sin Lee

[1]Department of Mechanical Engineering, the University of Melbourne, Australia
[2]Faculty of Engineering, National University of Singapore, Singapore,
[3]School of Engineering and Applied Sciences, Harvard University, USA
Email: mokhtarzadeh.hossein@gmail.com

INTRODUCTION

ACL injury is common among young athletes. Video-based, cadaver and simulation studies do not support a solely sagittal plane injury mechanism. Multiplanar mechanisms should be considered to assess possible ACL injury. At the onset of ACL injury, tibial rotation occurs and aggravates ACL strain. Knee muscles may protect the knee from ACL injury if they are able to resist tibial rotational torques generated by landing impact loads. This study investigated the effects of these loads on tibial rotational torques at different knee flexion angles. We hypothesized that at low flexion angle, axial impact loads induce less torque as compared to a higher flexion angle during landing.

METHODS

To simulate landing manoeuvres, a rig was designed to allow four DOFs to tibia with respect to femur (Figure 1). Internal/external rotation and vertical displacement were provided by the top cup in which tibia was cemented. Femur was attached to the bottom cup sitting on an X-Y table. Three porcine knee specimens were sectioned at proximal ends. A hydraulic machine (Instron 8874 UK) was used to apply an axial load in the direction of the long axis of the tibial shaft, with the knee held at certain flexion angles. The three specimens were tested at flexion angles of ~22.5, 37.5 and 52.5 degree respectively.

The axial rotation of tibia was fixed. At each flexion angle, compressive impact loads were applied using defined actuator displacement to the tibia at a single 10-Hz haversine wave [1] to simulate landing impact during landing. This protocol was repeated incrementally through five consecutive compressive displacements of 0.5mm. At each trial, the generated tibial torque and simulated landing impact loads were measured.

RESULTS AND DISCUSSION

The maximum impact load (GRF) at 3.5mm displacement for 22.5, 37.5, 52.5deg flexion angles were 1.96±0.83kN, 3.11±2.10kN and 4.02±1.05kN respectively. The axial impact load required to achieve the 5 prescribed displacement from 1.5mm to 3.5mm was greater at lower flexion angle. As the load increased, tibial torque increased for all flexion angles (Figure 2). However, at low flexion angle of 22.5degree, this increase was not significant.

In this study, muscles were absent. Therefore, the tibial torque detected was mainly contributed by the landing impact load. We demonstrated that increased loads generated larger tibial torque, together with higher axial displacements, especially for flexion angles of 37.5 and 52.5 degrees. This may suggest that ACL injury will likely occur if the knee muscles are unable to generate sufficient transverse torque to resist the externally-induced tibial torque. In addition, higher loads did not significantly increase torque at low flexion angle, which may imply that the ACL injury mechanism at low knee flexion angle may be dominated by valgus and anterior tibial translation (ATT), rather than tibial rotation.

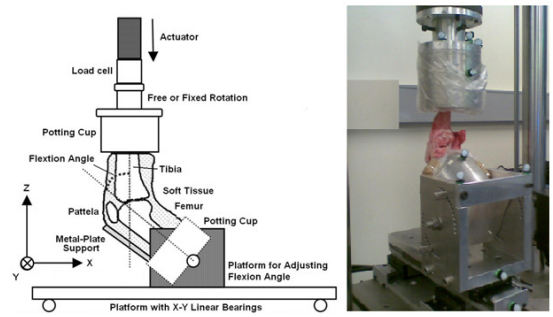

Figure 1: Impact test setup drawing (Left) with a soft tissue-intact porcine knee specimen (Right)

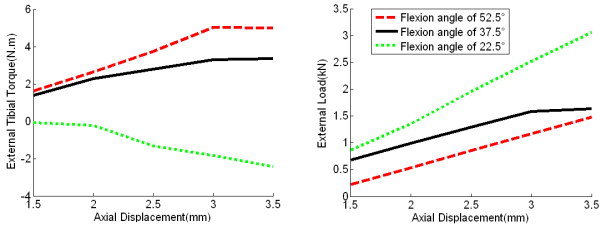

Figure 2: A representative curve of generated tibial torque (tibia resistant moment) (Left) and external force (impact load) in different flexion angles (Right)

CONCLUSIONS

Resistant tibial torques due to axial load changed in different flexion angles. Our finding suggests that ACL injury could be dominantly due to valgus and ATT rather than tibia rotation at low flexion angle. Also, any additional external tibia torque may exacerbate the joints' capacity to endure internal tibia rotation at the onset of ACL injury.

REFERENCES

1. Yeow C.H., et al, *J Biomech*, **42**(8): 972-981. 2009

SESSION 4 - ABSTRACTS

PhD Award

DAY 2: Friday, 31 August

3:00 PM – 4:25 PM

TARGETING HDAC1 TO SUPPRESS BONE LOSS IN PERI-PROSTHETIC OSTEOLYSIS

[1]Melissa D Cantley, [2]David P Fairlie, [3]P Mark Bartold and [1]David R Haynes

[1]Discipline of Anatomy and Pathology, School of Medical Sciences, University of Adelaide, South Australia.
[2]Institute for Molecular Bioscience, University of Queensland, Brisbane.
[3]Colgate Australian Clinical Dental Research Centre, School of Dentistry, University of Adelaide, South Australia.

INTRODUCTION

Inhibition of the histone deacetylase (HDAC) enzymes that regulate gene transcription is becomingly increasing popular to treat inflammatory diseases such as rheumatoid arthritis. These compounds have demonstrated suppression of bone loss [1,2] and could be a potential treatment for peri-prosthetic (PP) osteolysis which is the leading cause for joint revision surgeries. There are two main classes of the HDAC enzymes – HDAC class I includes HDAC 1,2,3 and 8 whereas class II includes HDAC 4,5,6,7, 9 and 10. Specifically targeting HDACs up regulated in PP osteolysis could result in more efficient acting compounds and reduce chances of side effects. The aim of this study was to determine which HDACs are up regulated in human tissue samples from sites of PP osteolysis and assess the effects of a novel HDACi that selectively targets HDAC 1 on inflammation and bone loss *in vitro*.

METHODS

Tissue Expression: Expression of HDACs enzymes 1-10 near sites of bone loss in human PP osteolysis tissues was assessed using real time PCR and immunohistochemistry. PP tissues were obtained during revision surgeries conducted at the Royal Adelaide Hospital (RAH) (n=10) and compared with osteoarthritic (OA) synovial tissues (n=5) from patients undergoing a primary implant at the RAH. mRNA expression of HDACs 1-10 was determined relative to hARP. For immunohistochemistry a rabbit polyclonal to HDAC1 (ab19845) was used to determine protein expression in the tissues.

In vitro effects: The effect of a novel HDACi specifically targeting HDAC 1 (NW-21) on human osteoclast activity *in vitro* was assessed. Human peripheral blood mononuclear cells were obtained from healthy blood buffy coats from the Australian Red Cross Blood Service. Cells were stimulated with Macrophage Colony stimulating factor (M-CSF) and receptor activator of nuclear factor κB ligand (RANKL). Cells were treated with five fold dilutions of NW-21 starting at 100nM. Effects on osteoclast formation and activity were assessed using a TRAP stain and pit resorption analysis. Inflammatory effects were also investigated by stimulating monocytes with either *E.coli* lipopolysaccharide (LPS) or tumour necrosis factor (TNF-α) and treating cells with NW-21 for 24 hours. Real time PCR was conducted to assess effects on mRNA expression for inflammatory cytokines and chemokines – TNF-α, interleukin 1 (IL-1β), monocyte chemotactic protein (MCP1) and macrophage inflammatory protein MIP1-α.

RESULTS AND DISCUSSION

HDAC 1 mRNA expression was significantly up regulated in human PP tissues compared to OA controls. Immunohistochemistry revealed that HDAC 1 was strongly expressed by multinucleated 'osteoclast like' cells in PP tissues compared to little or no expression in the OA control. HDACi NW-21 (targets HDAC 1) was found to suppress human osteoclast mediated bone resorption *in vitro* at concentrations higher than 0.8nM *in vitro* as shown in figure 1.

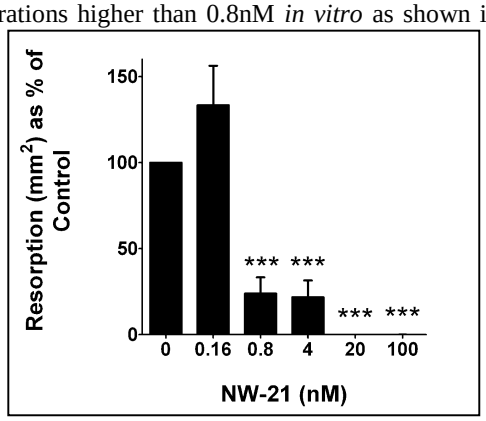

Figure 1: The effect of five-fold dilutions of NW-21 on osteoclast bone resorption expressed as a % of control resorption. Bars represent mean±SEM. *** $p<0.001$

Treatment of stimulated human monocytes with NW-21 significantly suppressed mRNA expression of MCP1 and MIP1-α but demonstrated no significant effect on reducing TNF-α, IL-1β mRNA expression.

CONCLUSIONS

mRNA expression class I HDAC 1 was found to be significantly up regulated in human PP tissue. Inhibition of HDAC 1 with novel HDACi NW-21 (targets HDAC 1) demonstrated both anti-resorptive and anti-inflammatory effects *in vitro*. HDAC1 is therefore a promising target for treatmen oft PP osteolysis and could reduce the incidence of revision surgeries.

ACKNOWLEDGEMENTS

This work was funded by a NHMRC Project Grant.

REFERENCES

1. Cantley MD et al, *J Periodont Res*, 2011.
2. Cantley MD et al, *J Cell Physiol* **226** (12), 3233 2011

AN *IN VITRO* MODEL TO STUDY THE REGULATION OF OSTEOCYTE METABOLISM BY CHONDROCYTES

[1]Anjali Jaiprakash, [1]Nishant Chakravorty, [3]Jerry Feng, [1, 2]Ross Crawford, [1]Yin Xiao

[1]Institute of Health and Biomedical Innovation, Queensland University of Technology, Brisbane, Australia
[2]Prince Charles Hospital, Brisbane, Queensland, Australia
[3]Texas A&M Health Science Center, Baylor College of Dentistry, Texas, USA
Email: anjali.jaiprakash@qut.edu.au

INTRODUCTION

Osteoarthritis (OA) is the most common type of joint disease, affecting millions of people worldwide. OA is not exclusively a cartilage-disorder. Multiple components of the joint are adversely affected by OA, including the bone, synovial joint lining and adjacent supporting connective tissue elements. Many structural alterations of the joint have been reported, but the pathogenesis remains poorly defined. Therefore current pathophysiological concepts focus on OA as a disease of the whole joint, rather than a "chondro-centric" or "osteo-centric" model [1, 2]. Although osteocytes are the most abundant bone cells, they have received little attention in OA pathophysiology. Our recent studies suggest that dysregulated osteocytic proteins contribute to the pathological changes in OA subchondral bone [3]. However, a significant knowledge gap exists in understanding the role of osteocytes and the extent of interaction and cross-talk between articular cartilage chondrocytes (ACCs) and osteocytes in bone remodeling. We hypothesized that soluble factors from OA ACCs play an important role in osteocyte metabolism, leading to the characteristic OA-osteocyte phenotype and bone remodeling. This study investigated the effects of conditioned media from OA ACCs on osteocytes metabolism *in vitro*.

METHODS

To study the synergistic relationship between osteocytes and chondrocytes, knee tissue from donors undergoing total knee replacement surgery was collected. Cartilage was classified using Mankin's score [4]. Sections with a score of 0-1 were used as control (C) ACCs and sections with a score over 3 were used as OA ACCs. Cells were enzymatically harvested with 0.15% collagenase (Fig. 1 shows a representative control and OA sample of the bone cartilage unit). To confirm their phenotypic stability, 3D cultures were set up in serum free chondrogenic media and characterized by their phenotype and expression of chondrogenic and hypertropic markers. After 14 days of differentiation, media was removed, serum free fresh media was added for 24 hrs, and conditioned media was collected and mixed with equal volumes of fresh media and given to the well established osteocyte cell line MLOY4. After 3 days of culture with conditioned media, cell proliferation (MTT assay) and total RNA amount were determined. Expression levels of bone formation (ALP, OPN), bone resorption (RANKL) and osteocyte/mineralization (E11, DMP1, OSX) mRNA were analyzed using qPCR. A Statistical significance was determined using student t-test, and a p-value <0.05 was considered significant (n=3).

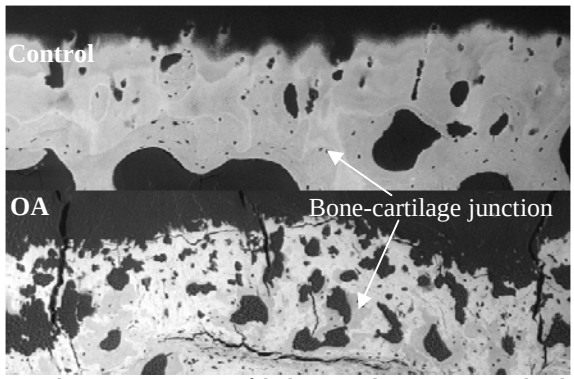

Fig 1: Back scatter SEM image of the bone-cartilage unit in control and OA samples from patients undergoing knee replacement surgery.

RESULTS AND DISCUSSION

MLOY4 cells demonstrated increased proliferation when treated with OA-ACC-conditioned media compared to C-ACC-conditioned media. qPCR revealed a statistically significant increase in the relative expression of the bone formation markers ALP and OPN. RANKL, a bone resorption marker, was found to be increased as well. Furthermore, cells showed an increased expression of E11 (immature osteocyte marker), DMP1 and OSX (osteocyte/mineralization markers), indicating a possible role of soluble factors from OA ACCs on osteocyte regulation and subchondral bone mineral metabolism. Further experiments have to be performed to determine if the soluble factors promote bone formation or bone resportion.

CONCLUSIONS

The findings of this study demonstrate the influence of soluble factors from OA ACCs on osteocytes which may lead to increased subchondral bone volume and hampered mineral metabolism as observed in OA. This *in vitro* model could contribute to a better understanding of OA pathophysiology.

REFERENCES

1. Rik J.Lories, et al., *Nat Rev Rheumatol*, 7: 43-49, 2011.
2. Anjali Jaiprakash, et al., *Int J Biol Sci*, 8(3):406-417, 2012.
3. David M Findlay, *Arthritis Res Ther*, 12:119,2010.
4. Van der Sluijs, et al., *J Orthop Res*, 10**:**58-61,1992

ULTRASOUND TRANSIT TIME SPECTRAL ANALYSIS FOR DERIVATION OF DENSITY OF CANCELLOUS BONE

[1]Marie-Luise Wille, [2]Mark B Flegg, and [1]Christian M Langton

[1]Institute of Health & Biomedical Innovation and Faculty of Science & Engineering, Queensland University of Technology, QLD
[2]Oxford Centre for Collaborative Applied Mathematics, Mathematical Institute, University of Oxford, UK
m.wille@qut.edu.au

INTRODUCTION

Dual Energy X-ray Absorptiometry (DXA) derived Bone Mineral Density (BMD) is currently the 'gold standard' tool to diagnose osteoporosis utilising WHO criteria. Broadband ultrasound attenuation (BUA) has been shown to reliably predict osteoporotic fracture risk, depending on both the material and structural properties of cancellous bone [1]; however, the relationships are yet to be fully elucidated, limiting the world-wide acceptance of the technique. Here we aim to verify a new theory proposing that the primary ultrasound attenuation mechanism is phase interference due to lateral inhomogeneity in transit time [2].

METHODS

We consider a simple model of parallel phonon rays travelling from the transmitting transducer to the receiving transducer with the sample in between. The resulting transmitted signal is assumed to be the sum of all rays. A 1 MHz ultrasound signal was transmitted through magnified stereolithography replicas of four cancellous bone samples that had previously been scanned with microCT (Figure 1).

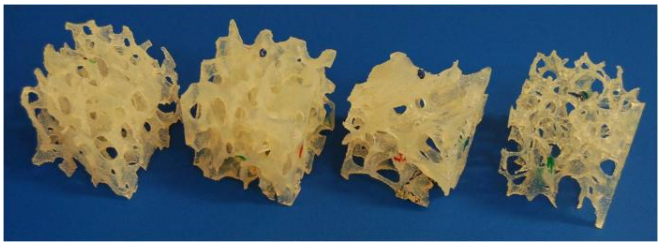

Figure 1: Magnified STL bone models. From left to right: calcaneus, femoral head, iliac crest, lumbar spine.

Transit time spectra were generated via deconvolution of the input and the measured output signal. We substantiated this model by comparing computer simulations with experiments. From the transit time spectra (TTS) we estimated the bone volume fraction.

RESULTS AND DISCUSSION

Good quantitative agreement was obtained between experimental and computer simulated output signals and transit time spectra. Figure 2 shows the experimentally derived and computer simulated mean value of the obtained TTS for the three orthogonal orientations of the four STL bone models. Bone volume fraction values were determined from both, the simulated (R^2=99%) and experimental data (R^2=97%) compared to the true values derived from the microCT scans.

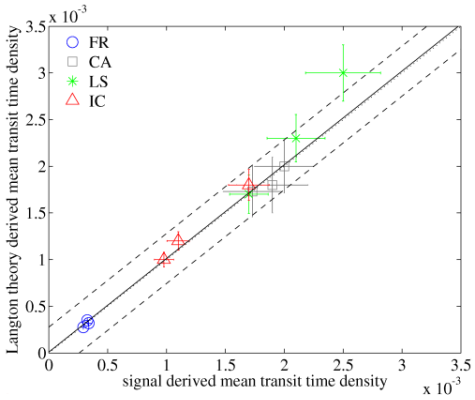

Figure 2: Mean values and standard errors of the signal derived versus simulated transit times.

CONCLUSIONS

This study is a new approach to determine both bone volume fraction and bone structure with broadband ultrasound. The observed phase interference in transit time spectra indicates indeed the structural properties of cancellous bone. Future work will be aimed at deriving a unified model relating ultrasound transit time spectra (function of bone volume fraction and bone structure) with the properties of a propagating ultrasound wave; and hence BUA. Furthermore in vitro and in vivo validation should be considered in order to implement the new findings in clinical systems.

REFERENCES

1. Njeh CF, et al., *Osteoporosis International.* **12**(1):1-15, 2001.
2. Langton CM, *Proc Inst Mech Eng Part H-J Eng Med.* **225**(H2):113-125, 2011.

EXPRESSION AND POTENTIAL FUNCTION OF NEUROTROPHIC FACTORS AND THEIR RECEPTORS IN GROWTH PLATE CARTILAGE BONY REPAIR AND SKELETAL CELL FORMATION

Yu-Wen Su, Rosa Chung, Fiona Zhou, Tristan King, Kristen Georgiou, Bruce Foster, Xin-Fu Zhou and Cory J. Xian

School of Pharmacy and Medical Sciences, Sansom Institute for Health Research, University of South Australia, SA
Email: suyyy009@mymail.unisa.edu.au

INTRODUCTION

The growth plate cartilage is responsible for bone growth in children and yet its injuries are often repaired undesirably by bony tissue causing bone growth defects, for which the mechanisms are not clear [1]. Neurotrophic factors (NTs) have been shown to regulate bone fracture healing [2]; however their potential roles in growth plate cartilage bony repair are unknown.

We investigated expression of NTs and receptors in the bony repair at the injured growth plate cartilage and during skeletal cell formation *in vitro*.

METHODS

Using a rat model of tibial growth plate injury, the expression of neurotrophic factors (NGF, BDNF, NT-3, and NT-4) and their receptors (TrkA, TrkB, TrkC and p75) at the injury site was investigated by RT-PCR and immunohistochemistry at different time points after injury.

In addition, expression of neurotrophic factors and receptors was investigated by RT-PCR during chondrogenesis, osteoblastogenesis, mineralisation and osteoclastogenesis *in vitro* in rat bone marrow cells.

RESULTS AND DISCUSSION

Upregulated levels of mRNA expression of NTs (NGF, BDNF, NT-3 and NT-4) and their high affinity receptors (TrkA, TrkB and TrkC) were observed at different times (days 5, 8, 14 and 28) at the growth plate injury site, where NT-3 showed the highest expression by 50 to 100 folds compared to non-injured control (Figure 1). The localization of NTs in mesenchymal cells, chondrocytes, osteoblasts and osteocytes at the injury site was also observed by immunostaining.

Furthermore, differentially regulated expression of the factors and their receptors was also detected during *in vitro* chondrogenesis, osteoblastogenesis, mineralisation and osteoclastogenesis in cultured bone marrow progenitor cells from normal rats, in which NT-3 mRNA displayed the greatest upregulation by 250 to 350 folds during chondrogenesis.

CONCLUSIONS

Neurotrophic factor signalling may be involved in the skeletal cell formation and in the repair processes at injured growth plate.

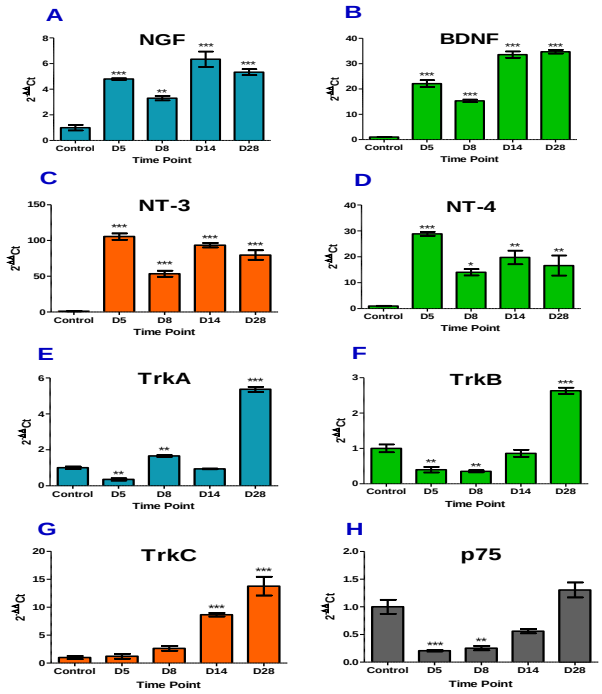

Figure 1: Time course gene expression of neurotrophic factors (NGF, BDNF, NT-3 and NT-4) and their receptors (TrkA, TrkB, TrkC and p75) at the injury site after growth plate injury by RT-PCR. The changes in mRNA expression levels of NGF (A), BDNF (B), NT-3 (C), NT-4 (D), TrkA (E), TrkB (F), TrkC (G) and p75 (H) are presented as fold change compared to non-injury control after being normalised to expression levels of Cyclophilin-A. N=6 per time point, *p<0.05, **p<0.01, ***p<0.001 compared with control group.

ACKNOWLEDGEMENTS

The project was funded in parts by research fund from Bone Health Foundation, and from the Australian National Health and Medical Research Council (NHMRC). Xin-Fu Zhou and Cory J. Xian are senior research fellows of NHMRC Australia.

REFERENCES

1. Xian CJ, et al., *Curr Stem Cell Res Ther*. **1**:213-229, 2006.
2. Asaumi K, et al., *Bone*. **26**:625-633, 2000.

AGGRECAN MOLECULAR MECHANICS MEETS CARTILAGE TISSUE NANOMECHANICS: RELEVANCE TO CARTILAGE REPAIR VIA BMSCS IN HYDROGEL SCAFFOLDS

[1,2,3]Alan J. Grodzinsky, [2]Hadi Tavakoli Nia, [3]Hsu-Yi-Lee [4]Lin Han [4]Christine Ortiz

[1]Center for Biomedical Engineering and Department of Biological Engineering, MIT, Cambridge, MA, USA
[2]Department of Mechanical Engineering, MIT, Cambridge MA, USA
[3]Department of Electrical Engineering and Computer Science, MIT, Cambridge, MA, USA
[4]Department of Materials Science and Engineering, MIT, Cambridge, MA, USA
email: alg@mit.edu

INTRODUCTION

Aggrecan is a ~300 kDa proteoglycan composed of a core protein substituted with ~100 chondroitin sulfate (CS) glycosaminoglycan (GAG) chains [1] (Fig. 1). Aggrecan associates noncovalently with hyaluronan and the ~45 kDa link protein to form high molecular weight aggregates (>200 MDa), which are enmeshed within the collagen fibrillar network of cartilage. Electrostatic repulsion and osmotic interactions between CS-GAGs provide >50% of the equilibrium compressive modulus of cartilage. Here we review studies to quantify physical mechanisms at equilibrium and higher frequencies by which aggrecan confers mechanical properties to native cartilage. We used AFM-based oscillatory loading to study the dynamic compressive properties of dense aggrecan layers and compared the results to recent findings [2] on the nanoscale dynamic modulus of cartilage.

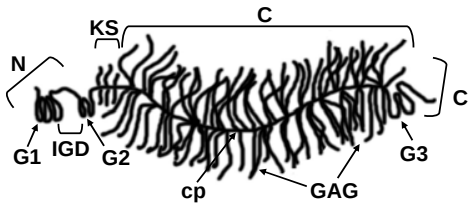

Figure 1: Schematic of aggrecan showing N and C terminal domains; cp = core protein; CS and KS (keratan sulfate) GAG chains; G1, G2, G3globular and IGD (inter-globular) domains.

METHODS

Purified bovine aggrecan was chemically end-grafted onto gold-coated planar substrates at physiological packing densities [3]. AFM-based wide-frequency dynamic force spectroscopy was performed using gold-coated AFM colloidal probe tips, (45 um diameter; cantilever spring constant 7.5 N/m) via previously described methods [2] but with an enhanced high frequency range of 1Hz – 10 kHz [4]. Results were compared to AFM-based dynamic force spectroscopy of intact bovine cartilage disks using similar methodology to explore the poroelastic properties of cartilage at the nanoscale.

RESULTS AND DISCUSSION

The experimentally measured magnitude (Fig. 2a) and phase of the dynamic nanoindentation modulus were well-predicted by a fibril-reinforced poroelastic model over a three-decade frequency range [2]. The peak frequency of the phase angle scaled linearly with the inverse square of the contact distance between probe tip and cartilage, as predicted by poroelasticity theory. Importantly, the dynamic stiffness of the aggrecan layer showed similar trends as in Fig. 2a, exhibiting low and high frequency asymptotes and a peak in the phase angle close to that of native cartilage.

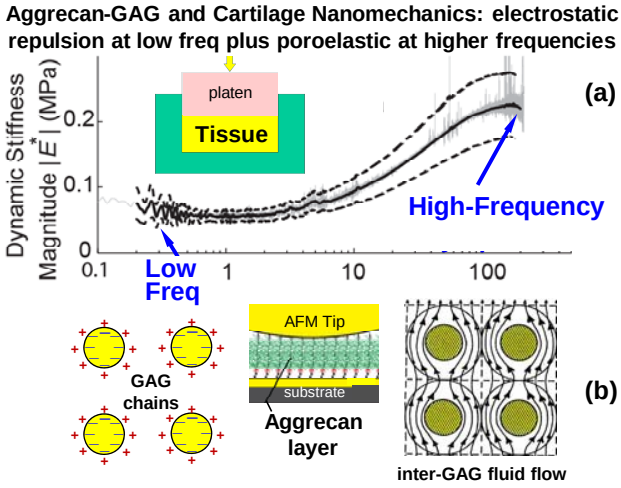

Figure 2: **(a)** Mean ± 95% confidence intervals for magnitude of dynamic nanoindentation modulus of bovine cartilage showing quasi-static and high frequency asymptotes (adapted from [2]). **(b)** GAG-GAG repulsion and osmotic swelling dominates quasi-static modulus; fluid flow restricted by GAGs dominates poroelastic response at higher frequencies.

CONCLUSIONS

At the molecular scale, aggrecan appears to provide the source of the frequency-dependent behavior of cartilage. At quasistatic frequencies, GAG-GAG repulsion interactions dominate, whereas fluid flow between GAGs induced by higher loading rates leads to increased stiffness and fluid pressurization (Fig 2b).

ACKNOWLEDGEMENTS

NSF Grant CMMI-0758651 and NIH Grant AR033236.

REFERENCES

1. Ng L, et al., *J Structural Biol.* **143**:242-257, 2003.
2. Nia, HT et al., *Biophysical J*, **101**:2302-2313, 2011
3. Dean D et al., *Macromolecules*, **38** :4047-4049, 2005
4. Nia, HT et al., Trans 58th ORS, Feb 3-7, 2012

IN VIVO SYNERGY BETWEEN rhBMP-2 AND IKK-INHIBITOR PS-1145

[1]David Carr[1,2], Nicole Y.C Yu[1,2], Marie Gdalevitch[1], Jane Fitzpatrick[4], Lauren Peacock[1], Kathy Mikulec[1], Andrew J. Ruys[2], Justin C. Cooper-White[4], David G. Little[1,3] and Aaron Schindeler[1,3]

[1] Department of Orthopaedic Research & Biotechnology, The Children's Hospital at Westmead, NSW
[2] School of Aerospace, Mechanical and Mechatronic Engineering, University of Sydney, NSW
[3] Discipline of Paediatrics and Child Health, Faculty of Medicine, University of Sydney, NSW
[4] Tissue Engineering and Microfluidics Laboratory, University of Queensland, QLD
email: nicole.yu@sydney.edu.au

INTRODUCTION

Bone tissue engineering can be optimized by modulating the anabolic and anti-catabolic responses. Recombinant human Bone Morphogenetic Protein-2 (rhBMP-2) is a bone anabolic clinically used for healing of critical-sized bone defects and delayed/non-unions. IKK inhibitor PS-1145 is emerging as a potent anti-catabolic, but has not yet been explored in the context of bone tissue engineering.

In this study we described two rodent models for the local co-delivery of anabolic recombinant human Bone Morphogenetic Protein-2 (rhBMP-2) and anti-catabolic IKK inhibitor PS-1145. As proof of concept, an ectopic mouse muscle pouch surgical model was used comparing PS-114 co-treatment via local delivery versus systemic injection. To demonstrate clinical efficacy, a rat critical-sized defect model was subsequently tested.

METHODS

Highly porous scaffold implants were manufactured from poly(lactide-co-glycolide) (PLGA) by thermally-induced phase separation (TIPS). rhBMP-2 and the IKK inhibitor PS-1145 were incorporated into the polymer, which was made as discs (3mm diameter x 1mm height) or cylinders (3mm x 5mm height). Discs were used in a C57BL6/J mouse muscle pouch bone ectopic bone formation model and cylinders in a Wistar rat critical sized defect model.

For the mouse ectopic bone model, all implants contained rhBMP-2 (10µg) and groups received local PS-1145 (0µg, 40µg or 80µg) or systemic PS-1145 (50mg/kg, days 11-20) (N=8 mice per group). For the rat defect model, all implants contained rhBMP-2 (20µg) and groups received local PS-1145 (0µg, 100µg) (N=20 rats per group). PGLA scaffolds were also compared with porous collagen scaffolds (Medronic).

Mice and rats were sacrificed at week 3 and 6 weeks, respectively. Samples were harvested for X-ray and microCT analyses and descriptive histology.

RESULTS AND DISCUSSION

In the mouse ectopic bone model, local and systemic delivery PS-1145 both significantly increased the net rhBMP-2 induced bone at 3 weeks (Figure 1A). A maximal response was seen with the 40µg PS-1145 group (111% increase over rhBMP-2 alone, p=0.02), although 40µg and 80µg PS-1145 showed no significant difference. Histology showed that PS-1145 did not cause local cytotoxicity.

In the rat model, regenerate bone volume (BV, mm^3, Figure 1B) was quantified by microCT. The addition of IKK inhibitor increased BV by 49% ($p<0.05$) versus rhBMP-2 alone (TIPS). 3D reconstructions from microCT data demonstrated significantly denser callus region in IKK groups compared to rhBMP-2 alone controls. TIPS scaffolds were able to restrict bone to the implant region more effectively than collagen controls, but this led to a suboptimal bone-scaffold interface.

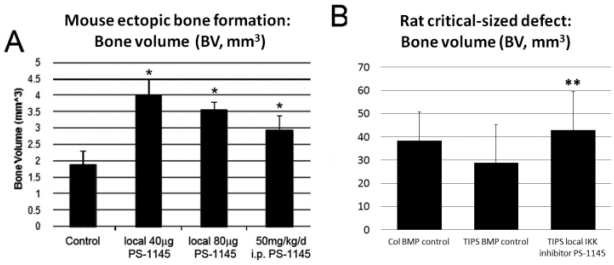

Figure 1: MicroCT quantification of 3D bone volume of **(A)** ectopic bone nodules induced in mouse muscle and **(B)** regenerate region in rat critical-sized bone defect (*=$p<0.05$ vs. mouse TIPS control and **=$p<0.05$ vs. rat TIPS control).

CONCLUSIONS

Local co-delivery of rhBMP-2 and PS-1145 via a porous PLGA scaffold represents a new tissue engineering approach for maintaining new bone in an unloaded ectopic bone formation environment. Based on the 3D reconstructions, an overlapping design between the defect bone ends and the PGLA implants may yield superior results.

For clinical translation, optimizing anabolic and anti-catabolic agents may result in improved bone formation and greater healing strength compared to current commercially available BMP-delivery alternatives.

ACKNOWLEDGEMENTS

Nicole Y. C. Yu was supported by the Australian National Health & Medical Research Council (NHMRC) Biomedical Postgraduate Research Scholarship. Dr Schindeler receives salary support from NHMRC Project Grant APP1003478. This work was supported by NHMRC Project Grant APP1020987.

SESSION 5 - ABSTRACTS

Bone Biology & Joint Regeneration (1)

DAY 3: Saturday, 1 September

9:00 AM – 10:40 AM

IMPLANTATION OF OSTEOGENIC DIFFERENTIATED DONOR MESENCHYMAL STROMAL CELLS CAUSES RECRUITMENT OF HOST CELLS

[1]Yinghong Zhou, [1,2]Ross Crawford and [1]Yin Xiao

[1] Institute of Health and Biomedical Innovation, Queensland University of Technology, QLD
[2] Prince Charles Hospital, Brisbane, Queensland, Australia
email: yinghong.zhou@student.qut.edu.au

INTRODUCTION

The interaction between host and donor cells is believed to play an important role in osteogenesis [1]. However, it is still unclear how donor osteogenic cells behave and interact with host cells *in vivo*. The purpose of this study was to track the interactions between transplanted osteogenic cells and host cells during osteogenesis.

METHODS

In vitro migration assay was carried out to investigate the ability of osteogenic differentiated human mesenchymal stromal cells (O-hMSCs) to recruit host MSCs.

At the *in vivo* level, hMSCs were isolated and cultured on type I collagen scaffolds with or without osteogenic differentiation. These cell-carrying scaffolds were implanted subcutaneously or into skull bone defects in severe combined immunodeficient (SCID) mice. Scaffold alone was used as blank control. Four weeks after the implantation, tissue samples were collected, fixed, embedded and sliced. Tissue mineralization and new bone formation were assessed by micro-CT, histological and immunohistochemical methods. *In situ* hybridization (ISH) against human repetitive Alu sequences was performed to distinguish donor cells from host cells.

RESULTS AND DISCUSSION

In vitro migration assay revealed an increased migration potential of hMSCs by co-culturing with O-hMSCs.

It was noted that significantly increased tissue mineralization was detected in both ectopic and orthotopic sites when O-hMSCs were transplanted *in vivo*. H&E and immunohistochemical staining against bone markers revealed remarkable new bone formation within the skull defects transplanted with O-hMSCs. ISH against human Alu sequences showed that host mouse MSCs migrated in large numbers into the transplantation site in response to O-hMSCs. Interestingly, host cells recruited by O-hMSCs were the major cell populations in newly formed bone tissues, indicating that O-hMSCs can trigger and initiate osteogenesis when transplanted in orthotopic sites.

CONCLUSIONS

The observations from this study demonstrated that *in vitro* induced O-hMSCs were able to attract host MSCs *in vivo* and were involved in the osteogenesis together with host cells, which may be of importance for bone tissue engineering applications [2].

REFERENCES

1. Greco S, et al., *Biologics.* **2**:699-705, 2008.
2. Lin C, et al., *Biomaterials.* **31**:3222-3230, 2010.

DESIGN AND FABRICATION OF BIPHASIC SCAFFOLD FOR OSTEOCHONDRAL REGENERATION

[1]Jiao Jiao Li, [2]Eun Seok Gil, [2]Rebecca Scholl Hayden, [1]Seyed-Iman Roohani-Esfahani, [2]David L. Kaplan, and [1]Hala Zreiqat

[1]Biomaterials and Tissue Engineering Research Unit, School of AMME, University of Sydney, Sydney, NSW, Australia
Email: jiaojiao.li@sydney.edu.au
[2]Department of Biomedical Engineering, Tufts University, Medford, MA, USA

INTRODUCTION

Articular cartilage injuries frequently arise due to trauma, disease, and age-related degeneration. Owing to the avascular nature of cartilage and its limited remodeling capacity, existing treatment procedures such as microfracture and autologous chondrocyte implantation (ACI) can alleviate pain and morbidity in the short term, but the effects of long term repair are barely satisfactory particularly for full-thickness osteochondral defects. Scaffold-based osteochondral tissue engineering is emerging as a novel treatment strategy that can address the growing unmet clinical need to develop more effective therapies. The present study describes the design and fabrication of a biphasic scaffold for the regeneration of both cartilage and subchondral bone in full-thickness osteochondral defects, which consists of two different phases with distinct material and structural properties tailored to their target tissues. The cartilage phase is a silk fibroin hydrogel, anchored to a composite silk-coated biphasic calcium phosphate (BCP-silk) scaffold that constitutes the bone phase. Characterisation of this biphasic scaffold shows optimistic results, indicating the potential for future clinical application.

METHODS

Biphasic calcium phosphate (BCP) ceramic powder (40% hydroxyapatite, 60% β-tricalcium phosphate) was prepared and fabricated into BCP scaffolds (5.5mm diameter, 4mm tall) as previously described [1]. BCP scaffolds were coated multiple times with 8wt% silk fibroin aqueous solution, which was prepared from cocoons of *B. mori* as previously described [2], to give BCP-silk composite scaffolds (bone phase). Silk fibroin hydrogel (cartilage phase) was prepared via sonication of silk fibroin aqueous solution mixed with DMEM powder as previously described [3]. The BCP-silk scaffold was partially immersed in the silk gelling solution and held in place by a silicone mold until gelation occurred, to give a biphasic scaffold with silk hydrogel mounted on top of a BCP-silk composite scaffold. Structural and biological properties of the biphasic scaffold were evaluated.

RESULTS AND DISCUSSION

Scanning electron microscopy (SEM) examination showed that the BCP-silk scaffold had internal architecture similar to cancellous bone, with highly interconnected pores and pore size ranges of 400-500µm (**Fig. 1A**). There was a coherent interface between the cartilage (hydrogel) and bone (scaffold) phases, with good integration of the hydrogel into the pores of the scaffold (**Fig. 1B**). Mechanical testing showed that the silk fibroin coating significantly improved the strength and toughness of the BCP-silk scaffold, making it more suitable for implantation in load-bearing defect sites (**Table 1**). *In vitro* testing using human bone marrow-derived mesenchymal stem cells (hMSCs) showed that the biphasic scaffold was able to induce tissue-specific differentiation responses in the two phases, with evidence of endochondral ossification observed in the BCP-silk scaffold after 6 weeks of culture (**Fig. 2**).

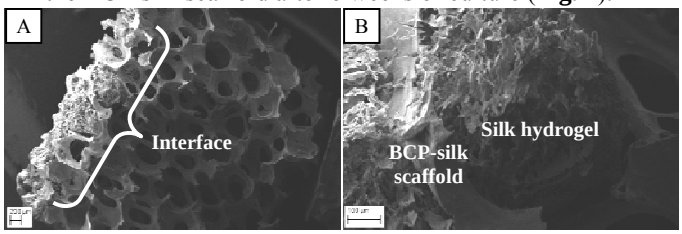

Fig. 1. SEM image of (A) biphasic scaffold, and (B) higher magnification of the interface between the two phases.

Table 1. Mechanical properties of BCP-silk and control BCP scaffolds.

	BCP Control	BCP-Silk
Compressive Strength (MPa)	0.043 ± 0.011	0.247 ± 0.032*
Compressive Modulus (MPa)	5.44 ± 0.87	5.06 ± 1.36
Energy for deformation (J/mm^2)	15.8 ± 6.5	176 ± 21*

* $p < 0.0001$

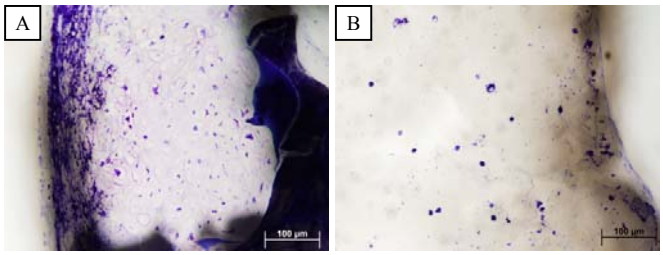

Fig. 2. Histological images of (A) BCP-silk scaffold, and (B) silk hydrogel, of biphasic scaffold cultured with hMSCs for 6 weeks (toluidine blue stain).

CONCLUSIONS

The biphasic scaffold developed in this study has two distinct phases with tailored properties to target the respective regeneration of cartilage and subchondral bone in full-thickness osteochondral defects. The biphasic scaffold has been shown to possess favourable structural and biological properties which advocate the potential for future clinical use.

REFERENCES

1. Roohani-Esfahani S.I., et al., *Biomaterials.* **31**:5498-5509, 2010.
2. Kim U.-J., et al., *Biomaterials*. **26**: 2775-2785, 2005.
3. Chao, P.-H.G., et al., *J Biomed Mater Res B*. **95B**: 84-90, 2010.

HIERARCHICAL DETERMINATION OF NUCLEAR DEFORMABILITY BY LAMINS DURING MARROW CELL DIFFERENTIATION: IMPLICATIONS IN BONE TISSUE ENGINEERING

[1]Jae-Won Shin, [1]Kyle R. Spinler, [1]Joe Swift and [1]Dennis E. Discher

[1]Biophysical Engineering Laboratory, University of Pennsylvania, Philadelphia, USA
mail: jaewons@mail.med.upenn.edu

INTRODUCTION

Bone is a porous tissue that marrow resident cells, including mesenchymal stem cells (MSCs), bone-remodeling cells, and hematopoietic cells must migrate through. Understanding design principles behind deformability of marrow cells is critical in formulating appropriate parameters for bone tissue engineering, such as pore size and elasticity, to accommodate natural processes of cell differentiation and trafficking. Cellular deformability is determined both by membrane and nuclear elasticity, the latter that is dynamically regulated by changes in gene expression and structural reorganization [1]. Here, we demonstrate that nuclear deformability is hierarchically programmed by differential expression of the nucleoskeletal lamin A/C and B isoforms during differentiation, which in turn influence the ability of marrow cells to migrate through pores in 3D.

METHODS

Lamin protein quantification and transwell migration assay: Single cell intracellular flow cytometry was used to evaluate mean intensity of lamin A/C and B isoforms across different bone marrow (BM) and peripheral blood (PB) cell types using antibodies against lamins and surface antigens, including: MSCs, CD34$^-$ cells, hematopoietic stem cell and multipotent progenitors (HSC/MPPs); Common-potent progenitors (CPP); granulocyte (CD33$^+$ mid) and monocyte (CD33$^+$ hi) lineages; erythroid (Ery) lineages (pro and late); megakaryocyte progenitors (MKPs) and differentiated cells (MKs); red blood cells (RBCs) and platelets (plts); Each mean intensity value was normalized by a value from the reference cell line COS-1 for internal fluorescence control. The value was then calibrated against the ratio between lamin A/C and B peptides in A549 cells from mass spectrometry analyses to estimate absolute values of lamins. Boyden chamber migration assay was done under chemotatic gradient of stromal derived factor-1 (SDF-1) as published [2] using 3-8 μm pores.

RESULTS AND DISCUSSION

Comprehensive profiling of lamins across different cell types reveals the lineage map of nuclear deformability (Fig 1, left), verified by nuclear micropipette aspiration (data not shown). Mesenchymal stem cells usually remain resident within marrow, and show higher nuclear stiffness and high lamin intensity than most hematopoietic cells. Myeloid CD34$^-$ cells have the potential to give rise to osteoclasts with stiff nuclei and high lamin expression. In hematopoietic lineages, lymphoid (T and B cells) and granulocyte/monocyte show decreased total lamin intensity and pliable nuclei, consistent with their ability to transmigrate into blood. In contrast, MKs remain in marrow because their polyploid nuclei are too large and rigid, indicated by high lamin intensity, but they do extend membrane projections into blood, where shear generates circulating platelets. Erythroid lineages share the progenitor with MKs and migrate into blood as enucleated RBCs, likely because of high lamin intensity in the progenitors and stiff chromatin. As predicted from the lineage map, lamin A/C overexpression increases MK and erythroid differentiation (data not shown), while the knockdown increases migration through pores (Fig 1, right).

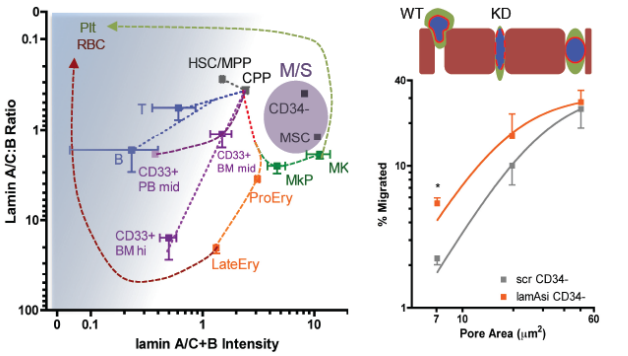

Figure 1: Functional roles of lamins in marrow cell differentiation. (Left) Lineage map showing hierarchy of lamin expression. M/S: Mesenchymal/Stromal. Color gradient represents BM vs PB barrier. (Right) Migration of marrow cells through pores is limited by nuclear stiffness. *P<0.05 (n=3, ±SEM) WT: Wildtype; KD: Lamin siRNA knockdown.

CONCLUSIONS

Expression profiling and functional experiments reveal critical roles of lamins in regulating marrow cell differentiation and migration through pores. The findings here will be helpful in bone tissue engineering designed to support physical characteristics of marrow cells and ultimately their functions.

ACKNOWLEDGEMENTS

This study was supported by the National Institutes of Health (P01DK032094) and the Human Frontier Science Program.

REFERENCES

1. Pajerowski JD, et al. *PNAS.* **104**:15619-24, 2007.
2. Peled A, et al. *Science* **283**: 845-848. 199.

ONE'S POISON IS ANOTHER'S FOOD - HEPARANASE FOR FRACTURE HEALING

[1,2]Rachel W Li, [1]Paul N Smith, [1]Yongliang Yang, [2]Craig Freeman, [2]Chris R Parish

[1]Trauma and Orthopaedic Research Unit, Department of Surgery, The Canberra Hospital, ACT
[2]Department of Immunology and Genetics, John Curtin School of Medical Research, Australian National University, ACT
email: rachel.li@anu.edu.au

INTRODUCTION

Heparanase (HPSE) specifically degrades heparan sulfate proteoglycans ubiquitously associated with the cell surface and extracellular matrix (ECM) that are capable of initiating signaling pathways [1-2]. However, its effects and mechanism in bone remodeling remains unclear. We sought to determine the effects of exogenous HPSE in stimulation of siHPSE osteoblasts (OBs) and fracture healing *in vivo*.

METHODS

Exogenous HPSE was prepared from human platelets [3]. Its purity and specific activity were verified by Western Blot. Human primary OB cells isolated were treated below: (1) transfected with siHPSE; (2) untransfected; and (3) transfected with siHPSE and exposed to exogenous HPSE. The OBs were cultured for 24, 48 and 96 h. HPSE mRNA expression and osteogenic gene expression were compared to that of non-exogenous HPSE treated cells. Measurements included alkaline phosphatase (ALP) assay, RT-qPCR Array and Western blot, and a fractured femur mouse model for fracture healing.

RESULTS AND DISCUSSION

Upon *HPSE* suppression, cell proliferation and ALP activity in the OB cell culture decreased. The altered OB cell proliferation and ALP activity were reversed by the exogenous HPSE in the siHPSE cells (Figure 1a and b). We found that genes and key proteins in osteogenesis signaling, such as TGFβ1 and receptor, SMAD2, BMP2, MMP9 and ALPL, were up/down regulated by the intervention of exogenous HPSE (Figure 1c and d).

In vivo, histomorphometric measurements using micro-CT showed significant increases in callus area (anterior-posterior, p=0.032), bone volume/tissue volume (BV/TV, p=0.001), and trabecular bone numbers (Tb.N, p=0.003) of fractured femurs in mice with exogenous HPSE treatment compared to the control groups at 7 days post-fracture. At 14 days post fracture the difference was also apparent with the exogenous HPSE treatment group demonstrating a significantly higher BV/TV (p=0.001) Tb.N (p=0.003) than the control groups.

In establishing *HPSE* siRNA human primary OB cells, we have shown that exogenous HPSE stimulates OBs proliferation and differentiation. Our results using the mouse femoral fracture model suggest that a single dose of exogenous HPSE significantly enhances the healing of fracture. Our results indicate that HPSE affects bone formation likely via the TGFβ1/SMAD signalling pathway.

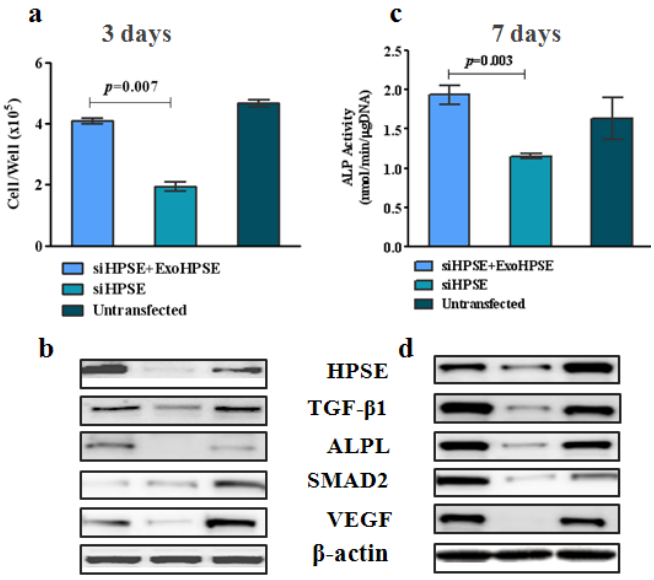

Figure 1: (a). Comparison of cell proliferation of siHPSE OBs treated with exogenous HPSE (3μg/mL) to siHPSE OBs and untransfected OBs at 3days cultures; (b). Protein expression in 3 groups of OBs; (c). Comparison of ALP activity in 3 groups of OBs at 7 days cultures; and (d). Protein expression in 3 groups of OBs at 7 days culture.

CONCLUSIONS

These initial laboratory findings in human bone cell culture systems and in the mouse model support a potential novel therapeutic use of heparanase as an anabolic agent in the treatment of fractures.

ACKNOWLEDGEMENTS

Authors thank the support by AOA Research Foundation Grant and Australian Bone Growth Foundation Grant.

REFERENCES

1. Li RW, et al., *Arthritis and Rheumatism*. **58(6)**:1590-1600, 2008.
2. Smith PN, et al., *J Orhtop Res*. **28**:1315-1322, 2010.
3. Freeman C and Parish CR, *J Biochem*. 330:1341-1350, 1998.

Expression of angiogenic related cytokines in cartilage of osteoarthritis

Xufang Zhang, Indira Prasadam, Ross Crawford, *Yin Xiao

Institute of Health & Biomedical Innovation, Queensland University of Technology, Brisbane, Queensland 4059, Australia.

INTRODUCTION

Inflammation and angiogenesis are closely integrated process in osteoarthritis (OA) [1,2], which involved a broad range of cytokines[3,4]. This study was aimed to investigate the difference of cytokine profiles between OA and normal cartilage, especially focusing on the expression of angiogenic factors.

METHODS

Human knee samples were collected from three OA patients undergoing joint replacement surgery. Proteins and RNA were extracted from normal and OA cartilages. The protein microarray which designed to detect 54 growth factors, cytokines, or chemokines were used to investigate the cytokine expression profiles in OA cartilage. Angiogenesis PCR array were performed to investigate the expression pattern of angiogenic factors in cartilage.

RESULTS AND DISCUSSION

From cytokine array analysis, totally twenty proinflammatory cytokines or chemokines showed significantly increased levels in OA compared to normal cartilage. Several factor related to angiogenesis were highlighted which showed upregulation in OA sample such as PECAM-1, PDGF AA, VE-Cadherin, Tie-2, MMP-9, VEGFR3, IP-10. Gene expression pattern of these angiogenic factors were also upregulated in OA samples demonstrated by PCR array.

CONCLUSIONS

These results suggest that upregulated angiogenic factors contained in cartilage may contribute to the chondrocyte hypertrophy and cartilage degradation.

REFERENCES

1. Suri S, et al. Bone. 2011, doi:10.1016.
2. Fransès R.E, et al. Osteoarthritis Cartilage. 2010, 18(4): 563–571.
3. Ashraf S, et al. Current Opinion in Rheumatology 2008, 20:573–580.
4. Walsh DA, et al. Rheumatology 2010;49:1852–1861.

CONFLICT OF INTEREST DECLARATION

In the interests of transparency and to help reviewers assess any potential bias, ANZORS requires authors of original research papers to declare any competing commercial interests in relation to the submitted work. Referees are also asked to indicate any potential conflict they might have reviewing a particular paper.

If you have accepted any support such as funds or materials, tangible or intangible, concerned with the research by the commercial party such as companies or investors, choose YES below, and state the relation between you and the commercial party.

If you have not accepted any support such as funds or materials, choose NO.

Do you have a conflict of interest to declare? (DELETE TEXT as appropriate)

NO (DELETE all text below)

Lithium (Li)-containing bioactive scaffolds improved cementogenic differentiation of periodontal ligament cells via the activation of Wnt/β-catenin signalling pathway by released Li^+ ions

[1]Pingping Han, [2*]Chengtie Wu, [2]Jiang Chang, [1]*Yin Xiao

1. Institute of Health & Biomedical Innovation, Queensland University of Technology, Brisbane, Queensland 4059, Australia.
2. State Key Laboratory of High Performance Ceramics and Superfine Microstructure, Shanghai Institute of Ceramics, Chinese Academy of Sciences, Shanghai 200050, People's Republic of China.

INTRODUCTION

Lithium (Li) has been widely used as a long-term mood stabilizer in the treatment of bipolar and depressive disorders [1,2]. Li^+ ions are thought to enhance the remyelination of peripheral nerves and also stimulate the proliferation of neural progenitor cells and retinoblastoma cells via activation of the Wnt/β-catenin signalling pathway [3].

METHODS

In this study, we incorporated the Li^+ ions into the mesoporous bioactive glass (MBG) scaffolds and showed that this approach yielded scaffolds with a favourable composition, microstructure and mesopore properties for cell attachment, proliferation, and cementogenic differentiation of hPDLCs. We went on to investigate the biological effects of Li^+ ions themselves on cell proliferation and cementogenic differentiation.

RESULTS AND DISCUSSION

The results showed that Li^+ ions by themselves significantly enhanced the proliferation, differentiation, cementogenic gene expression of PDLCs. Further study demonstrated that 5% Li^+ ions incorporated into MBG scaffolds enhanced the proliferation and cementogenic differentiation of hPDLCs on scaffolds, most likely via activation of Wnt/β-catenin signalling pathway.

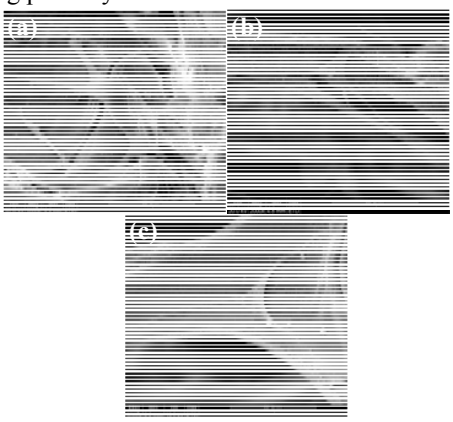

Figure1. The attachment of PDLCs on 0Li-MBG (a), 2Li-MBG (b) and 5Li-MBG scaffolds after culturing for 7 day.

CONCLUSIONS

Our results indicate that incorporation of Li^+ ions into bioactive scaffolds is a viable means of enhancing the Wnt canonical signalling pathway to stimulate cementogenic differentiation of PDLCs.

ACKNOWLEDGEMENTS

Funding for this study was provided by One Hundred Talent Project, SIC-CAS, and ARC Discovery DP120103697.

REFERENCES

1. Cade JFMed J Aust 1949; 2: 349-352.
2. Allagui MS, et al. Neurochem Res 2009; 34: 453-462.
3. Makoukji J, et al. Proc Natl Acad Sci U S A 2012;109: 3973-3978.
4. Hedgepeth CM, et al. Dev Biol 1997; 185: 82-91.

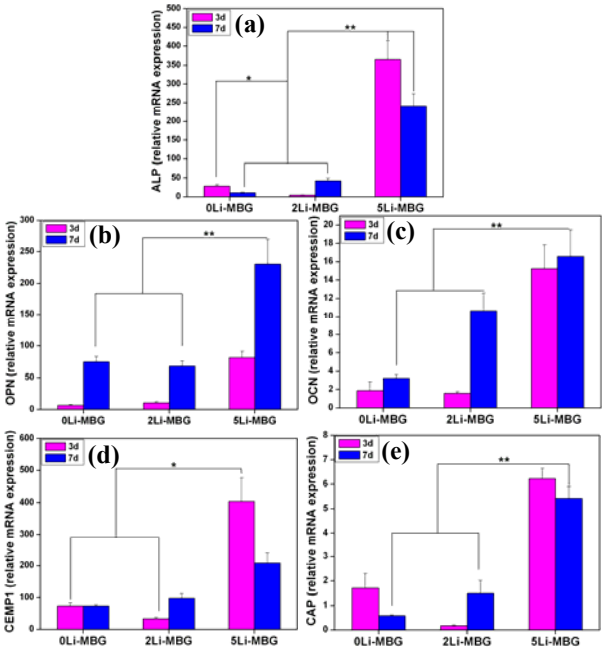

Figure2.The effect of Li contents in MBG scaffolds on bone-related gene expression of ALP (a), OPN (b), OCN (c) and cementum-specific markers of CEMP1 (d) and CAP (e) for hPDLCs.

DESIGN OF PROTEIN-BASED BIOMATERIALS FOR SKELETAL TISSUE ENGINEERING

Sarah C. Heilshorn

Department of Materials Science & Engineering, Stanford University, USA

A key goal in designing biomaterials is to harness the functionality found in nature to create materials that mimic critical components of the natural extracellular matrix (ECM). We design such materials using the tools of recombinant protein engineering to synthesize block-copeptide scaffolds, hydrogels, coatings, and fabrics. Dictating the specific amino acid sequences of these designed proteins affords us molecular-level control to incorporate biochemical and biomechanical elements of natural ECM. In addition, by altering the sequences of the designed proteins, the assembly mechanisms, mechanical properties, and cell-material interactions can be modulated. Given their cytocompatibility and bioactivity, these materials are ideal candidates for use as cell and drug delivery vehicles, implant coatings, and biomaterials for reconstructive surgeries. Two examples of protein-based biomaterials will be discussed: (1) MITCH, a 3D physical hydrogel designed with thixotropic, shear-thinning, and self-healing properties to act as an injectable cell delivery vehicle and (2) an elastin-like, photocrosslinkable biomaterial developed for use as a cell-adhesive, thin film implant coating.

ROLES OF WNT/β-CATENIN SIGNALLING IN BONY REPAIR OF INJURED GROWTH PLATE IN YOUNG RATS

[1]Rosa Chung, [1]Derick SK Wong, [1,2]Carmen E Macsai, [3]Alessandro Piergentili, [3]Fabio Del Bello, [3]Wilma Quaglia, [1,2]Cory J Xian

[1]Sansom Institute for Health Research, and School of Pharmacy & Medical Sciences, University of South Australia, Adelaide, SA
[2]Discipline of Paediatrics, School of Paediatrics and Reproductive Health, University of Adelaide, Adelaide, SA
[3]School of Pharmacy, University of Camerino, Camerino, Italy
email: cory.xian@unisa.edu.au

INTRODUCTION

Growth plate cartilage is responsible for bone lengthening in children, and its injury is often repaired undesirably by bony tissue, which can cause limb length discrepancy and/or bone angulation deformities. Whilst our earlier studies on growth plate injury repair have identified inflammatory, mesenchymal infiltration, osteogenesis and remodeling repair responses, the molecular mechanisms involved in the bony repair remain unknown.

Since the Wnt-β-catenin signalling pathway is known to play a crucial role in the osteogenic differentiation of mesenchymal progenitor cells, this study investigated the potential roles of Wnt-β-catenin signalling pathway in the bony repair of injured tibial growth plate in rats.

METHODS

Proximal tibial growth plate was disrupted centrally (about 30% area) using a dental drill as described [1,2]. Repair tissue within the injury site only was dissected at post-injury days 4, 8, and 14 and was subjected to fixation and processing for paraffin embedding for histological analyses or subjected to RNA isolation, cDNA synthesis, amplification, and Affymetrix gene microarray analysis or quantitative RT-PCR gene expression analysis [3].

To examine potential roles of Wnt/β-catenin signalling pathway in the bony repair of the injured growth plate, β-catenin inhibitor ICG-001 was orally gavaged at 200mg/kg/day to the injured rats till tissue collection on day 10. Treatment effects were examined by quantitative histological image analysis (for proportions of different repair tissues) and by RT-PCR (for expression of osteogenesis or chondrogenesis-related genes). In addition, β-catenin inhibitor ICG-001 was investigated with isolated and cultured normal rat bone marrow stromal cells for its dose-dependent effects in inhibiting expression of β-catenin target genes and on the osteogenic or chondrogenic differentiation potential of the treated stromal cells [4].

RESULTS AND DISCUSSION

Suggestive of a role of Wnt/β-catenin signalling pathway in the early stage of the repair, our Affymetrix gene microarray analysis with RNA isolated from laser-capture microdissected injury site tissue identified an increase in β-catenin and yet a decrease in expression of Wnt signalling inhibitors sFRP1 & 4 at day 4 post-injury vs later time points. Compared to the vehicle control, treatment of the injured rats with the β-catenin inhibitor ICG-001 enhanced collagen-2 gene expression (by qRT-PCR) and increased proportion of cartilage tissue, but decreased level of osterix expression (by qRT-PCR) and amount of bone tissue (by histological analysis), at the injury site by day 10 post-injury (n=8, $P<0.001$). Consistently, in vitro studies with bone marrow stromal cells from normal rats showed that β-catenin inhibitor ICG-001 dose-dependently decreased mRNA expression of β-catenin target genes survin and cyclin-D1 and at 25mM suppressed osteogenic (by CFU-f-ALP assay) but enhanced chondrogenic (by pellet culture) differentiation of the treated bone marrow stromal cells.

CONCLUSIONS

Our data suggest that Wnt-β-catenin signalling promotes osteoblast differentiation and suppresses chondrogenic differentiation during bony repair of the injured growth plate, and intervention of this signalling could represent a potential approach in enhancing cartilage regeneration and preventing the faulty bony repair after growth plate injury.

ACKNOWLEDGEMENTS

This work was funded in part by project grants from NHMRC, Bone Growth Foundation, and Channel-7 Children's Research Foundation. CM was a recipient of PhD Scholarship of University of Adelaide. CJX is a recipient of NHMRC Senior Research Fellowship.

REFERENCES

1. Xian CJ, Zhou FH, McCarty RC, & Foster BK (2004). Intramembranous ossification mechanism for bone bridge formation at the growth plate cartilage injury site. *J Orthop Res* 22, 417-426.
2. Zhou FH, BK Foster, XF Zhou, CJ Xian (2006). TNF-α mediates p38 MAP kinase activation and negatively regulates bone formation at the growth plate injury site in rats. *J Bone Miner Res* 21, 1075-1088
3. Macsai CE, Georgiou KR, Zannettino AC, Foster BK, Xian CJ (2012). Microarray expression analysis of genes and pathways involved in growth plate cartilage injury responses and bony repair. *Bone* 50, 1081–1091
4. McCarty RC, Gronthos S, Zannettino AC, Foster BK, Xian CJ (2009). Characterisation and Developmental Potential of Ovine Bone Marrow Derived Mesenchymal Stem Cells. *J Cell Physiol* 219: 324-33

SESSION 6 - ABSTRACTS

ECR Award

DAY 3: Saturday, 1 September

11:00 AM – 12:25 PM

TNF-α Preconditioning Promotes Osteogenic Differentiation of Adipose-derived Mesenchymal Stem Cells by Modulating BMP-2 Signalling Pathway

Lu ZF[1], Wang GC[1], Dunstan C[1], and Zreiqat H[1]

[1.] *Biomaterials and Tissue Engineering Research Unit, School of AMME, the University of Sydney, Sydney, 2006, Australia*

email: zufu.lu@sydney.edu.au

INTRODUCTION

Mesenchymal stem cells (MSCs) hold a great promise for tissue repair or regeneration, while there are still lacking the safe and effective strategies to direct MSCs into osteogenic lineage for the ultimate clinical applications. Pre-conditioning of MSCs by some factors such as growth factors may overcome the concerns of dosage or safety using traditional gene therapy strategy or drug delivery, while still effective in improving the efficacy of MSCs for tissue repairing or regeneration.

The aim of this study was to investigate whether tumour necrosis factor-α (TNF-α) preconditioning is capable of directing adipose tissue-derived mesenchymal stem cells (ASCs) into osteogenic differentiation and its underlying mechanisms.

METHODS

First, after ASCs were treated with TNF-α (1 ng/ml) for three days, the medium containing TNF-α was replaced with normal growth medium and ASCs were then cultured for up to 14 days and osteogenic gene expression (collagen I, Runx2, osteopontin and osteocalcin) and alkaline phosphatase (ALP) activity of ASCs were analyzed in the ASCs at day 4 and 14. Second, bone morphogenetic protein-2 (BMP-2) protein expression was measured in ASCs in the presence of TNF-α, and the osteogenic differentiation of ASCs induced by TNF-α pre-conditioning was investigated when BMP-2 expression in ASCs was knocked down by transfecting BMP-2 siRNA into ASCs. ASCs were also pre-conditioned by three days of BMP-2 (50 ng/ml) to investigate its effect on osteogenic differentiation of ASCs. In addition, phosphorylated and total Smad1/5 proteins were measured by western blot in the presence and after the withdrawal of TNF-α. Finally, phosphorylated and total erk1/2 and p38 mitogen-activated protein kinase (MAPK) proteins were measured in the presence of TNF-α, and the effects of inhibition of erk1/2 (PD09059) and p38 (SB203580) signaling pathways in ASCs on BMP-2 induction as well as the osteogenic induction by TNF-α pre-conditioning were investigated.

RESULTS AND DISCUSSION

Three days of TNF-α pre-conditioning significantly increased collagen I, Runx2, osteopontin and osteocalcin gene expression and ALP activity of ASCs after 4 and 14 days of culturing following the withdrawal of TNF-α pre-conditioning, and TNF-α significantly induced BMP-2 protein expression in ASCs while blocking BMP-2 expression by siRNA partially inhibited the osteogenic differentiation of ASCs induced by TNF-α pre-conditioning; three days of BMP-2 pre-conditioning also significantly increased osteogenic gene expression and ALP activity of ASCs after 4 and 14 days of culturing but their expression levels were significantly lower than those induced by TNF-α pre-conditioning **(Fig.1)**. In addition, TNF-α directly inhibited Smad1/5 signaling pathway despite elevated BMP-2 protein expression in ASCs. Finally, we showed that TNF-α promoted erk1/2 and p38 mitogen-activated protein kinase (MAPK) signaling pathways, but only the inhibition of erk1/2 signaling pathway in ASCs reduced BMP-2 induction as well as the osteogenic induction by TNF-α pre-conditioning **(Fig.2)**.

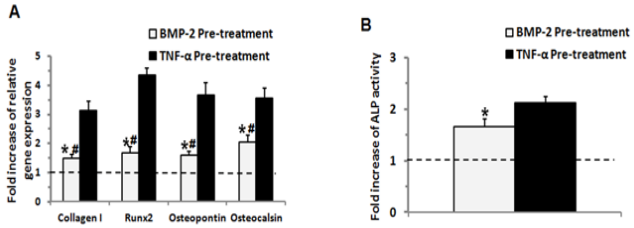

Figure 1 The effects of TNF-α and BMP-2 pre-conditioning on osteogenic differentiation of ASCs. *Dash line: control (no TNF-α or BMP-2 preconditioning); *: compared with control, P<0.05; #: compared with BMP-2 preconditioning, P<0.05;*

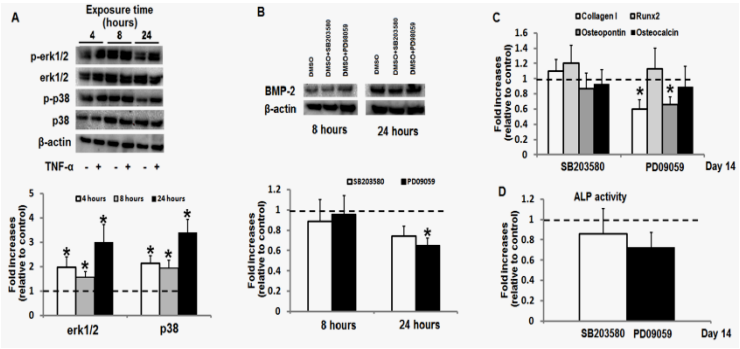

Figure 2 The roles of* erk1/2 and p38 signaling pathways in *TNF-α preconditioning-induced osteogenesis of ASCs. *A: TNF-α promoted erk1/2 and p38 signaling pathways, Dash line: control (no TNF-α preconditioning); B: Only the inhibition of erk1/2 signaling pathway partially reduced BMP-2 induction as well as the osteogenic induction by TNF-α pre-conditioning; dash line: control (no inhibitors); *: compared with control, P<0.05;.*

CONCLUSIONS

It was concluded that TNF-α preconditioning promotes osteogenic differentiation of ASCs at least in part by modulating BMP-2 signalling. TNF-α preconditioning might serve as an effective strategy to direct stem cells into osteogenic lineage for clinical applications.

ACKNOWLEDGEMENTS

The authors acknowledge the Australia National Health and Medical Research Council (NHMRC) for endowing my Early Career Fellowships (ECFs, 2012-2015) and its funding for the research. The authors also acknowledge Rebecca Cooper Foundation.

HIGH-RESOLUTION MICRO-CT EXAMINATION OF HUMAN BONE: TOWARDS THE ENTIRE ORGAN

[1]Egon Perilli, [2,3]Ian H Parkinson, and [1]Karen J Reynolds

[1]Medical Device Research Institute, School of Computer Science, Engineering and Mathematics, Flinders University, SA
[2]Bone and Joint Research Laboratory, SA Pathology and Hanson Institute, SA
[3]Discipline of Anatomy and Pathology, The University of Adelaide, SA
email: egon.perilli@flinders.edu.au

INTRODUCTION

Micro-CT systems are available that facilitate *ex vivo* examinations of human bones as large as entire vertebrae, with spatial resolutions in the 10-micrometer range. Accurate 3D-description of the microarchitecture of entire organs can be obtained, at resolutions previously achievable only on biopsies [1,2]. These high-resolution scans produce large datasets, with costs and benefits, which have to be considered.

The aim of this study is to present whole human vertebrae scanned at high resolution (17 µm/pixel). The datasets were down-sampled to 34 and 68 µm pixel size, their morphometric parameters compared to those at 17 µm pixel size, and discussed in relation to data size and calculation time.

METHODS

Five human L3 vertebrae were used, from 5 cadavers. Posterior vertebral elements were removed. Scans were performed with an *in vivo* micro-CT system (model 1076, Skyscan NV, Kontich, Belgium), at 17.4 µm isotropic pixel size [1]. For each vertebra, the full height (32 mm) was reconstructed (68x68 mm cross-sections). The computer was equipped with two dual-core Intel Xeon CPUs, each at 3.00 GHz, 4 GB memory, OS Windows XP 64 bit. Morphometric parameters were calculated over the entire vertebra, using 3D-methods [1]: trabecular bone volume fraction (BV/TV), trabecular thickness (Tb.Th), trabecular separation (Tb.Sp), structure model index (SMI), cortical thickness (Ct.Th).

Next, vertebral datasets were down-sampled by a factor of two and four (34 and 68 µm/pixel), and the 3D-morphometric parameters recalculated. To test for changes in morphometric values at varying pixel size, ANOVA for repeated measures was performed. Where statistical significance was found, a paired t-test between morphometric data at lower resolutions (34 and 68 µm/pixel) and highest resolution (17 µm/pixel) was performed. Significance level was set to $p = 0.05$.

RESULTS AND DISCUSSION

High-resolution imaging of entire vertebrae produced large datasets (26 GB, Tab.1). Down-sampling of the datasets did substantially reduce calculation times for 3D-analysis, from days to minutes (Tab.1).

Table 1: Data size and calculation times at varying pixel sizes, per vertebra.

Pixel size:	17 µm	34 µm	68 µm
Entire vertebra, dataset size:	26.4 GB	3.3 GB	423 MB
3D morphometry, calculation times:	5 days	114 min	5 min

The 3D-morphometric parameters for both trabecular and cortical bone showed significant monotonic changes at varying pixel size, compared to 17 µm/pixel data ($p < 0.05$) (Fig.1). The biggest changes were found for Ct.Th, Tb.Th, and Tb.N (+56%, +53%, and -45%, at 68 µm/pixel).

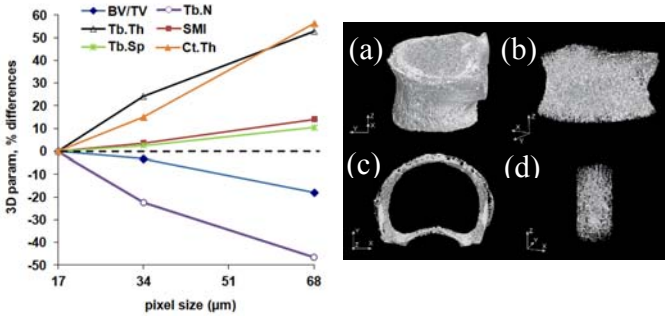

Figure 1: Left: Percentage changes of 3D-morphometric parameters at varying pixel size, with reference to 17µm/pixel. Right: (a) Micro-CT 3D-rendering of a vertebral body, (b) trabecular bone, (c) cortical bone, (d) virtual cylindrical trabecular bone biopsy.

CONCLUSIONS

As shown in this study, high-resolution micro-CT imaging of entire vertebrae produces large datasets, challenging for 3D-analysis. Down-sampling introduced losses in accuracy in morphometric parameters, as expected [3]. Nonetheless, down-sampling was very effective in speeding up calculations.

One might ask whether it is really necessary to use a high-resolution micro-CT scan (17 µm/pixel), if data might later be down-sampled, for practicality [1]. The answer depends on the research question, the minimum acceptable error for the study purpose, and on computational resources available.

High-resolution micro-CT scans of entire bones give freedom of choice: regions of interest can be extracted *ad hoc*, ranging from the whole organ to sub-volumes of various sizes and shapes, virtual biopsies (Fig.1, right). High-resolution scans ensure higher accuracy even after down-sampling, compared to low-resolution scans with similar large pixel size [3]. This confirms high-resolution micro-CT as an invaluable tool for bone investigations in 3D.

REFERENCES

1. Perilli E, et al., *Ann Ist Super Sanita.* **48:**75-82, 2012.
2. Perilli E, et al., *Bone.* **50:**1416-25, 2012.
3. Kim DG, et al., *Bone.* **35:** 1375-82, 2004.

COMPARISON OF TWO TYPES OF EXERCISE FOR PROMOTING BONE GROWTH IN THE FEMORAL NECK

[1]Saulo Martelli, [1]Mariana E. Kersh, [1]Anthony G. Schache, [1]Marcus Pandy

[1]Department of Mechanical Engineering, University of Melbourne, Australia
email: saulo.martelli@unimelb.edu.au

INTRODUCTION

Osteoporosis, falls and related fragility fractures are public health problems affecting an increasing number of individuals every year. There is evidence that bone loads induced by physical exercises can counteract the bone resorption process. To date, physical exercises are widely recommended to mitigate the detrimental effect of osteoporosis but no consensus can be found in the literature on the recommended exercises and the frequency required [1]. In this context, a clear understanding of the mechanical stimulus for bone apposition induced by different motor tasks might help the design of more effective exercise protocols. The aim of this study was to compute and compare the mechanical stimulus for bone apposition in two types of exercise: 1) single-joint exercises performed in the anatomical planes of motion; and 2) weight-bearing exercises typically recommended for post-menopausal women with severe osteoporosis.

METHODS

Medical image and dissection data available from a public data collection (www.physiomespace.com) were used to create a patient-specific musculoskeletal model of the lower limb and a finite element (FE) model of the proximal femur using MR, CT and dissection data obtained from one osteoporotic subject (female, 81 yr, 63 kg, 167 cm) (Figure 1). The musculoskeletal model was generated during a previous study from the full-body dissection data and validated by common procedures. Two different models were generated by assuming the highest and the lowest muscle tetanic stress within the published range. The FE model of the right femur was created from computer-tomography images following a well-established procedure [2].

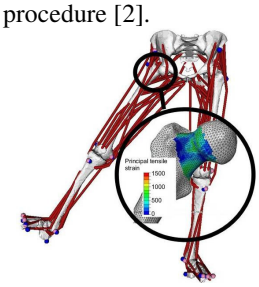

Figure 1: Patient-specific lower-limb musculoskeletal model and FE model of the proximal femur used in this study.

Joint motion and ground reaction forces were recorded from a body-matched volunteer (female, 25 yr, 57kg, 165cm) during walking, stair rising and descending, chair up, step up and down and squatting. Exercises in the anatomical planes (hip adduction, abduction, flexion, extension and, knee extension and flexion) were studied by applying a resistance load that induced maximal muscle activation. The forces acting on the femur were computed using Opensim. Strain energy stored in the femoral neck was used as an indicator of the mechanical stimulus for bone apposition [3]. Peak principal tensile strain was used as an indicator of bone fracture [2]. All analyses were solved with Abaqus© (Dassault Systèmes Inc., USA).

RESULTS AND DISCUSSION

We found that different activities can stimulate bone apposition in different ways (Figure 2). Knee flexion had the highest potential to stimulate bone apposition. However, resisted motions of knee flexion and hip extension may contribute to osteoporotic bone fracture, more likely at the extremes of joint range of motion and for physiologically strong muscles. Therefore, extreme ranges of joint motion should be avoided during these exercises, and a through estimation of muscle strength is important in patient-specific analyses. For movements below the fracture threshold, resisted hip adduction in average resulted in the lowest strains while inducing a consistent mechanical stimulus for bone apposition (149 mJ). Further research is necessary to elucidate the mutual interactions between bone quality, muscle strength and anatomy.

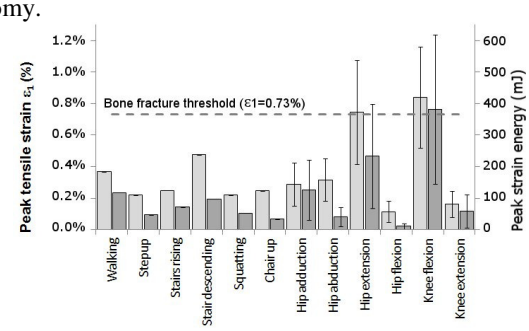

Figure 2: Peak values during motion of bone strains and neck strain energy. The error bar represents extreme values obtained for extreme muscle tetanic stresses.

CONCLUSIONS

The current analysis suggests that it is possible to design dedicated training protocols to maximize bone apposition while minimizing the risk of bone fractures.

REFERENCES

1. Nikander, et al., *BMC Medicine*, **8**:47, 2010
2. Schileo, et al., *J Biomech*, **41**:356-67, 2008
3. Huiskes, et al., *J Biomech*, **20**:1135-50, 1987

Strontium increases the bioactivity and degradability of magnesium silicate based scaffolds

[1]Seyed-Iman Roohani-Esfahani, [2]Kai Yuen Wong, [1]Zufu Lu, [1]Jiao Jiao Li, [1]Colin R Dunstan and [1]Hala Zreiqat

[1]Tissue Engineering & Biomaterials Research Unit, School of AMME/Faculty of Engineering and IT and Bosch Institute, The University of Sydney, NSW
[2]The Imperial College of Science, Technology and Medicine, United Kingdom
Email: iman.roohani@gmail.com

INTRODUCTION

Silicon (Si), magnesium (Mg) and strontium (Sr), are the essential elements in skeletal development found to be uniquely localized in the active areas of new bone and involved in the early stage of bone calcification. Magnesium silicate (Mg_2SiO_4) (FS) ceramic has been introduced as a potential biomaterial for bone regeneration. However its low degradation rate compromises its ability to release bioactive ions. The aim of this study was to introduce Sr to the FS ceramic to enhance its bioactivity and degradability.

METHODS

The pure FS powder and Sr doped FS powders (Table 1) were prepared by the sol-gel method. Scaffolds with 85% porosity and pore size of 500µm were fabricated by the polymer sponge method Beta-tricalciumphoshate/Hydroxyapatite (TCP/HA) scaffolds were used as a control for biological studies. In vitro investigation of cytocompatibility and bioactivity of FS and Sr doped FS scaffolds were assessed using of primary human osteoblast cells (HOBs).

Table 1: Designation of the prepared scaffolds.

	FS	FS1	FS2	FS5	FS10	FS20
Sr content(mol%)	0	1	2	5	10	20

RESULTS AND DISCUSSION

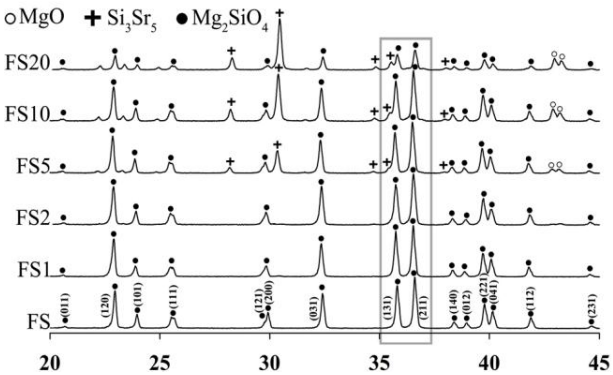

Figure 1. X-ray diffraction and crystal refinement analysis of the FS and Sr doped FS scaffolds

X-Ray diffraction analsyis demonstates that pure FS has been successfully prepared (Fig 1). Doping Sr (> 2 Mol%) resulted in the formation of MgO and Si_3Sr_5 phases. 5% Sr doping maintained the phase composition however the shift to the left in the peaks indicated an increase in volume and planar distances of FS crystals.

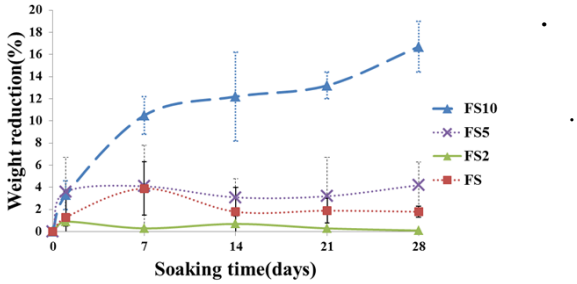

Figure 2: Weight reduction of FS and Sr doped FS scaffolds at simulated body fluid.

Doping of Sr (10 mol%) into the FS structure (FS10) significantly enhanced the degradability of the scaffolds. Furthermore, HOB cultured on the (FS10) scaffolds displayed significantly higher expression levels of Runx2, osteopontin, BSP and osteocalcin (Fig. 3) compared to other groups tested on day 7 ($p<0.05$). FS scaffolds displayed higher expression levels of Runx2, BSP and osteocalcin genes compared to TCP/HA groups on day 3 and day7 ($p<0.05$).

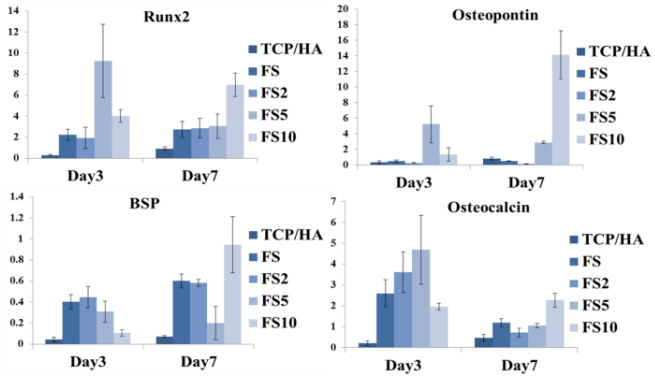

Figure 3. Osteogenic gene expression profile for FS and Sr doped scaffolds compared to TCP/HA scaffolds. (Y-axis denotes "relative gene expression (/GAPDH)".

CONCLUSIONS

The Strontium doped Mg_2SiO_4 scaffolds displayed dramatic increase in in vitro bioactivity, and degradation rate compared to the Mg_2SiO_4 scaffolds. Doping 10 mol% Sr in FS (FS10) resulted in formation of a new degradable magnesium silicate based scaffold able to release bioactive ions (Mg, Si and Sr) into aqueous environments. FS10 scaffolds showed the strongest osteoblast differentiation profile in comparison to other scaffolds.

Moving Towards Population Based Computational Modelling of Total Joint Replacement

[1]Mark Taylor

[1]Medical Device Research Institute, School of Computer Science, Engineering and Mathematics, Flinders University, SA
Email: mark.taylor@flinders.edu.au

It is becoming increasingly difficult to differentiate the performance of new hip and knee replacement designs using current pre-clinical test methods. The majority finite element studies are performed on a representative subject's anatomy, with optimal implant placement, subjected to idealised loading conditions. Extrapolating these results to the larger patient population is unlikely to predict the potential risk of failure. There are significant differences between patients and accounting for anatomical variability is likely to lead to a better assessment of the risk of failure.

To date, the barrier to multi-subject FE studies has been the model generation process and this has limited the majority of studies to examining just a single bone segment. Multi-subject specific finite element studies have been performed on the intact femur, mainly investigating the risk of femoral neck fracture and have generated a few 10's of models. Only two studies have examined 100's of subjects to explore factors influencing fracture risk using cohorts of living subjects [1, 2]. In comparison, truly subject specific, multi model studies of implanted bone segments are rarer. This has been primarily due to the additional work required to align the prosthetic components and perform the Boolean operations to virtually implant the prosthesis into the bone. For example, Radcliffe and Taylor [3] adopted the brute force approach to generated 16 implanted proximal femur models and investigate the effect of cement mantle thickness and implant position on the performance of femoral head resurfacing.

In pre-clinical testing of joint replacement, the shift from a patient specific study to a population based study is significant. Population based studies offer the opportunity to identify patient factors, such a weight, loading, bone quality, bone size or anatomical features, as well as, the influence of implant design and surgical parameters on the performance of total joint replacement. An alternative approach to manually creating a database of subject specific bone models is to develop a statistical shape and intensity model (SSIM) of a bone segment, which is capable of describing the variation in both geometry and material property distribution based on a limited initial training set. This can then be used to synthetically generate new instances and has the potential to generate thousands of representative models from a much smaller training set. To date, there have only been a few studies which have used SSIM's to analysis the behaviour of an intact or implanted bone segment. This technique was successfully applied to study the risk of femoral neck fracture [4]. A population of 1000 femurs were synthetically generated, based on an initial training set of 21 femur models. The study simulated the impact of an oblique fall to the side. FE model generation, application of subject specific loading and boundary conditions, FE processing and post processing of the solutions were completed automatically. Based on an arbitrarily defined failure criteria, an at risk group of femurs was shown to have statistically different cortical bone volume, cortical bone modulus, neck shaft angle and anteversion angle as compared to a not at risk group.

A logical progression of this methodology is to convert these intact femurs into implanted models, thus providing a way for interpatient variability to be included in orthopaedic implant testing. In smaller scale studies, this can be done manually, although it is tedious. However, in studies comprising 100's to potentially 1000's of analyses, this simply becomes impractical. Bryan et al. [5] developed a fully automated methodology was devised to implant a resurfacing component into any given femur geometry. To find the correct implant size and alignment, algorithms were implemented to determine the diameter and centre of the femoral head and the axis of the femoral neck. The study then investigated the influence of head size on the early risk of fracture, as evidence from the Australian Joint Registry [6] has shown that there is a higher risk of failure in the first 6 post-operative months associated with small sized components. Using the population based analysis, Bryan et al. [5] was able to demonstrate that small femoral heads had elevated superior neck strains, which may contribute to the higher incidence femoral neck fracture.
It should be noted that SSIM's have their limitations, for example if you wish to study the behavior of osteoporotic femurs, the SSIM needs to be train using an osteoporotic population. However, coupled with the probabilistic techniques, SSIM's offers a potentially powerful tool for assessing the next generation of implant designs.

REFERENCES

1. Orwoll, E.S., et al., J Bone Miner Res, 2009. 24(3): p. 475-83; 2. Keyak, J.H., et al., Bone, 2011. 48(6): p. 1239-1245. 3. Radcliffe, I.A.J. and M. Taylor, Clinical Biomechanics, 2007. 22: p. 422-430; 4. Bryan, R. et al., J Biomech, 2009. 42(13): p. 2171-6; 5. Bryan, R., P.B. Nair, and M. Taylor, Journal of Biomechanics, 2012. 45: p. 1952-1958; 6. Australian Orthopaedic Association National Joint Replacement Registry Annual Report, 2008: Adelaide.

LOWER LIMB BIOMECHANICAL CHANGES THAT IMPAIR GAIT PERFORMANCE FOLLOWING TOTAL KNEE REPLACEMENT SURGERY

[1,2]Pazit Levinger, [2]Hylton B Menz, [2]Adam D Morrow, [3]John R Bartlett, [2]Julian A Feller and [3]Neil R Bergman

[1]Institute of Sport, Exercise and Active Living, Victoria University, VIC
[2]Musculoskeletal Research Centre, Faculty of Health Science, La Trobe University, VIC
[3]Warringal Private Medical Centre, VIC
email: pazit.levinger@vu.edu.au

INTRODUCTION

Normal biomechanical function of the knee during walking may not be fully restored in people following total knee replacement (TKR) and therefore compensation in other lower limb joints may occur. However, the mechanism causing gait changes in older people following TKR has been inadequately addressed, with most studies focusing on the knee joint only. Given the importance of maintaining adequate mobility in older people following TKR, identifying specific gait impairments following surgery may also help improve rehabilitation strategies. The purpose of this study, therefore, was to identify biomechanical changes in the lower limb in the sagittal plane that impair gait performance following TKR.

METHODS

Thirty two patients scheduled for TKR surgery (mean ± SD age 68.0 ± 6.4 years, height 167.7 ± 8.7 cm, mass 85.3 ± 12.7 kg and body mass index (BMI) of 30.4 ± 5.0 kg/m^2) were tested before surgery and at 12 months post-surgery. Twenty eight aged matched asymptomatic controls were also tested (mean ± SD age 65.1 ± 11.2 years, height 168.8 ± 10.5 cm, mass 72.6 ± 16.8 kg and BMI of 25.3 ± 4.5 kg/m^2). Gait analysis was performed using a 3D motion analysis system (VICON, Oxford Metrics) with ten camera (100HZ) and two (1000Hz) force plates. Lower limb kinematics and kinetics including motion, moments (%BW*H) and powers (W/kg) of the hip, knee and ankle in the sagittal plane were extracted. Assessment of physical function, pain and stiffness was also documented using the Western Ontario and McMaster University Osteoarthritis Index (WOMAC) and compared between pre and post-surgery using Paired t-tests. Comparisons were made for all selected gait variables between the groups at baseline (control vs surgical group pre-operatively) and at 12 months (control vs surgical group post-operatively) and within the surgical group (pre vs post-operatively) using a mixed-design ANOVA, with one fixed factor (surgical or control group) and one repeated measure (pre- and post-surgery gait pattern). Analysis of variance with Bonferroni-adjusted post-hoc tests were used to assess the differences for the gait variables with gait velocity entered as a covariate.

RESULTS AND DISCUSSION

Generally, no significant changes in temporo-spatial parameters, knee joint kinematics and kinetics during gait were observed in the surgical group following surgery, despite improvements in pain (180.6 ± 94.5 pre vs 152.1 ± 251.3 post; $p = 0.013$) and self-reported function (594.6 ± 315.0 pre vs 126.2 ± 151.4 post; $p < 0.001$). Only knee flexion moment significantly increased following the surgery (2.27 ± 1.33 vs 3.20 ± 1.22; $p = 0.029$). Changes in ankle joint moments were observed following the surgery, with increases in peak plantarflexion (-0.86 ± 0.31 vs -1.22 ± 0.38; $p = 0.001$) and dorsiflexion (7.41 ± 0.99 vs 8.22 ± 1.07; $p = 0.005$) moments and ankle power generation during push off (2.80 ± 0.87 vs 3.70 ± 0.98; $p<0.001$). It is possible that the ankle joint compensated for the impaired knee function to increase forward momentum and allow sufficient power generation for propulsion. Following the surgery, the surgical group showed reduced peak knee extension motion (8.89 ± 5.55° vs 1.83 ± 4.63°; $p = 0.002$), peak knee extension moment (-0.77 ± 1.03 vs -1.97 ± 0.88; $p = 0.002$) and peak knee power absorption (-1.09 ± 0.40 vs -1.70 ± 0.43; $p = 0.029$) during stance compared to the control group. Significantly greater ankle dorsiflexion motion was also observed for the surgical group compared to the control group (17.26 ± 2.68° vs 14.37 ± 2.58°; $p = 0.005$).

CONCLUSIONS

Several biomechanical changes in the knee and ankle were identified in the surgical group before and following TKR compared to the control group. Differences in gait parameters observed at the knee may arise as a result of the presence of osteoarthritis and mechanical changes associated with TKR as well as retention of the pre-surgery gait pattern. Consequently, the gait alterations observed at the ankle joint may be a compensatory response to facilitate forward momentum and allow sufficient power generation for propulsion. This highlights the potential role the ankle joint plays in compensating for the impaired knee function before and following the surgery. Rehabilitative strategies may therefore need to focus not only on improving knee function, but also on distal joints function and gait retraining to optimise recovery following TKR.

ACKNOWLEDGEMENTS

This study was funded by the Clive and Vera Ramaciotti Foundation and the Arthritis Foundation of Australia. PL is currently funded through the Australian Government's Collaborative Research Networks program. HBM is currently a National Health and Medical Research Council Senior Research Fellow (ID: 1020925).

SESSION 7 - ABSTRACTS

Biomaterials & Tissue Engineering

DAY 3: Saturday, 1 September

1:20 PM – 2:30 PM

Human adult mesenchymal stem cell cultivation on a Bio-Oss hydroxyapatite matrix

[1]Jaydeep Ubeja, [1]Ashvind Prabahran, [1]Lipi Shukla, [1]Qin Liu, [2]Frauke Warnke, [1]Patrick Warnke
[1]Faculty of Health Sciences and Medicine, Bond University, Gold Coast, Australia
[2]School of Dentistry, Griffith University, Gold Coast, Australia
Email: jaydeep.ubeja@hnehealth.nsw.gov.au

INTRODUCTION

In recent times mesenchymal stem cells have been incorporated as part of an emerging concept known as *tissue engineering*[3]. This involves the use of artificial or inert scaffold materials and living cells, with an aim to grow the desired osseous tissue with its characteristic biological function.

Bio-Oss is a natural granular form of hydroxyapatite matrix derived from bovine cancellous bone[1,4]. In the practice of orthopaedic surgery, it is used in the promotion of osteoblastic activity at a site where an osseous defect or injury is present. It has an especially effective role in the promotion of fracture healing whereby there is regeneration and restoration of the structural and functional stability of damaged osseous tissue[2].

The aim here was to evaluate the ability for human adult mesenchymal stem cells to be cultivated on a Bio-Oss hydroxyapatite matrix.

METHODS

Primary human mesenchymal stem cells (MSCs) were cultured with DMEM media containing 10% Fetal Calf Serum and 1% Penicillin/Streptomycin over 16 days. The media was changed every second day to promote cell survival. Human mesenchymal stem cells were cultured on scaffolds of Bio-Oss for 10 days with a WST proliferation test used to measure cellular proliferation at days 3, 7, and 10. A comparison was made against cells cultured on scaffolds of synthetic hydroxyapatite matrix, as well as those cells cultured without scaffolds as an effective control group. Light microscopy was used to assess cellular behaviour over this time.

RESULTS AND DISCUSSION

Figure 1 on the opposite column provides the cumulative data gathered from the WST tests.

As has been demonstrated by the graphs, the overall values suggest that there is limited proliferation of Bio-Oss when compared against the synthetic hydroxyapatite matrix (HAP), control, and blank groups.

The WST tests do illustrate that the Bio-Oss scaffold does allow for cellular proliferation. It is limited when compared against the synthetic hydroxyapatite matrix and control groups in particular.

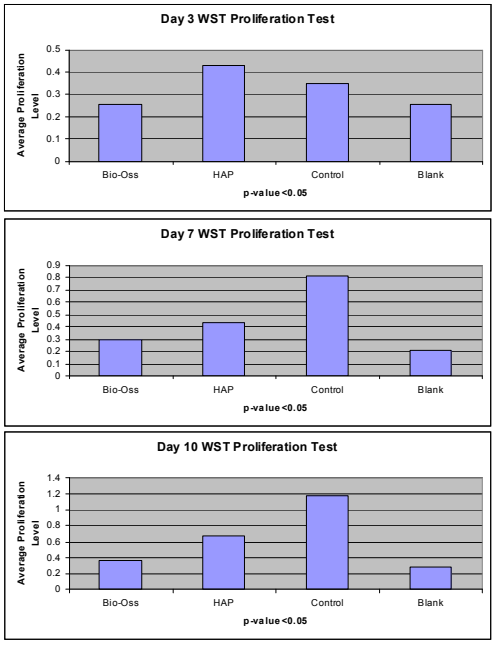

Figure 1: Collective WST proliferation results for study. Y axis indicates the average proliferation levels.
P value given for difference between control and Bio Oss

CONCLUSIONS

The findings from the study may indicate a limited effectiveness of Bio-Oss as a scaffold but further investigation would still be required including in-vivo based tests.

REFERENCES

1) Warnke PH, Seitz H, Warnke F, Becker ST, Sivananthan S, Sherry E, Liu Q, Wiltfang J, Douglas T
Ceramic scaffolds produced by computer-assisted 3D printing and sintering: Characteristics and Biocompatibility Investigations J Biomed Mater Res B Appl Biomater **93**(1):212-7, 2010.

2) Alwatter BJ, Schwarzkopf R, Kirsch T
Stem cells in orthopaedics and fracture healing Bull NYU Hosp Jt Dis **69**(1):6-10, 2011

3) Tuan RS, Boland G, Tuli R
Adult mesenchymal stem cells and cell based tissue engineering Arthritis Res Ther **5**(1):32-45, 2003

4) Liu Q, Douglas T, Zamponi C, Becker ST, Sherry E, Sivananthan S, Warnke F, Wiltfang J, Warnke PH
Comparison of in vitro biocompatibility of NanoBone and Bio Oss for human osteoblasts Clin Oral Implants Res **22**(11):1259-64, 2011

TOPOGRAPHICALLY AND CHEMICALLY MODIFIED TITANIUM IMPLANT SURFACES INITIATE DIFFERENTIAL REGULATION OF MICRO-RNAS IN OSTEOBLASTS

[1]Nishant Chakravorty, [2]Saso Ivanovski, [1]Anjali Jaiprakash, [1,3]Ross Crawford, [1]Adekunle Oloyede and [1]Yin Xiao

[1]Institute of Health and Biomedical Innovation, Queensland University of Technology, Australia
[2]School of Dentistry and Oral Health, Centre for Medicine and Oral Health, Griffith University, Australia
[3]Prince Charles Hospital, Brisbane, Queensland, Australia
email: n.chakravorty@qut.edu.au

INTRODUCTION

Titanium implants are commonly used in orthopedics and dentistry to provide a supporting framework for restoration of fractures or replacing missing teeth. Micro-roughened and chemically modified titanium implant surfaces like the sand-blasted, large grit, acid etched (SLA) and modSLA (hydrophilic SLA) titanium implant surfaces are recognized to have improved osseointegration and osteogenic properties [1, 2]. However, the molecular mechanisms responsible for these observations have remained a challenge to interpret. Studies on the molecular regulation of these properties have demonstrated the up-regulation of the TGFβ/BMP and Wnt (especially Wnt/Ca^{2+}) pathways, early in the process of osteogenic differentiation on these surfaces [3,4]. MicroRNAs (miRNAs) are vital regulators of the differentiation process [3] that influence gene expression by translational repression and gene silencing [4]. This study aimed to determine whether modSLA and SLA surfaces regulate these small RNAs differentially in osteoprogenitor cells that eventually lead to differential regulation of TGFβ/BMP and Wnt/Ca^{2+} pathways.

METHODS

Primary human osteoprogenitor cells established from redundant alveolar bone tissue obtained following third molar extraction surgery were used for this study. The osteogenic potential of the cells was confirmed using ALP activity and Alizarin Red-S staining. The effect of smooth (SMO), SLA and modSLA surfaces on the TGFβ/BMP (BMP2, BMP6, ACVR1) and non-canonical Wnt/Ca^{2+} (WNT5A, FZD6) pathways, as well as the integrins (ITGB1, ITGA2) was determined using quantitative real time polymerase chain reaction (qPCR). The expression pattern of miRNAs related to cell development and differentiation was evaluated after 24 hours of culture and statistically significant miRNAs (p-value <0.05, fold-change beyond +/-2) were identified. Target predictions for the differentially regulated miRNAs were performed using TargetScan [5]. The predicted targets were screened for genes related to TGFβ/BMP and Wnt/Ca^{2+} pathways (for down-regulated miRNAs) and inhibitors of osteogenesis (for up-regulated miRNAs).

RESULTS AND DISCUSSION

The osteogenic potential of the osteoprogenitor cells and the ability of the modified titanium surfaces to induce the expression of TGFβ/BMP and non-canonical Wnt/Ca^{2+} signaling genes were confirmed. The relative expression of the genes (BMP2, BMP6, ACVR1, WNT5A, FZD6, ITGB1, and ITGA2) was higher on modSLA and SLA surfaces than on SMO. The miRNA expression profiling revealed 35 miRNAs on modSLA and 32 miRNAs on SLA surfaces to be down-regulated (compared with SMO). Among these, 31 miRNAs were common to both modSLA and SLA. There were 10 miRNAs up-regulated on modSLA and 9 on SLA surfaces, amongst which 8 were the same as observed on modSLA. Relatively minor differences were observed between modSLA and SLA. TargetScan predictions for potential targets for the down-regulated miRNAs identified several genes of the TGFβ/BMP and Wnt/Ca^{2+} pathways. Osteogenesis inhibitors were predicted as targets for up-regulated miRNAs.

CONCLUSIONS

This study demonstrated the influence of topographically and chemically modified titanium surfaces on the expression profile of miRNAs in osteoprogenitor cells. The majority of the miRNAs were down-regulated in response to the SLA and modSLA surfaces compared to the SMO surfaces, with only relatively minor differences observed between SLA and modSLA. Screening of the predicted gene targets for the differentially regulated miRNAs revealed that modified titanium implant surfaces induce down-regulation of miRNAs potentially regulating the TGFβ/BMP and WNT/Ca^{2+} pathways during osteogenic differentiation and thereby influence genetic mechanisms leading to osteogenic differentiation on modified titanium implant surfaces.

ACKNOWLEDGEMENTS

The project is partly supported by the ITI foundation and the Australian Dental Research Foundation.

REFERENCES

1. Wennerberg A, et al., *Clinical Oral Implants Research*. **20**:172-184, 2009
2. Wall I, et al., *Bone*. **45:**17-26, 2009
3. Vlacic-Zischke J, et al. *Biomaterials.* **32(3):**665-671, 2011
4. Olivares-Navarrete R, et al. *Acta Biomat.* **7(6):**2740-2750, 2011
5. Lewis BP, et al. *Cell.* **120:**15-20, 2005

RAPID SCREENING OF STEM CELLS AND ENGINEERING INTERFACE TISSUES USING NANOSCALE GRADIENT BIOMATERIALS

Murugan Ramalingam

Institut National de la Santé Et de la Recherche Médicale U977, Faculté de Chirurgie Dentaire, Université de Strasbourg, Strasbourg 67085, France
Centre for Stem Cell Research, CMC Bagayam Campus, Vellore-632002, India
WPI-Advanced Institute for Materials Research, Tohoku University, Sendai 980-8577, Japan
*Email: ramalingam@unistra.fr; rmurug2000@gmail.com

Biomaterials that have gradients in material composition and functional properties may be used to engineer interfaces between two different tissues (soft-to-hard, for example) or for rapid screening of cell response to scaffold properties suitable for tissue engineering applications. This talk reports a method for generating nanofiber scaffold libraries containing gradients in material composition and properties. The method is based on "bi-spinnerret electrospinning" system, wherein the gradients are obtained by using two syringes where one is filled with poly(ε-caprolactone) (PCL) solution and the other with PCL solution containing calcium phosphate particles, nano hydroxyapatite (nHA) for example. The electrospun scaffolds consisted of non-woven PCL nanofibers containing a linear gradient of nHA, as a single scaffold specimen, which facilitated screening of the effect of nHA composition on human bone marrow stromal cells (hBMSCs) response. The cellular responses were studied by qualitative (fluorescence imaging) and quantitative (Picogreen DNA assay) analysis. The cell culture data showed presence of nHA enhanced the cell adhesion and proliferation compared to pure PCL. In addition, an increased alkaline phosphatase activity has observed on the nHA rich side compared to other end of the scaffold specimen (nHA absence side). These data confirm that the hBMSCs respond to material composition and properties along the graded libraries and can be controlled or tuned their growth and differentiation. Therefore, gradient approach can be utilized to systematically identify scaffold composition and properties that optimize cell responses for tissue engineering applications, in particular when engineering interface tissues.

THE OSTEOGENIC EFFECTS OF A PROTEIN COMPONENT EXTRACTED FROM A HYDROXYAPATITE-BASED PRODUCT

David S Musson[1*], Maureen Watson[1], Karen E Callon[1], Dorit Naot[1], Craig McIntosh[2], Jillian Cornish[1]

[1] Department of Medicine, University of Auckland, New Zealand.
[2] Waitaki Biosciences, Christchurch, New Zealand.
email: d.musson@auckland.ac.nz

INTRODUCTION

Hydroxyapatite (HA) is a microcrystalline, mineral structure that is the primary constituent of mineralised bone. HA products derived from extracellular matrices have been used extensively in regenerative medicine as a base for biomaterial scaffolds, a carrier for controlled drug delivery, as "fillers" in bone and dental defects, or as coatings for metallic implants to promote osteoinduction,. Here we analyse some growth factor content of the protein component of a HA product and assess what effect it has on the growth and differentiation of primary osteoblasts.

METHODS

Using EDTA extraction, approximately 0.1mg/ml protein was extracted from bovine-derived MCH-CAL™, a microcrystalline HA product (Waitaki Biosciences, NZ). Levels of IGF-1, IGF-2 and osteocalcin were assessed by ELISA. Subsequently, the protein extract was used to treat primary rat osteoblasts in 2D (plastic) and 3D (within a collagen gel). Proliferation, differentiation and mineralisation were assessed either through thymidine incorporation, alamarBlue®, real-time PCR and von Kossa staining. MCH-CAL™ particles (inclusive of the protein) were also incorporated into 3D cell-seeded collagen gels and their effect on osteoblast proliferation and differentiation was studied.

RESULTS AND DISCUSSION

Growth factors were detected at levels similar to those found in circulation, with IGF-1 and -2 found at 230ng/g and 170ng/g, respectively. In contrast, osteocalcin was detected at 604µg/g, much higher than reported in circulation. The extracted proteins produced a significant, dose-dependent decrease in the proliferation of osteoblasts in 2D cultures, while dose-dependently increasing osteoblast mineralisation. Cells treated with 100µl/ml protein extract decreased proliferation 2.5-fold ($P<0.05$), yet increased mineralisation 3.5-fold ($P<0.05$), compared to the control.
Cells cultured in 3D had a similar response to those cultured in 2D, with MCH-CAL™ protein digest dose-dependently decreasing cell mitogenesis. However, collagen Iα1 levels were 3-fold higher in 3D cultures treated with 100µl/ml extract, compared to untreated. Interestingly, the incorporation of MCH-CAL™ particles (including the protein) into cell-seeded gels had no change on cell mitogenesis, but did increase cell differentiation.

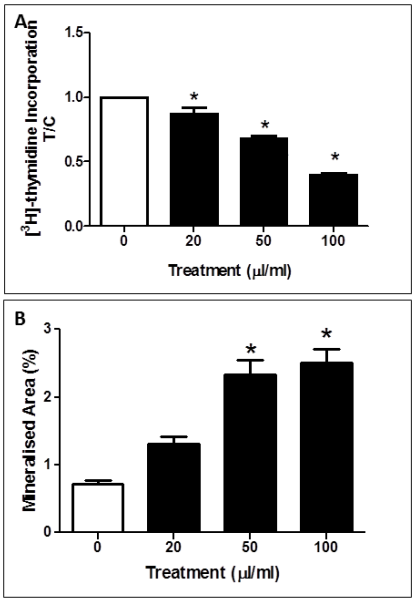

Figure 1: MCH-CAL™ protein extract: A) inhibits mitogenesis of primary rat osteoblasts after 24 hours of 2D culture and B) increases mineralisation in 2D primary rat osteoblast cultures. Data shown are mean (SEM); one-way analysis of variance ($p<0.05$) with post hoc Dunnett's test *$p<0.05$ versus control.

CONCLUSIONS

Currently, HA based products are used to promote osteoinduction through offering structural substrate that is similar to natural bone. However, here we have demonstrated that the protein component of these products can also play a prominent role in inducing bone regeneration. This could have significant implications in the use of such products in future regenerative applications.

ACKNOWLEDGEMENTS

Waitaki Biosciences

Auckland Medical Research Foundation

CONFLICT OF INTEREST DECLARATION

In the interests of transparency and to help reviewers assess any potential bias, ANZORS requires authors of original research papers to declare any competing commercial interests in relation to the submitted work. Referees are also asked to indicate any potential conflict they might have reviewing a particular paper.

If you have accepted any support such as funds or materials, tangible or intangible, concerned with the research by the commercial party such as companies or investors, choose YES below, and state the relation between you and the commercial party.

If you have not accepted any support such as funds or materials, choose NO.

Do you have a conflict of interest to declare? (DELETE TEXT as appropriate)

YES - This project was part funded by Waitaki Biosciences.

THE ROLE OF BMP2 IN BONE GRAFT HEALING

Vivianne Chappuis and Vicki Rosen

Harvard University

Bone graft incorporation depends on the orchestrated activation of numerous growth factors and cytokines in both the host and the graft. Prominent in this signaling cascade is BMP2. Although BMP2 is dispensable for bone formation, it is required in the initiation of bone repair, thus understanding the cellular mechanisms underlying bone regeneration driven by BMP2 is essential for improving future bone graft therapies. We assessed the role of BMP2 in bone graft incorporation using mice where Bmp2 was removed in the limb prior to skeletal formation (Bmp2cKO). When autograft transplantations were performed in Bmp2cKO mice, callus formation and bone healing were abolished. Transplantation of either a vital wild type (WT) bone graft into a Bmp2cKO host or a vital Bmp2cKO graft into a WT host also resulted in the inhibition of bone graft incorporation. Histological analyses of these transplants show that in the absence of BMP2 periosteal progenitors remain quiescent and healing is not initiated, suggesting that local BMP2 levels drive periosteal cell condensation and subsequent differentiation into chondrocytes that produce the callus. The lack of integrated healing in the absence of BMP2 was not due to the inability of periosteal cells to respond to BMP2 as healing occurred when grafts were pre-soaked in rhBMP2 protein, indicating that periosteal progenitors remain functional in the absence of BMP2. In contrast to the requirement for BMP2 in periosteal progenitor activation in vital bone grafts, our studies also showed that BMP2 present in devitalized bone matrix derived does not significantly enhance bone graft incorporation. Taken together, our data suggest that BMP2 is not required for the maintenance of periosteal progenitors within their niche, but is necessary for activation of these progenitors and their subsequent movement out of the niche during healing. Therefore the availability of BMP2 in the local environment is an essential driving force for the initiation of graft healing.

Development and optimization of *ex vivo* bioreactor system for tendon tissue engineering

Tao Wang, Zhen Lin, Euphemie Landao, Minghao Zheng

Centre of Orthopaedic Surgery, School of Surgery, University of Western Australia, Nedlands, WA 6009 Australia
Email: louis@mech.uwa.edu.au

INTRODUCTION

Tendon injury is a common orthopaedic disease but the treatment options remain poorly defined. Tendon/ligament engineering might be an alternative option of surgical replacement of injured tendon. Tendon/ligament ex vivo bioreactor system may provide a controllable environment that mimics the dynamics of *in vivo* situation for tendon/ligament maturation, therefore serve as a systematic study model for specific biological, biochemical and biomechanical effects on engineering of tendon tissue. Programmable mechanical stimulation is the key component of a bioreactor system for tendon engineering.

The aims of the study were to design a bioreactor system with cyclic mechanical stimulation to mimic the condition that Achilles tendon undergoes *in vivo*, and to define the optimal tensile loading strain for maintaining the tendon homeostasis.

METHODS

An ex vivo bioreactor system with programmable dynamic tensile stretch was designed and manufactured. Achilles tendons from New Zealand white rabbits were loaded in the bioreactor with or without cyclic tensile loading (0.25Hz for 8 hours per day). A range of tensile strains, from 0% to 9%, were applied on the rabbit Achilles tendon for 6 days or 2 weeks. General histology, immunohistochemical staining of type III collagen, TUNEL assay and quantitative-PCR were applied to examine the structural integrity and matrix turnover of the tendons.

RESULTS AND DISCUSSION

The bioreactor system contains 6 individual culture chambers (FIG.1), a step motor and a programmable logic controller. It can provide maximum 198N peak force and accuracy up to ±5μm. The mechanical loading regimes, such as frequency and loading period, can be preprogrammed through a computer. Furthermore, the study shown that without tensile loading, Achilles tendon lost its structure integrity as evidenced by disorientated collagen fiber, increased type III collagen production and expression, and increased cell apoptosis. Tendons with 3% of tensile loading did not prevent matrix deterioration, whilst 6% of tensile loading was able to maintain the structural integrity and cellular function. Exceeded loading regime of 9% caused massive tendon rupture.

A proper cyclic tensile loading is required to maintain the tendon homeostasis. Completed/partial loading deprivation or overload results in abnormal matrix structure and cellular function in tendon, which are observed in clinical tendinopathy. Our bioreactor system could be programmed to provide a suitable dynamic culture condition to mimic the *in vivo* situation for tendon tissue engineering purposes, and moreover a study model to define the tendon-specific biological, biochemical and biomechanical profiles under physical/pathological conditions.

SESSION 8 - ABSTRACTS

Bone Biology & Joint Regeneration (2)

DAY 3: Saturday, 1 September

2:50 PM – 4:05 PM

MONOSODIUM URATE CRYSTALS INHIBIT TENOCYTE VIABILITY AND FUNCTION: IMPLICATIONS FOR PERIARTICULAR INVOLVEMENT IN CHRONIC GOUT

Ashika Chhana[1], Karen E Callon[1], Bregina Pool[1], Dorit Naot[1], Greg Gamble[1], Brendan Coleman[2], Fiona M McQueen[3], Jillian Cornish[1] and Nicola Dalbeth[1]

[1]Bone & Joint Research Group, Department of Medicine, University of Auckland, Auckland, New Zealand
[2]Department of Orthopaedic Surgery, Middlemore Hospital, Auckland, New Zealand
[3] Department of Molecular Medicine and Pathology, University of Auckland, Auckland, New Zealand
email: a.chhana@auckland.ac.nz

INTRODUCTION

Recent advanced imaging studies have demonstrated that urate deposition in periarticular structures is common in gout. Urate deposition has been observed both adjacent to and within tendons, suggesting that monosodium urate monohydrate (MSU) crystals are likely to be in direct contact with tenocytes, the stromal cells of tendons. The aim of this study was to determine the effects of MSU crystals on tenocyte viability and function.

METHODS

Cultures of primary rat tenocytes were prepared from Wistar rat tails, and primary human tenocytes from patients undergoing orthopaedic surgery. MTT and flow cytometry assays were used to assess tenocyte viability following culture with MSU crystals. Real-time PCR was used to determine changes in gene expression and Sirius red staining was used to determine changes in collagen deposition in tenocytes cultured with MSU crystals.

RESULTS AND DISCUSSION

MSU crystals rapidly reduced viability in a dose-dependent manner in both primary rat and human tenocytes. Differing MSU crystal lengths and increased serum levels in cultures did not alter this effect. The reduction in tenocyte viability was specific to MSU crystals, as soluble uric acid did not reduce cell viability. Culture with MSU crystals reduced mRNA expression of collagen types 1 and 3; and tenocytic markers, including tenomodulin, scleraxis and tenascin-C. Collagen deposition was inhibited in tenocytes cultured with MSU crystals in a dose dependent manner.

CONCLUSIONS

These data indicate that MSU crystals directly interact with tenocytes to reduce cell viability and function. These interactions may contribute to tendon damage in patients with chronic gout.

Central control of bone resorption: Neuropeptide Y, Y6 receptor signalling in the regulation of bone homeostasis

[1]Driessler F, [1]Yulyaningsih E, [1]Khor EC, [1]Enriquez RF, [2]Xu J, [1]Sainsbury A, [1]Eisman JA, [1]Herzog H and [1]Baldock PA

[1]Neuroscience Program, Osteoporosis and Bone Biology, Garvan Institute of Medical Research, St Vincent's Hospital, Sydney, Australia.
[2]School of Pathology and Laboratory Medicine, University of Western Australia, Perth, Australia.
email: e.khor@garvan.org.au

INTRODUCTION

The past decade has seen the Neuropeptide Y system identified as a novel regulatory axes between the nervous system and bone cells. Gene knockout studies have shown that signalling through Neuropeptide Y receptors in the hypothalamus and osteoblast are required for normal bone formation. Here, we demonstrate that the lesser characterised Y6 receptor is also an important regulator of bone resorption.

METHODS

Y6R gene knockout mice were generated to assess the bone phenotype DXA and micro-CT. Tissues were collected from the Y6R KO mice for histology and to measure gene expression by RT-PCR. Bone cell activity was measured using bone histomorphometry. Bone marrow was extracted to examine RANKL-osteoclastogenesis in Y6R KO mice.

RESULTS AND DISCUSSION

Y6R-deficient mice displayed a significant decrease in whole body and femoral BMD and BMC. In addition, micro-CT analysis revealed that Y6R KO mice showed a significant decrease in trabecular bone volume due to reduced trabecular number. Cortical thickness was also reduced in Y6R KO. Interestingly, Y6R KO mice had reduced body weight associated with increased energy expenditure. Nevertheless, the restoration to WT body weight levels due to fat-feeding failed to rescue the bone phenotype. Bone histomorphometry revealed no changes in osteoblast activity, whereas osteoclast activity was significantly increased in Y6R KO. Despite the lack of Y6R gene expression in osteoclast precursors and mature osteoclasts, ex vivo Y6R KO osteoclast cultures showed increased osteoclast number similar to the in vivo phenotype.

CONCLUSIONS

The deletion of Y6R has uncovered an additional pathway by which the NPY system controls bone homeostasis. Moreover, the Y6R is expressed solely in the hypothalamus and is activated by a different member of the NPY family, pancreatic polypeptide (PP), which is produced by F-cells in the gut. Thus the role of Y6R in bone highlights the multi-level regulation of bone homeostasis by peripheral factors through central relay mechanisms.

TNF-LIKE WEAK INDUCER OF APOPTOSIS (TWEAK) AND ITS RECEPTOR, FN14, ARE EXPRESSED BY MULTINUCLEATED CELLS IN REVISION TISSUES AND ELEVATED DURING OSTEOCLAST DEVELOPMENT STIMULATED BY POLYETHYLENE PARTICLES *IN VITRO*.

Anak ASSK Dharmapatni, [1]Tania N Crotti, [1]Christopher A Holding, [2]David M Findlay, [2]Gerald J Atkins, [1]David R Haynes.

[1]Discipline of Anatomy and Pathology, University of Adelaide, Adelaide, SA, Australia, 5005.
[2]Bone Cell Biology Group, Discipline of Orthopaedics and Trauma, University of Adelaide, Adelaide, SA, Australia, 5005.

INTRODUCTION

TWEAK has been reported to be a mediator of inflammation and bone erosion in several chronic inflammatory pathologies such as rheumatoid arthritis (RA) [1] and chronic periodontitis [2]. In this study we aim to investigate if TWEAK and its receptor Fn14 have a role in bone erosion associated with implant loosening and polyethyene (PE) particles.

METHODS

In vivo studies: Soft tissues adjacent osteolysis from 7 patients was obtained from patients undergoing revision surgery loosening of implants containing PE. Soft tissues from 10 OA patients undergoing primary hip/knee replacement were obtained as control. TWEAK was detected using inmmunohistology with a monoclonal antibody (P2D10), a gift from Dr Timothy Zheng (Biogen Inc) and Fn14 monoclonal antibody (clone Item4, R&D Systems) as previously described [1, 2]. Semiquantitativeanalysis (SQA) of TWEAK expression levels were carried out using previously published methods [1, 2]. The difference in expression in PP and OA was analysed using Mann Whitney U test and $p<0.05$ was considered as being a statistically significant difference.

In vitro studies: Human Osteoclasts were differentiated from peripheral blood monocytes (PBMCs) obtained from healthy donors using our previously published methods [3]. Briefly, cells were incubated in collagen and PE particles (500 ng/ml) containing media for the first three days in the presence and absence of high and low levels of RANKL (50 or 10 ng/ml respectively). After three days the collagen was digested and the cells washed before they were placed in complete medium (alpha MEM, 10% v/v Foetal Calf Serum, 2 mM L glutamine, 5 μg/ml penicillin and 50 μg/ml Streptomycin) contain MCSF (25ng/ml) and RANKL (50ng/ml). Total RNA was isolated from the cells at day 17. cDNA was generated from the total RNA and real time PCR for TWEAK was performed with hARP as the house keeping gene, according to previously published methods [4]. Osteoclast formation was confirmed by TRAP staining and osteoclast function by assessing dentine pit resorption using Scanning Electron Microscope.

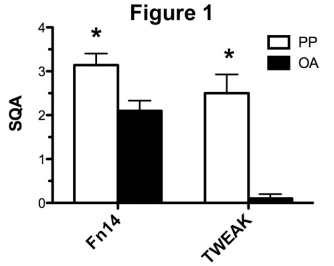

RESULTS AND DISCUSSION

TWEAK and Fn14 protein expression was significantly higher ($p<0.05$) in PP tissues compared to OA tissues (Figure 1). TWEAK was strongly expressed by multinucleated cells containing PE particles in the peri-prosthetic tissues. *In vitro* studies showed that TWEAK mRNA expression was higher in pre-osteoclasts cultured with PE compared to those without PE during the terminal stages of osteoclast maturation (Figure 2). Interestingly, TWEAK mRNA was highest in cells stimulated with low levels of RANKL (10ug/ml). PE significantly enhanced osteoclast activity in the presence of low (10ng/ml) and high (50ng/ml) RANKL (Figure 3) similar to that previously reported for the high level of RANKL [3].

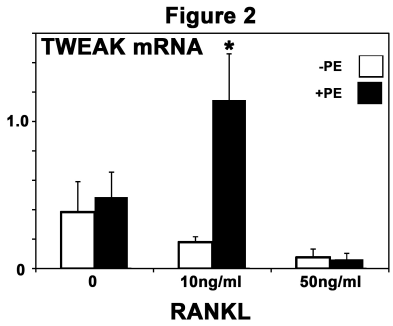

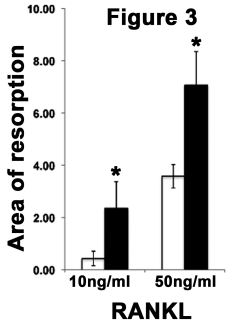

CONCLUSIONS

TWEAK and Fn14 are highly expressed by "osteoclast like" cells in peri-prosthetic tissues associated with PE wear particles. This is consistent with the *in vitro* findings showing that low levels of RANKL induce TWEAK expression in the presence of PE particles. In addition, PE particles induce significantly elevated levels of osteoclast-mediated resorption *in vitro*. These finding suggest a role for TWEAK/Fn14 signalling in the induction of resorption associated with PE particles.

REFERENCES

1. Dharmapatni, A. A.; Smith, M. D.; Findlay, D. M.; Holding, C. A.; Evdokiou, A.; Ahern, M. J.; Weedon, H.; Chen, P.; Screaton, G.; Xu, X. N.; Haynes, D. R. Arthritis Res Ther.13(2):R51. 2009

2. Kataria NG, Bartold PM, Dharmapatni AASK, Atkins, G. J. Holding, C. A. Haynes, D. R. Journal of Periodontal Research : 45 : 4 : 564-573 2010

3. Alias E, Dharmapatni A.S.S.K, Holding AC, Atkins G.J., Findlay D.M., Howie D.W., Crotti T.N. and Haynes D.R. Acta Biomaterialia (accepted for publication 26 April 2012).

ENU-INDUCED CHEMICAL MUTAGENESIS REVEALS THAT CHOLINE KINASE BETA IS AN IMPORTANT REGULATOR OF OSTEOPOROSIS

[1]Jasreen Kular, [1]Jennifer Tickner, [2]Nathan Pavlos, [3]Helena M. Viola, [4]Tamara Abel, [1]Baysie Lim, [3]Livia C. Hool, [2]Ming-Hao Zheng and [1]Jiake Xu

[1]School of Pathology and Laboratory Medicine, University of Western Australia
[2]Centre for Orthopaedic Research, School of Surgery, University of Western Australia
[3]Cardiovascular Electrophysiology Laboratory, University of Western Australia
[4]Centre for Microscopy, Characterisation and Analysis (CMCA), University of Western Australia
email: jiake.xu@uwa.edu.au

INTRODUCTION

The maintenance of bone homeostasis requires a tight balance between bone formation and bone resorption by osteoblasts and osteoclasts. The molecular mechanism(s) underlying the fundamental activities of these cells still remains largely unclear. In search of novel molecules that potentially play an important role in bone homeostasis we screened a number of ENU-induced mutant mouse lines. We identify choline kinase beta, a kinase that phosphorylates the first reaction in the biosynthesis of phosphatidylcholine, as a novel candidate regulator of bone homeostasis.

METHODS

The choline kinase beta mutant mice were generated at the Australian Phenomics facility at the Australian National University. MicroCT and histological analysis was carried out to assess the bone phenotype of the choline kinase beta mutant mice. Osteoclasts were generated from bone marrow macrophages isolated from the long bones of wildtype and choline kinase beta mutant mice and cultured *in vitro* with macrophage colony stimulating factor (M-CSF) and receptor activator of nuclear factor kappa B ligand (RANKL). Osteoblasts for *in vitro* analysis were cultured from bone marrow and induced to differentiate and form bone nodules by the addition of dexamethasone, beta-glycerophosphate and ascorbate. *In vitro* intracellular calcium assays were performed using the fluorescent indicator Fura-2 and measuring 340/380nm ratiometric fluorescence. *In vivo* rescue experiments were performed by injecting CDP-choline into wildtype and choline kinase beta mutant mice for 3 weeks before analysis.

RESULTS AND DISCUSSION

Choline kinase beta mutant mice exhibit an osteoporotic phenotype as evidenced by microCT and histological assessment. *In vivo* and *in vitro* analysis reveals elevated osteoclast numbers in the mutant mice. Furthermore, osteoclasts from choline kinase beta mutant mice exhibit increased resorptive activity compared to those of littermate controls. Interestingly, exposure to elevated extracellular calcium results in a significant increase in intracellular calcium in osteoclasts derived from control mice, however this response is significantly attenuated in osteoclasts derived from choline kinase beta mutant mice. This may account for the increased resorptive activity in osteoclasts derived from the mutant mice. Treatment with CDP-choline *in vivo* and *in vitro* reduces osteoclast numbers, thereby rescuing the osteoclast phenotype. *In vitro* assays show a reduction in bone mineralisation in osteoblast cultures derived from the bone marrow of mutant mice.

CONCLUSIONS

Taken together, our data documents, for the first time, that choline kinase beta plays an important role in bone homeostasis by regulating both osteoclasts and osteoblasts.

ACKNOWLEDGEMENTS

This work was supported by the National Health and Medical Research Council of Australia.

SEMINAL VESICLE SECRETION (SVS) 7 IS EXPRESSED BY MATURE OSTEOCLASTS AND ACTS TO REGULATE OSTEOCLAST PRECURSOR PROLIFERATION, DIFFERENTIATION AND BONE HOMEOSTASIS

[1]William Cundawan, [1]Jennifer Tickner, [3]Tamara Abel, [1]Shek Man Chim, [2]Nathan Pavlos, [2]Minghao Zheng, and [1]Jiake Xu

[1]School of Pathology and laboratory Medicine, The University of Western Australia, WA
[2]Centre for Orthopedic Research, School of Surgery, The University of Western Australia, WA
[3]Centre for Microscopy, Characterization, and Analysis, The University of Western Australia, WA
email: jiake.xu@uwa.edu.au

INTRODUCTION

Bone is remodeled throughout life by complementary activites of bone-forming osteoblasts and bone-resorbing osteoclasts. The intercellular communication between osteoblasts and osteoclasts is achieved by the production of various cytokines, growth factors, and proteins produced by these cells.

Using subtractive hybridization-based differential screening, SVS7, also known as calcium-transport inhibitor (caltrin), was identified to be expressed by mature osteoclasts, not by their precursors or osteoblasts**.** SVS7 expression is upregulated during RANKL-induced osteoclastogenesis. The aim of this study is to investigate the role of SVS7 in bone homeostasis.

METHODS

To investigate the role of SVS7 in bone, we generated global SVS7 knockout mice. MicroCT was then used to characterize the bone phenotype of these mice versus WT. Bone marrow of WT and KO mice were extracted and used for *in vitro* osteoclastogenesis and bone resorption assay, mineralization and alkaline phosphatase assays for both osteoclast and osteoblast activity respectively.

To further investigate the mechanism on how SVS7 regulates bone homeostasis, proliferation assays on WT and KO bone marrow osteoclast precursors and calvarial osteoblasts were carried out. RANKL stimulation on osteoclast precursors has been shown to induce calcium oscillation, which is necessary for the induction and activation of NFATc1 transcription factor, a master regulator of osteoclastogenesis [1,2]. To determine the effect of SVS7 in RANKL-induced calcium oscillation in osteoclast precursors, intracellular calcium assay on WT and KO bone marrow osteoclast precursor was carried out.

RESULTS AND DISCUSSION

By microCT we find that SVS7 KO mice exhibit an osteopenic phenotype. *In vitro* osteoclastogenesis revealed that KO bone marrow produced significantly more osteoclasts than that of WT following RANKL stimulation. There was a trend of larger resorption pit/osteoclast in KO osteoclasts compared to WT in bone resorption assays. No significant differences in mineralization and alkaline phosphatase activity between WT and KO bone marrow-derived osteoblasts were observed. Alamar blue proliferation assays on WT and KO bone marrow osteoclast precursors showed a significantly increased proliferation rate after 72hrs of M-CSF stimulation in KO compared to WT, whereas the proliferation rates of WT and KO calvarial osteoblasts remained constant. Intracellular calcium assays revealed that there were more KO osteoclast precursors undergoing calcium oscillation than WT after 24hrs RANKL stimulation**.** These results indicate that SVS7 is expressed by mature osteoclasts and acts to regulate precursor cell proliferation and differentiation within bone marrow.

CONCLUSIONS

We posit SVS7 as a novel regulator of bone homeostasis.

ACKNOWLEDGEMENTS

This research was supported by the National Health and Medical Research Council (NHMRC) grant

REFERENCES

1. Yarilina A, et al., *PNAS.* **108(4)**: 1573, 2011.
2. Nakashima T, et al., *Annals of the New York Academy of Sciences*. **1240(1)**:E13-E18, 2011

CONFLICT OF INTEREST DECLARATION

In the interests of transparency and to help reviewers assess any potential bias, ANZORS requires authors of original research papers to declare any competing commercial interests in relation to the submitted work. Referees are also asked to indicate any potential conflict they might have reviewing a particular paper.

If you have accepted any support such as funds or materials, tangible or intangible, concerned with the research by the commercial party such as companies or investors, choose YES below, and state the relation between you and the commercial party.

SCAFFOLD MECHANICAL PROPERTIES AND COMPOSITION REGULATES STEM CELL FATE

[1, 2, 3] Ciara M Murphy, [2, 3] Amos Matsiko, [2, 3] Matthew G Haugh, [2, 3] John P Gleeson and [2, 3] Fergal J O'Brien

[1] Kids Research Institute, Children's Hospital at Westmead, NSW
[2] Department of Anatomy, Royal College of Surgeons in Ireland, Dublin, Ireland
[3] Centre for Bioengineering, Trinity College Dublin, Dublin, Ireland
email: ciara.murphy@sydney.edu.au

INTRODUCTION

The rigidity of a substrate and the mechanical input generated by its deformation has been shown to regulate adult stem cell differentiation [1]. However, many of these investigations have been carried out on 2-D surfaces which do not necessarily mimic the native ECM. Utilising a collagen-glycosaminoglycan (CG) scaffold as a 3-D analogue of the ECM, this study aimed to investigate the effect of CG scaffold stiffness on osteogenic and chondrogenic differentiation of mesenchymal stem cells (MSCs). Furthermore, we sought to determine if MSC differentiation is further up-regulated towards a specific lineage depending on the GAG type used within the CG scaffold.

METHODS

Two CG scaffold groups (**CCS** = Collagen 0.5wt%, chondroitin sulphate 0.05wt%, **CHyA** = Collagen 0.5wt%, hyaluronic acid 0.05wt%) were fabricated using a previously described freeze-drying technique [2] and then crosslinked with either a dehydrothermal process or with one of two concentrations of 1-ethyl-3-(3-dimethyl aminopropyl) carbodiimide (3mM or 6mM). This resulted in 3 scaffolds with the same composition but 3 different stiffness values: 0.5, 1 and 1.5 kPa [3]. The scaffolds were seeded with rat MSCs in standard non-conditioned growth media. Blebbistatin (50µM), a non muscle myosin II inhibitor was added to media as a negative control as it hinders the cells ability to sense the elasticity of the matrix, preventing mechanotransduction. Real-time PCR was used to assess the expression of osteogenic and chondrogenic transcription markers to determine lineage specification and differentiation. N=6 was analysed for each assay with $p \leq 0.05$ considered significant.

RESULTS AND DISCUSSION

Our results demonstrate that scaffold mechanical properties influence the fate of MSCs (Fig. 1). Scaffolds with the lowest stiffness (0.5 kPa) demonstrated a significant up-regulation in *Sox9* expression indicating that MSCs are directed towards a chondrogenic lineage within the more compliant scaffolds (Fig. 1 A&B). In contrast, the greatest level of *Runx2* expression was observed in the stiffest of the scaffold groups (1.5 kPa) indicating that MSCs are directed towards an osteogenic lineage within these scaffolds (Fig. 1 C&D). These results were observed in the absence of any differentiation supplements. In addition, when Blebbistatin was added to the culture media, there was no up-regulation in transcription markers in any of the scaffold groups. This indicates that the transcriptional changes result from the cells sensing scaffold elasticity.

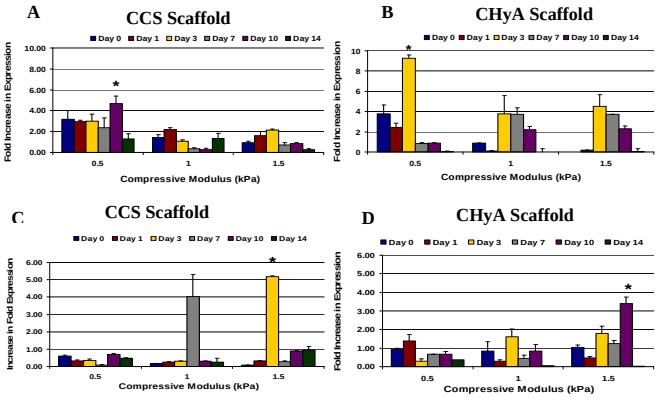

Figure 1: Comparison of ***Sox9*** expression in CCS scaffolds (A) and CHyA scaffolds (B) and ***Runx2*** expression in CCS scaffolds (C) and CHyA scaffolds (D), across the stiffness range. *P<0.001

Although the mechanical properties influence the lineage specification of the MSCs, GAG type further affects the direction of stem cell differentiation. This was apparent when the expression of *Runx2* and *Sox9* were compared in both composition types. The level of up-regulation of *Sox9* was higher within the CHyA scaffolds in comparison to the CCS scaffolds indicating that hyaluronic acid further influences chondrogenic differentiation. Enhanced *Runx2* expression was observed in the CCS scaffolds in comparison to the CHyA scaffolds suggesting an osteogenic influence of chondroitin sulphate on MSC differentiation.

CONCLUSIONS

This study has significant implications for the therapeutic uses of stem cells in bone tissue engineering. Due to the complex nature of native ECM, these results enhance our understanding of the physical effects of the *in vivo* microenvironment on stem cell behaviour.

ACKNOWLEDGEMENTS

European Research Council (grant agreement #239685), Integra Life Sciences provided collagen for the study.

REFERENCES.

1. Engler A.J., et al., *Cell.* **126**(4): 677-689, 2006.
2. O'Brien, F. J. et al., *Biomaterials*, **25**(6): 1077-1086, 2005
3. Haugh M.G., et al, *Tissue Eng Part A*, **17**(9-10): 1201-1208, 2011.

EGFL7 is Differentially Expressed in Osteoclasts and Osteoblasts and Mediates Endothelial Cell Migration through the Activation of Extracellular Signal-regulated Kinase

Shek Man Chim, Siu To Chow, Jiake Xu

School of Pathology and Laboratory Medicine, The University of Western Australia, Western Australia, Australia
Email: jiake.xu@uwa.edu.au

INTRODUCTION

Angiogenesis plays a pivotal role in bone formation, remodeling, and fracture healing [1-3]. The regulation of angiogenesis and bone remodeling is highly complex and orchestrated by multiple intercellular communication between bone cells and endothelial cells [4-6]. However, local factors contributing to the cross-talk in bone microenvironment is still unclear. The aim of our study was to identify novel secreted factors expressed by bone cells, which regulate angiogenesis and bone homeostasis. Here, we report that EGF-like domain 7 (EGFL7), a member of the epidermal growth factor (EGF) repeat superfamily proteins is differentially expressed in osteoclasts and osteoblasts and regulates endothelial cell activities.

METHODS

Microarray analysis was used to identify the gene expression of EGFL7 in osteoclasts and osteoblasts. RT-PCR was used to determine the gene expression profile of EGFL7 during osteoclast and osteoblast differentiation. Molecular cloning of mouse EGFL7 and transient transfection in COS-7 cells was used to produce conditioned medium containing recombinant mouse EGFL7 for functional study. Scratch wound healing assays was used to examine the effect of EGFL7 on SVEC (A simian virus 40-transformed mouse microvascular endothelial cell line) cell migration. Moreover, Western blot was used to examine signaling pathways involved in EGFL7-induced endothelial cell migration.

RESULTS AND DISCUSSION

Microarray analysis revealed that EGFL7 is differentially expressed during osteoclast and osteoblast differentiation. The gene expression of EGFL7 in osteoclast and osteoblast was confirmed by semiquantitative RT-PCR. An expression construct encoding the full-length of mouse EGFL7 was generated using expression vector pcDNA3.1A-EGFL7-c-myc/his. COS-7 cells were transfected with EGFL7 expression construct to produce conditioned medium containing recombinant EGFL7 as a 32 kDa protein, confirming that the EGFL7 is a secreted protein. Using scratch wound healing assay, we found that conditioned medium containing recombinant EGFL7 potentiates SVEC (A simian virus 40-transformed mouse microvascular endothelial cell line) cell migration. Furthermore, we show that EGFL7 recombinant protein induces phosphorylation of ERK in SVEC endothelial cells.

CONCLUSIONS

Together, these results demonstrate that osteoblasts and osteoclasts express EGFL7, a secreted factor that is capable of promoting endothelial cell migration via ERK activation. Understanding the mechanisms by which EGFL7 regulates the intercellular communication in bone local environment should aid in advancing our knowledge of bone remodeling and angiogenesis and might offer an important new target for the potential treatment of bone diseases, including osteoporosis, and bone fracture healing.

ACKNOWLEDGEMENTS

This work was supported in part by the National Health and Medical Research Council of Australia

REFERENCES

1. Carano RA, et al., *Drug Discov Today* **8**:980-989, 2003.
2. Fang TD, et al., *J Bone Miner Res* **20**:1114-1124, 2005.
3. Gerber HP, et al., *Trends Cardiovasc Med* **10**:223-228, 2000.
4. Eriksen EF, et al., *J Bone Miner Res* **22**:1-6, 2007.
5. Brandi ML, et al., *J Bone Miner Res* **21**:183-192, 2006.
6. Chim SM, et al., *J Biol Chem* **286**:22035-22046, 2011.

ANZORS 18th Annual Scientific Meeting
List of registered delegates at time of printing
(surname alphabetical order)

Surname	First name	Title	Affiliation	E-mail address
ABRAHAMS	John	Mr	University of Adelaide, SA	john.abrahams@student.adelaide.edu.au
BUENZLI	Pascal	Dr	University of Western Australia, WA	pascal.buenzli@uwa.edu.au
CALLARY	Stuart	Mr	Royal Adelaide Hospital, SA	Stuart.Callary@health.sa.gov.au
CANTLEY	Melissa	Miss	University of Adelaide, SA	melissa.cantley@adelaide.edu.au
CHAKRABARTY	Adhiraj	Dr	Royal Adelaide Hospital, SA	adhirajc@gmail.com
CHAKRAVORTY	Nishant	Dr	Queensland University of Technology, QLD	n.chakravorty@qut.edu.au
CHEN	Song	Mr	Australian National University, ACT	song.chen@anu.edu.au
CHHANA	Ashika	Miss	University of Auckland, NZ	a.chhana@auckland.ac.nz
CHIM	Shek Man (Jacky)	Dr	University of Western Australia, WA	shek.chim@uwa.edu.au
CORNISH	Jillian	Prof	University of Auckland, NZ	j.cornish@auckland.ac.nz
COSTI	John	Dr	Flinders University, SA	john.costi@flinders.edu.au
CUNDAWAN	William	Mr	University of Western Australia, WA	cundaw01@student.uwa.edu.au
DAVIDSON	John	Dr	University of Western Australia, WA	john.davidson@uwa.edu.au
DISCHER	**Dennis**	**Prof**	**University of Pennsylvania, USA**	**discher@seas.upenn.edu**
DUNSTAN	Colin	Prof	University of Sydney, NSW	colin.dunstan@sydney.edu.au
FINDLAY	David	Prof	University of Adelaide, SA	david.findlay@adelaide.edu.au
GRODZINSKY	**Alan**	**Prof**	**Massachusetts Institute of Technology, USA**	**alg@mit.edu**
HAN	Ping Ping	Miss	Queensland University of Technology, QLD	pingping.han@student.qut.edu.au
HAYNES	David	A/Prof	University of Adelaide, SA	david.haynes@adelaide.edu.au
HE	Bo	Mr	University of Western Australia, WA	hebo@mech.uwa.edu.au

Surname	First name	Title	Affiliation	E-mail address
HEILSHORN	**Sarah**	**Assist. Prof**	**Stanford University, USA**	**heilshorn@stanford.edu**
JAIPRAKASH	Anjali Jumkur	Miss	Queensland University of Technology, QLD	anjali.jaiprakash@qut.edu.au
JONES	Claire	Dr	SA Pathology, SA	claire.jones2@health.sa.gov.au
KHOR	Ee Cheng	Dr	Garvan Institute of Medical Research, NSW	e.khor@garvan.edu.au
KULAR	Jasreen	Dr	University of Western Australia, WA	jasreen.kular@uwa.edu.au
LEVINGER	Pazit	Dr	Victoria University, VIC	pazit.levinger@vu.edu.au
LI	Jiao Jiao	Ms	University of Sydney, NSW	jiaojiao.li@sydney.edu.au
LI	Rachel	Dr	Australian National University, ACT	rachel.li@anu.edu.au
LOW	Stephanie	Dr	University of Adelaide, SA	low.wiles@adam.com.au
LU	**William**	**Prof**	**University of Hong Kong, HK**	**wwlu@hku.hk**
MARTELLI	Saulo	Dr	University of Melbourne, VIC	saulo.martelli@unimelb.edu.au
MCDONALD	Michelle	Dr	Garvan Institute of Medical Research, NSW	m.mcdonald@garvan.org.au
MOKHTARZADEH	Hossein	Mr	University of Melbourne, VIC	mokhtarzadeh.hossein@gmail.com
MURPHY	Ciara	Dr	Kids Research Institute, NSW	ciara.murphy@sydney.edu.au
MUSSON	David	Dr	University of Auckland, NZ	d.musson@auckland.ac.nz
PAVLOS	Nathan	A/Prof	University of Western Australia, WA	nathan.pavlos@uwa.edu.au
PERILLI	Egon	Dr	Flinders University, SA	egon.perilli@flinders.edu.au
PETERS	James Robert	Mr	Drexel University, USA	jrp345@drexel.edu
PIVONKA	Peter	Prof	University of Western Australia, WA	peter.pivonka@uwa.edu.au
REDDY	Silpa	Ms	Drexel University, USA	sr444@drexel.edu
ROOHANI-ESFAHANI	Seyed-Iman	Mr	University of Sydney, NSW	iman.roohani@gmail.com
ROSEN	**Vicki**	**Prof**	**Harvard University, USA**	**vicki_rosen@hsdm.harvard.edu**
SMITH	David	Prof	University of Western Australia, WA	david.smith@uwa.edu.au
SOLOMON	Bogdan	A/Prof	Royal Adelaide Hospital, SA	bogdan.solomon@health.sa.gov.au
SU	Yu-Wen	Miss	University of South Australia, SA	suyyy009@mymail.unisa.edu.au

Surname	First name	Title	Affiliation	E-mail address
TAYLOR	**Mark**	**Prof**	**Flinders University, SA**	**mark.taylor@flinders.edu.au**
THEWLIS	Dominic	Dr	University of South Australia, SA	dominic.thewlis@unisa.edu.au
THOMAS	David	Mr	University of Melbourne, VIC	cdthomas@unimelb.edu.au
WANG	Tao	Mr	University of Western Australia, WA	louis@mech.uwa.edu.au
WILLE	Marie-Luise	Miss	Queensland University of Technology, QLD	m.wille@qut.edu.au
XIAN	Cory	Prof	University of South Australia, SA	cory.xian@unisa.edu.au
XIAO	Yin	Prof	Queensland University of Technology, QLD	yin.xiao@qut.edu.au
XU	Jiake	Prof	University of Western Australia, WA	jiake.xu@uwa.edu.au
YELICK	**Pamela**	**Prof**	**Tufts University, USA**	**pamela.yelick@tufts.edu**
YU	Nicole	Dr	Kids Research Institute, NSW	nicole.yu@sydney.edu.au
ZHANG	Xu Fang	Miss	Queensland University of Technology, QLD	xufang.zhang@student.qut.edu.au
ZHOU	Ying Hong	Ms	Queensland University of Technology, QLD	yinghong.zhou@student.qut.edu.au
ZOEHRER	Ruth	Dr	University of South Australia, SA	ruth.zoehrer@flinders.edu.au
ZREIQAT	Hala	A/Prof	University of Sydney, NSW	hala.zreiqat@sydney.edu.au